The Effects of Imposed Deformations on the Behaviour of Loaded Concrete Structures

Alemo, Jan

1976

LUND INSTITUTE OF TECHNOLOGY · LUND · SWEDEN · 1976
DIVISION OF STRUCTURAL MECHANICS AND CONCRETE CONSTRUCTION · BULLETIN 53

JAN ALEMO

THE EFFECTS OF IMPOSED DEFORMATIONS ON THE BEHAVIOUR OF LOADED CONCRETE STRUCTURES

LUND INSTITUTE OF TECHNOLOGY LUND SWEDEN 1976

DIVISION OF STRUCTURAL MECHANICS AND CONCRETE CONSTRUCTION

THE EFFECTS OF IMPOSED DEFORMATIONS ON THE BEHAVIOUR OF LOADED CONCRETE STRUCTURES

JAN ALEMO

LUND, AUG 1976

Offsettryck. Elegant-tryck, Växjö 1976

CONTENTS

ACKNOWLEDGEMENTS

This paper is the final report from a research project sponsored by the Swedish Council of Building Research. The author wishes to thank the Council for this support.

The author wants to thank the initiator of the project, Professor Arne Hillerborg with whom the project has been performed in close cooperation, for his fruitful ideas and encouraging support.

The author also wishes to thank the whole staff of the Division of Structural Mechanics and Concrete Construction and particularly the persons listed below.

Professor Ove Pettersson, the head of the division

Lisbeth Henning who has translated the original manuscript into English

Ulf Wickström and Sven Strandberg for their help with the calculation of the drying process

Sven Thelandersson who has read through the manuscript and made many helpful suggestions

Ann Schollin for making the drawings and

Tarja Aunola who has typed the manuscript.

Lund, August 1976

Jan Alemo

ABSTRACT

The effects of cracking, creep, shrinkage and support displacements on the deflection and the force distribution at serviceability limit state and on the rotation requisite at ultimate limit state have been investigated for loaded beams, columns and frames.

The problem has been tackled by establishing first refined calculation models based on the behaviour of the concrete and the reinforcement and then simplified models, the reliability of which is controlled in relation to these, and at last by putting the simplified models together in models describing the behaviour of the whole structure.

The investigation has resulted in relations for the determination of the deformations of concrete on account of tensile and compressive stresses, basic creep, drying creep and shrinkage and regard has been taken to stress changes in these relations. Furthermore simplified force-deformation relations have been established for reinforced concrete subjected to normal force, moment, moment plus normal force and shear force at the same time as creep and shrinkage. Calculation methods for beams and columns based on the stated simplified bilinear moment-curvature relations have been evaluated and are accounted for and descriptions are given on how to use them for more complicated structures. A systematized calculation method has been established for frames based on the load-deformation relations for beams and columns and conditions have been given, for which frames may be calculated by a simple method.

A great number of calculations have been performed to show the effects of imposed deformations on loaded beams and they are accounted for in diagrams and tables by which the deflection, moment distribution and rotation requisite may be determined.

NOTATIONS

SI-unites are used unless otherwise stated.

A_c	area of concrete
A_s	area of tensile reinforcement
A'_s	area of compressive reinforcement
A_{sf}	area of tensile reinforcement in span
A_{ss}	area of tensile reinforcement at support
C	diffusivity m^2/days
C_1	diffusivity at high pore humidity
E_a	modulus of elasticity of aggregate
E_c	modulus of elasticity of concrete
E_m	modulus of elasticity of cement paste
E_s	modulus of elasticity of reinforcement
E_o	secant modulus of elasticity of concrete at maximum stress
$(EI)_r$	flexural rigidity at cracked state for an additional moment loading
$(EI)_{rc}$	flexural rigidity at cracked state for an additional moment loading at creep
$(EI)_{rcs}$	flexural rigidity at cracked state for an additional moment loading at creep and shrinkage
$(EI)_{rcsN}$	flexural rigidity at cracked state for an additional moment loading at creep, shrinkage and normal force
$(EI)_o$	flexural rigidity at uncracked state
$(EI)_{oc}$	flexural rigidity at uncracked state and creep
$(EI)_{ocs}$	flexural rigidity at uncracked state and creep and shrinkage
$(EI)_{ocsN}$	flexural rigidity at uncracked state and creep, shrinkage and normal force
F	concentrated lateral load
GA	shear rigidity
H	relative humidity, pore humidity
H_{en}	ambient relative humidity
K	slip modulus

M	moment
M_f	maximum moment in span
M_p	plastic moment
M_{pf}	plastic moment in span
M_{ps}	plastic moment at support
M_r	cracking moment, the moment for which the flexural rigidity passes from uncracked to cracked state
M_{rcs}	cracking moment at creep and shrinkage
M_{rcsN}	cracking moment at creep, shrinkage and normal force
M_s	moment at support
M_y	yield moment
N	normal force
T	temperature ^oC
V	shear force
W_o	original water content in concrete ℓ/m^3
a	deflection, support displacement, slip
a_c	deflection at creep
a_{cs}	deflection at creep and shrinkage
a_o	deflection at short-term load
b	width
c	distance from the centroid of the tensile and compressive reinforcement to the edge in tension and compression respectively
d	effective depth
f	function
f_{cbm}	mean flexural strength of concrete
f_{ccm}	mean compressive strength of concrete
f_{ctm}	mean tensile strength of concrete
f_{st}	tensile strength of reinforcement
h	total depth
k	constant
ℓ	length of member, span length, distance between cracks

ℓ_{max}	maximum shortest cracking distance
q	distributed load
$1/r$	curvature
$1/r_o$	curvature at zero moment
s	safety factor
t	time, days
t_o	age at loading, days
x, y	depth of neutral axis
z	lever arm
α	E_c/E_s, coefficient
α_c	material coefficient governing creep
α_{ct}	coefficient governing the influence of age at loading on creep
α_o	ratio between the diffusivities at low and high pore humidity
β	shear strain, coefficient
β_c	coefficient governing the time function of creep
γ	ratio between the final shrinkage in upper and lower edge
Δ	increment
ε	strain
ε_c	concrete strain, stress-related strain of concrete
ε_{cc}	creep (total or basic) of concrete
ε'_{cc}	specific creep of concrete
ε_{ccs}	drying creep of concrete
ε_{ci}	instantaneous strain of concrete
ε_{cs}	shrinkage strain
ε_{css}	final shrinkage strain
ε_ℓ	strain in a local coordinate system
ε'_{mc}	specific creep of cement paste
$\varepsilon_{p\ell}$	plastic strain
ε_r	tensile strain at which concrete cracks
ε_s	reinforcement strain
ε_{sa}	average strain of reinforcement

ε_o	strain at maximum tensile stress
ε'_o	strain at maximum compressive stress
ζ	coefficient
η	coefficient
θ	rotation, rotation requisite, slope
λ	coefficient
ξ	coefficient
ξ_s	coefficient
ρ	$A_s/(b \cdot h)$
ρ'	$A'_s/(b \cdot h)$
σ	stress
σ_a	stress in aggregate
σ_c	stress in concrete
σ_{cc}	compressive stress in concrete
σ_{ct}	tensile stress in concrete
σ_{cta}	average tensile stress in concrete
σ_m	stress in cement paste
σ_r	fictitious tensile strength at shrinkage
σ_s	stress in tensile reinforcement
σ'_s	stress in compressive reinforcement
ϕ	creep coefficient
ψ	$(1+\phi) \cdot \alpha \cdot A_s/(b \cdot h)$
ψ'	$(1+\phi) \cdot \alpha \cdot A'_s/(b \cdot h)$

Other notations are explained where they are used.

1 INTRODUCTION

In the present Swedish design methods schematic rules are followed for the consideration of the effects of imposed deformations. The effects of imposed deformation is the name for those redistributions of forces which take place in statically indeterminate structures as a consequence of imposed deformations combined with additional deformations, which must be such that the total deformation should be compatible with the external connections of the structure. As examples of imposed deformations shrinkage, temperature changes, support displacements and deformations in connection with imperfect fit of members may be mentioned. It may be an advantage to include in the imposed deformations all those deformations which do not correspond to the elastic effects of the applied forces and in this work also cracking and creep are regarded as imposed deformations, which is normally not the case.

The importance of the effects of imposed deformations is totally different for the serviceability limit state and the ultimate limit state. In serviceability limit state defections and crack widths are controlled with regard to integrity of secondary structures, impenetrability, the risk of corrosion as well as aesthetic demands. The analysis is normally carried out according to the elastic theory, in which the forces due to imposed deformations should be included. At ultimate limit state the safety against failure is controlled to be satisfactory. This is performed through a stability analysis, in which the imposed deformations should be regarded, and a control that the cross-sections can carry the section forces. These are generally determined by calculations according to the plastic theory without consideration to the effects of imposed deformations. Then, for the collapse mechanism assumed, a control must be done, that the rotation requisite at each plastic hinge does not exceed the rotation capacity. In order to determine the required rotations at the plastic hinges the rotations between the hinges must be calculated. Elastic behaviour is assumed in the regions between the plastic hinges. This implies that the imposed deformations should be included in the calculation of the rotations between the plastic hinges. The rotation capacity is influenced by creep and shrinkage. The present code does not take into consideration

the difference between the two states, but forms a compromise, which often seems to underestimate the importance of the effects of imposed deformations at serviceability limit state, and overestimate their importance at ultimate limit state.

As an example of a schematic and, from the previous section, diverging treatment of the influence of the effects of imposed deformations, it may here be mentioned that, at the design of bridges, a standardized support displacement should be used, that the influence of cracking on the variation of flexural rigidity of a structure is usually neglected, that, at calculation of the influence of support displacements, the structure should be assumed to be uncracked, and that, at ultimate limit state calculations, generally only an elastic analysis is done, where the effects of the imposed deformations are included in the same way as other loads. According to the suggestion for a new Swedish concrete code, the more differentiated design method described above will be used. This involves an increased amount of calculation, and a practice for a simplification of the calculation work has not yet been developed.

This investigation aims at presenting diagrams or formulae or calculation methods which can serve as a guidance for the designers, when they are to treat the influence of the effects of imposed deformations on loaded concrete structures at serviceability limit state as well as at ultimate limit state.

In order to make this guidance rest on a solid basis and to be as generally valid as possible, it has here been chosen to build up refined calculation models, departing from the force-deformation relation of the reinforcement and the concrete, and which, at the present state of knowledge, describe the behaviour of reinforced concrete as well as possible. With the aid of these refined calculation models, simplified calculation models have been built up, the reliability of which has been controlled against the more accurate calculation models. These simplified models have then been used on more complicated structures, and have resulted in diagrams, formulae or methods for the calculation of the influence of the effects of imposed deformations.

2 CALCULATION MODELS

The calculation work has been pursued according to three calculation methods with different degrees of division and accuracy. In method A (Fig. 2.1) one starts from elements of concrete and reinforcement for which a refined calcualtion model is valid, and then these are put together into segments which later are joined into beams and columns and finally into frames. In method B (Fig. 2.2) one starts from simplified force-deformation relations for the segments, and in method C (Fig. 2.3) from load-deformation relations for beams and columns which are based on the simplified force-deformation relations of the segments. References to these methods will be made in connection with the statement of calculation results in the following chapters. Below is a closer description of the models.

Calculation model A

The concrete and reinforcement elements of method A can only carry axial forces. The reinforcement is assumed to be ideally elasto-plastic. The force-deformation relations of concrete are built upon the condition that the total strain of concrete is identical with the sum of the stress related strain, the shrinkage, the basic creep, and the drying creep. Calculation models have been established for these different strains. The models take stress variations into consideration since great such variations normally appear during a drying process. At the establishment of the models great regard has been taken to the fact that, when they are entered into the integrated calculation model, then this should describe the behaviour of concrete as well as possible. The material dependent parameters of the models are determined by the consistency of the concrete at the time of concreting and the strength. In order to be able to determine the shrinkage and the drying creep of the concrete elements as a function of time, a calculation model has been established, by which the drying process of the segment may be calculated at a one- and two-dimensional drying process through an element division of the cross-section and a forward difference calculation in time. In the model the diffusivity is nonlinearly dependent on the relative humidity of the concrete.

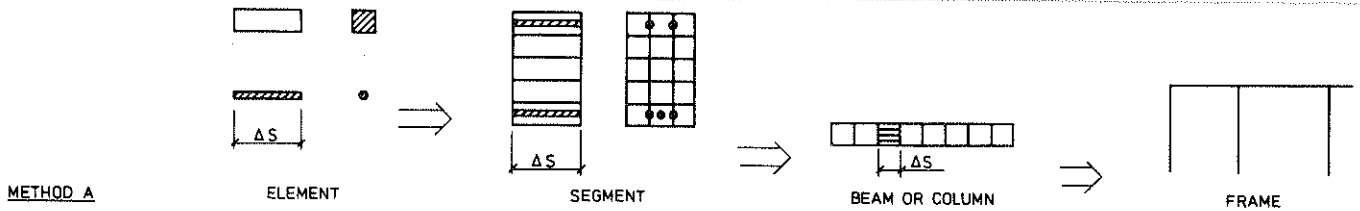

Figure 2.1 Calculation method A based on models of the behaviour of the reinforcement and concrete elements.

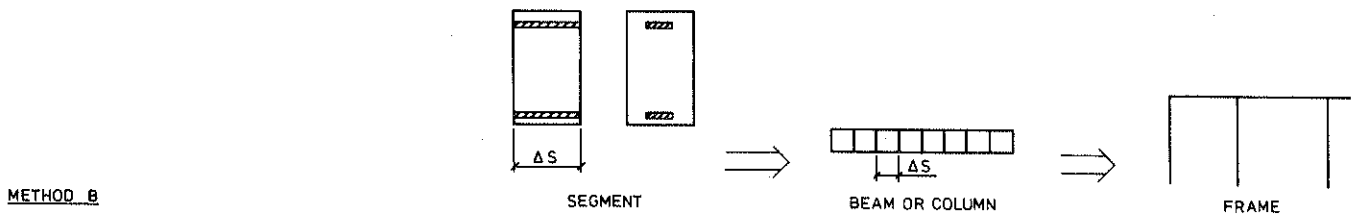

Figure 2.2 Calculation method B based on simplified force-deformation relations of the segments.

Figure 2.3 Calculation method C based on the load-deformation relations for beams and columns.

The material properties of concrete and the models for its behaviour are described in chapter 3.

At a calculation where the segments are divided into elements the depth of each concrete element has been put equal to a tenth of the depth of the segment, and the width of the concrete element has been put equal to the width of the segment at a one-dimensional drying process and equal to a tenth of the width at a two-dimensional drying process. The reinforcement element has been placed in the centres of gravity of the tensile and compressive reinforcements with the same areas as these. Regard has not been taken to the variation of the stresses over the elements, but the stresses have been assumed to be equal to those in the centres of gravity of the elements. For the segments it is assumed that plane cross-sections remain plane.

In the calculations several iteration processes have been used. For segments divided into elements two processes are required to fulfil the conditions of equilibrium. If creep occurs an additional one must be used in order to make the creep proportional to the average stress of the elements within the time step, and for statically indeterminate structures, one more iteration process must be used to make the deformations of the segments fulfil the bond conditions.

Both the force and the deformation methods have been used in the calculations, the deformation method in order to determine the forces of the elements, and the force method in order to determine the rigidity of the segments, whereupon the section forces of the structure have been determined by the deformation method.

With this method (method A) the forces and deformations of a structure may be followed as a function of time at drying and varying loading. Furthermore, the reliability of the simplified force-deformation relations of method B as well as the accuracy of the calculation of a whole structure can be controlled with the use of the relations of method A.

Calculation method B

Generally, there is no interest in how forces and deformations develop as a function of time, but merely of the initial and final states. For these cases simplified calculation models have been worked out by which it is possible to determine the force-deformation relations of the segments. Such models are established for loading with normal forces, moments, moments and normal forces, and shear forces. Under creep and shrinkage it is assumed in the models that the loading of the segments is constant during the time lapse, whereas a model has been worked out for short-time loading, where the load may vary. The simplified force-deformation relations are treated in chapter 5.

The relations are derived with the assumption that the cross-sections of the segments remain plane. The rigidities of the segments are calculated by the force-method, and the section forces of the structure are calculated by the deformation method. For statically indeterminate structures an iterative process must be used to fulfil the boundary conditions.

The calculation method can be used for the final state at constant loading or at short-time loading when the load varies, for example to find out the influence of a support settlement during a loading process.(section 6.3).

Calculation method C

Method C can only be used for a calculation of the initial and final states. The load-deformation relations have been determined for simply supported beams loaded with lateral loads, end moments and normal forces. At the derivation of the relations (aid formulae in Appendix A4) the beam has been divided into uncracked and cracked sections after the moment distribution that occurs when all loads work simultaneously. At the determination of the deformations a simplified bilinear moment-curvature relation , which takes into consideration creep, shrinkage and normal force, has been used.

With the aid of these load-deformation relations a systematized frame calculation model has been worked out, by which loaded

concrete frames, subjected to support displacements, may be calculated. The model can be used at short-time loading, creep and non-uniform shrinkage with the consideration of partial cracking. The calculation is carried out according to the deformation method. The stiffness matrices for the beams and columns of the frame are calculated by the inversion of their flexibility matrices, which are determined from the load-deformation relations. An iteration must be performed to make the division of cracked and uncracked sections correspond to the distribution of forces. The frame calculation model is used in chapter 8, and the load-deformation relations of the beams are used in chapters 6 and 9.

3 THE MATERIAL PROPERTIES OF CONCRETE

A great many investigations describing the mechanical properties of concrete are reported in literature, but the coverage of important parts is still incomplete. The results of the investigations and their interpretations are often contradictory, the quality varies and the conditions are badly described in many cases. It is often difficult to discern the influence of individual parameters since the test results are accounted for as a function of the influence of several parameters at the same time. This depends on the complex behaviour of concrete, which involves difficulties in performing tests where the influence of individual parameters can be isolated.

Influences are generally described by parameters unknown to the designer. The investigations are seldom planned in such a way, that the results could be used as a basis for a description of the total behaviour of concrete under different influences, enabling a designer to make his estimate on the basis of his knowledge on the concrete structure in question.

An integrated description of the behaviour of concrete, based on an understanding of the processes in the microstructure of the cement paste, has been put forward by Bazant /69BA/. In order to use his theories, however, a vast experimental background is required to correlate the large number of parameters. This makes them very laborious to use in practical applications and it is doubtful whether such a correlation of parameters means anything else than a description on a phenomenological bases. In this work, an integrated phenomenological model, starting from submodels of the behaviour of concrete, has been developed, the description ultimately being based on parameters given for the structure. Great consideration has been taken to the fact that when the different submodels are put into an integrated calculation model, then this model will describe the known behaviour of the concrete as well as possible. Effort has been made not to complicate the models unnecessarily but to decrease the number of parameters controlling them, so that only parameters, the values of which can be stated with sufficient accuracy, have been used.

Submodels for, among other things, the stress-strain relation, the shrinkage, the basic creep and the drying creep of concrete have been constructed. Since the concrete in a structure during a drying process normally is subjected to big variations of stresses, the sign of which also may change, this has been considered in the models.

The description of the material properties has sometimes been made relatively comprehensive and the chapter contains passages of a more general character in order to facilitate the understanding of and to give a more integrated description of the total behaviour of concrete. At the same time this general information partly forms the basis of the motivation for the assumptions made.

The reliability of the simplified calculation models described later (chapters 5, 6) is controlled against the results from calculations made with the models in this chapter.

3.1 Stress-strain relation of concrete

The shape of the stress-strain curve for compressed concrete has little influence on the behaviour at serviceability limit state for a structure subjected to pure bending since the deviation from a linearity is then insignificant. At service condition, however, the structure is normally partly cracked. The deformation of the structure increases considerably upon cracking. Therefore it is important to know the stress-strain relation for concrete in tension in order to be able to judge whether the structure will crack, especially since both the cracking moment and the deformation at cracking are affected by the non-uniform shrinkage at drying.

In the ultimate limit state the stress-strain relation in compression has a greater influence, since it affects the rotation capacity and the ultimate moment expecially in strongly reinforced cross-sections. The stress-strain relation for concrete in tension affects the flexural rigidity and hence has importance for the determination of the rotation requisite and the buckling load as well as for calculations according to second order theory.

3.1.1 Stress-strain relation for concrete in compression

The stress-strain relation in Fig. 3.1 is on the whole linear up to a third of the maximum stress. The divergence from linearity depends on the fact that internal microcracks, some of which have existed from the beginning, develop in the bonds between the mortar and the coarse aggregate. At 70 to 90 % of the ultimate stress mortar cracks begin to increase noticeably, and at the same time new bond cracks form and develop continuous crack patterns, and the nonlinearity is further emphasized. The descending part of the curve is characterized by an increased breakdown of the bonds between aggregate and mortar, and by crack formation in the mortar and an interlinking of the cracks /72LIU, 63HSU/. The long term compressive strength of concrete is about 75 % of the short term strength /59RÜ/, i.e. the same as the stress at which cracks develop in the mortar. The maximum compressive strain at failure is about 6 to 8 times larger than the one at maximum stress /70SW/. The rise and fall of the curve are steeper at higher strength of concrete. In pure bending the peak point of the curve occurs at both higher stress (about 20 %) and higher strain (about 50 %) than it does at concentric compression /65ST/. A review of different formulae describing the stress-strain relations of concrete can be found in /70PO/.

An equation which describes the stress of concrete as a function of the strain should fulfil five conditions.

1. The curve passes through the origin, i.e. $\sigma_{cc} = 0$ when $\varepsilon_c = 0$
2. The slope of the curve in the origin equals the modulus of elasticity of the concrete, i.e. $d\sigma_{cc}/d\varepsilon_c = E_c$ when $\varepsilon_c = 0$
3. The curve passes through the peak point, i.e. $\sigma_{cc} = f_{ccm}$ when $\varepsilon_c = \varepsilon_o'$
4. The curve has a maximum, i.e. $d\sigma_{cc}/d\varepsilon_c = 0$ for $\varepsilon_c = \varepsilon_o'$
5. The curve passes through a certain point on its descending branch, i.e. $\sigma_{cc} = \sigma_1$ when $\varepsilon_c = \varepsilon_1$

The following equation suggested by Sargin /69SA/, which has proved to correspond well with experiments satisfies these conditions.

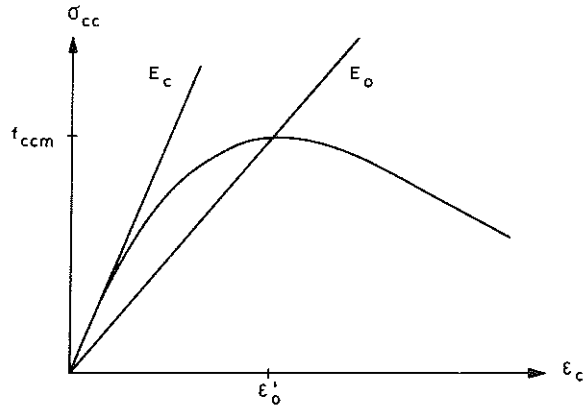

Figure 3.1 Principle diagram for the stress-strain relation for concrete in compression at constant strain rate.

$$\sigma_{cc} = f_{ccm} \cdot \frac{\alpha_1\alpha_3 + (\alpha_2 - 1)\cdot\alpha_3^2}{1 + (\alpha_1 - 2)\cdot\alpha_3 + \alpha_2\alpha_3^2}$$

where $\alpha_3 = \varepsilon_c/\varepsilon_0'$, $\alpha_1 = E_c\cdot\varepsilon_0'/f_{ccm} = E_c/E_0$ and α_2 is a parameter which mainly determines the slope of the curve after the peak point. The equation is relatively simple and has the advantage that the parameters are determined by factors which are known to the designer.

The modulus of elasticity of concrete exhibits a relatively large variation. It may therefore occur that the real modulus of elasticity diverges from the assumed one by 20-25 %. The variation of the modulus of elasticity with the strength of concrete at low stresses can be described by the equation

$$E_c = 5200\cdot\sqrt{f_{ccm}} \quad MN/m^2$$

In American codes the constant has been given the value 4740 whereas in Swedish codes it has been assigned a somewhat higher value (about 5400).

The magnitude of ε_0' is dependent on the shear reinforcement, the rate of loading and the strain gradient. Most researchers consider is also dependent on the strength of concrete. Sargin /69SA/ regards it independent of the strength of concrete. Here ε_0' has been given the value 0,0021 /69SA/ at concentric compression and the influence of the other factors mentioned above is disregarded. For bending ε_0' has been given the value 0.003.

Saeng /64SAE/ has stated that the value of E_c/E_0, i.e. α_1 varies from 1,3 to 4 when the strength of concrete varies from 70 to 7 MN/m^2. This will also be the case with the values assumed above of E_c and ε_0.

Here we will mainly treat structures at serviceability limit state which means that the slope of the descending curve will not have any greater significance. The parameter α_2 has therefore been given the value 1 instead of about 0,65 /69SA/. When the parameter α_2 has the value 1, the formula is somewhat simplified and is transformed into a formula originally proposed by Saeng /64SAE/.

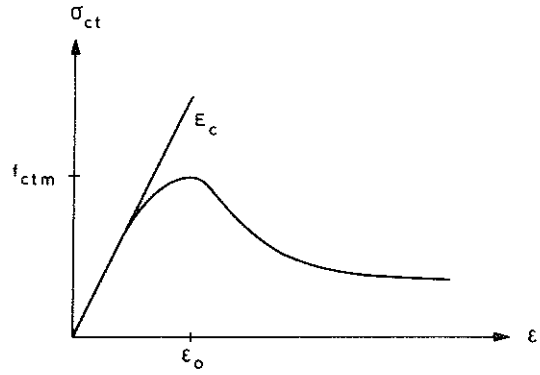

Figure 3.2 Principle diagram for the stress-strain relation for concrete in tension at constant strain rate.

3.1.2 Stress-strain relation for concrete in tension

The stress-strain relation in Fig. 3.2 is on the whole linear up to about 60 % of maximum stress after which the microcracks, that have existed from the start in the bonds between mortar and coarse aggregate, develop more strongly. At about 75 % of maximum stress also mortar cracks develop. The bond cracks and the mortar cracks propagate and interlink at the same time as new bond cracks develop, and the deviation from linearity between stress and strain is strongly emphasized /66WE/. In the post-peak state, the strain increases locally while it decreases in the surrounding areas /66WE, 69HE/ at the same time as the load decreases. The top of the curve and particularly the descending part of the curve is substantially dependent on the testing equipment, the dimensions of the test specimen and the measuring length /74HI/. The descending branch of the curve corresponds to the average strain within the measuring length where there is an increase of strain in certain sections, and simultaneously there is a decrease of strain in other sections. At the same time as the force is reduced strain reversal takes place in the test specimen outside the measuring length, in the fastening devices and in the testing machine itself. When the strain increases in the prospective failure zone without any additional movement in the testing machine the test specimen fails. The testing machine affects the result since its elastic deformation at unloading is different for different machines. The length of the test specimen has an influence by the fact that the reversing deformation gets larger when the test specimen is longer. A test specimen with a larger cross-section area causes larger changes of deformation at the unloading of the machine and the fastening devices than a test specimen with a smaller one. The factors enumerated above mainly influence the occurrence of the failure whereas the measuring length influences the shape of the curve. The measured average strains will be dependent on the size of that part of the measurement area within which the decrease of strain happens.

At normal testing failure occurs as early as at the top of the curve. By modifying the testing equipment we can also get the

descending part of the curve as reported by for instance /66HU, 66HUG, 68HU, 75MA, 68EV/. When measuring the strains on short lenghts with and without strain gradient, strains in the order of 2000 microstrains have been recorded /65ST, 66HU, 70IM, 68EV/. At a lower rate of loading larger strains are obtained /69KO/. The strain gradient has a great influence on both the maximum strain and the strain at maximum stress, and may increase these considerably.

The tensile strength of the concrete depends among other things on the strength of the cement paste and on the strength of the bonds between mortar and coarse aggreagte. The bond strength and hence the tensile strength decrease with increasing maximum size of aggregate /70JO, 66HU/. According to /69KO/ the influence of the aggregate grading is insignificant if the maximum aggregate size is constant whereas, according to /68HU/, the strength decreases considerably if the ratio between sand and coarse aggregate becomes smaller than a certain value. Johnston /70JO/ considers the stress strain curve to be independent of the composition of the concrete when stress and strain are expressed in per cent of their maximum values. The strain is about 40 % of maximum strain at 50 % of maximum stress. Johnston has performed his tests with a testing machine, where failure occurs at the top of the curve. The maximum tensile strength is attained 28-90 days after concreting and after this it remains constant /70KO/. The maximum strain increases with age /66WE/.

An assumed stress-strain relation for concrete subjected to tensile stresses should meet the following conditions. The stress should be zero when the strain is zero and the slope of the curve at this point should be the same as the modulus of elasticity for concrete in tension. The curve must pass the point (ε_0, f_{ctm}), where it must have a horizontal tangent. The moment capacity of a non-reinforced beam with a rectangular cross-section and of normal size should be about 20-80 % larger than that calculated under the assumption of a rectilinear stress-strain relation and the flexural stress being equal to the maximum tensile strength (f_{ctm}). The increase depends on the strength of the concrete and on the depth of the beam /76PE/. It will be smaller at a high strength /71NE/.

The ultimate moment will be about 25 % lower if the depth of the beam increases from 10 to 50 cm /67MA/. This can be explained theoretically with the aid of fracture mechanics and the assumption that forces remain in the cracks /76PE/. The moment must not decrease before cracking if the moment-curvature relation is drawn for a non-reinforced rectangular beam /71AB/. Neither must the moment decrease at cracking, if the moment-curvature relation is drawn for a rectangular beam which does not collaps when it cracks. By curvature is here meant the average curvature and not the one in the vicinity of the crack. When the tensile reinforcement yields the concrete around this does not carry any forces.

The modulus of elasticity for concrete in tension has been chosen equal to the one for compressed concrete.

The tensile strength of the concrete has been chosen to vary with the compressive strength according to the formula /70CEB/

$$f_{ctm} = 0{,}28 \cdot f_{ccm}^{2/3} \qquad \text{(Mpa)}$$

The American codes state about the same value ($0{,}498 \cdot f_{ccm}^{1/2}$) and the formula agrees well with the original value of tensile strength according to /67MA/, if it is assumed that the flexural strength is about 50 % higher than the tensile strength. The formula is assumed to be valid for totally water-saturated concrete. Most researchers and codes state lower values than the one stated here. This may depend on the fact that a relatively short period of drying will reduce the strength measured. CEB's formula is valid for the 28 days value of the strength. However, here the formula is supposed to be valid independently of the age of concrete, with the restriction that the tensile strength is not supposed to increase after 90 days /70JO/.

When the strains are smaller than the strain at which maximum tensile stress occurs the relation is supposed to have the same shape as the one for compressed concrete, viz.

$$\sigma_{ct} = \min \begin{cases} f_{ctm} \cdot \alpha_1 \cdot \alpha_3 / (1 + (\alpha_1 - 2) \cdot \alpha_3 + \alpha_3^2) \\ E_c \cdot \varepsilon_c \end{cases}$$

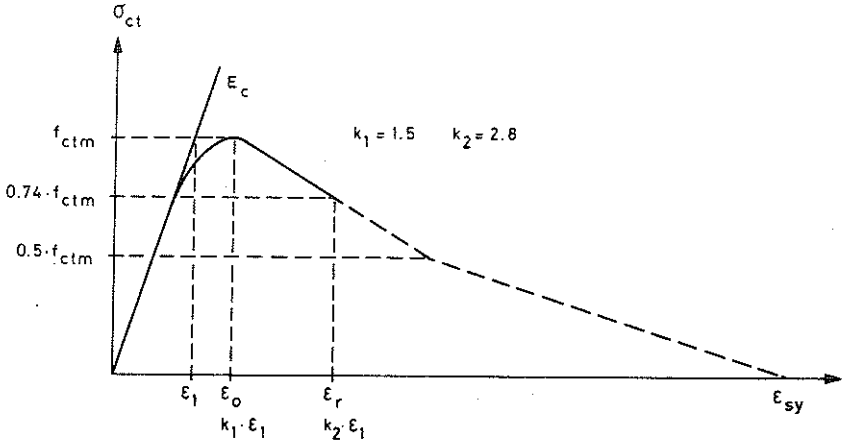

Figure 3.3 Stress-strain relation chosen for reinforced concrete in tension where ε_{sy} denotes the strain at which reinforcement starts yielding.

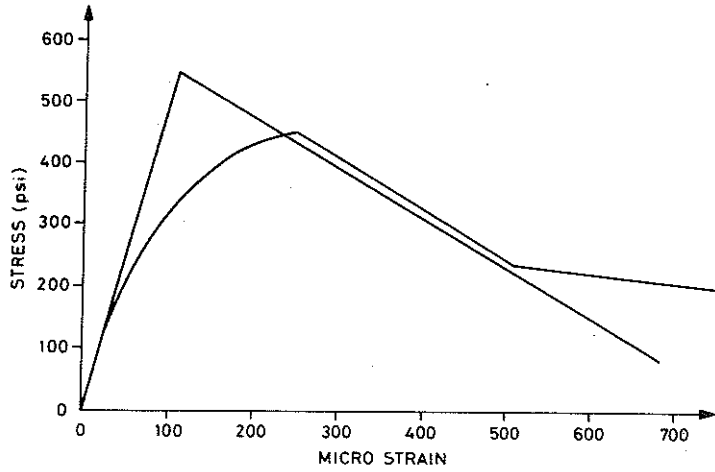

Figure 3.4 Models established by /74KU/ for the stress-strain relation for concrete in tension.

where $\alpha_1 = E_c \cdot \varepsilon_o / f_{ctm}$ and $\alpha_3 = \varepsilon_c / \varepsilon_o$

The values of maximum strains and of the shape of the descending branch of the curve, stated in the above-mentioned literature, are divergent. The values measured are strongly dependent on the testing method and therefore it is difficult to translate the measured strains into average strains. Consequently, testing results are lacking in order to make a more accurate determination of the shape of the descending part of the curve. It has therefore been given the schematic design according to Fig. 3.3. When the peak point of the curve has been passed then the strain consists of an average strain. If the concrete has cracked and is reinforced then the relation between average stress and average strain is supposed to follow the dashed lines. The curve meets the conditions that have been mentioned above and has the effect that the flexural strength becomes about 60 % higher than the tensile strength. In Fig. 3.4 models assumed by another writer /74KU/ for the relation between stress and strain are related .

A theoretical study of the relation between average stress of concrete and the strain for a centrically reinforced prismatic bar according to plastic theory and at a progressive cracking according to the theory of constant slip modulus (appendix A1) indicates that the assumed relation is correct. (The theory of constant slip modulus implies among other things that the shear forces between reinforcement and concrete are proportional to the slip between them.) However, the average stress should possibly be somewhat higher for large strains. This is shown in Figs 3.5 and 3.6 that have been calculated for different ratios between the areas of reinforcement and concrete with the aid of the theory of constant slip modulus. The thick curve in the figures constitutes an average value when the crack distances vary. In the calculations a linear stress-strain relation has been used for the concrete. At the beginning of the cracking, forces probably exist between the concrete on either side of a crack. This causes a greater uncertainty of the shape of the calculated curves shortly after the cracking. When the final crack distances have developed then the figures probably give a relatively correct image of reality.

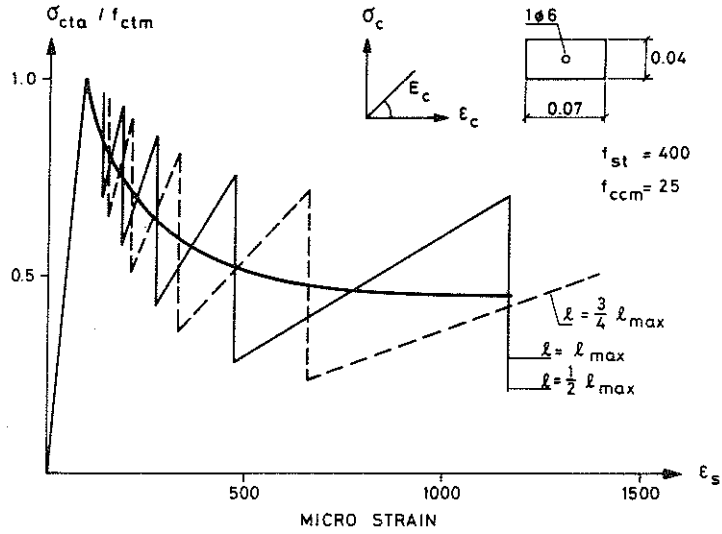

Figure 3.5 Relation between average strain of reinforcement and average stress/strength ratio of concrete for concentrically reinforced prismatic bar under successive cracking at constant rate of deformation.

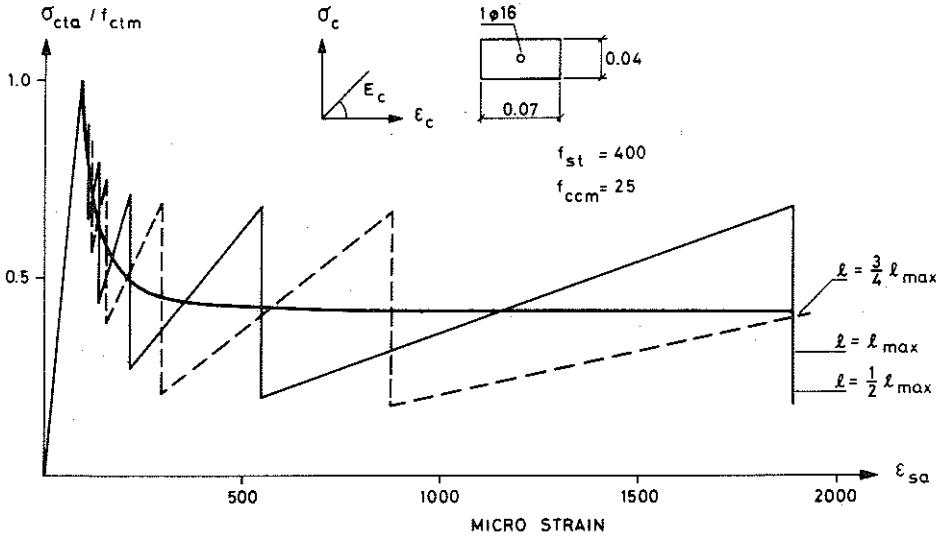

Figure 3.6 Relation between average strain of reinforcement and average stress/strength ratio of concrete for concentrically reinforced prismatic bar under successive cracking at constant rate of deformation.

3.2 Stress-strain relation for concrete at load changes

3.2.1 Concrete exposed to compressive stresses

According to tests made by /70SW, 70KA/ the stress-strain relation will be subjected to loops at unloading, followed by renewed loading, as shown in Fig. 3.7. In order to simplify, and as a satisfyingly good approximation for this work the loop will be represented by a straight line with the same slope as the modulus of elasticity at the origin.

$$\sigma_{cc} = \min \begin{matrix} f_c(\varepsilon_c) \\ E_c \cdot (\varepsilon_c - \varepsilon_{p\ell}) \end{matrix}$$

where f_c denotes the curve of the stress-strain relation for compressed concrete and $\varepsilon_{p\ell}$ the plastic strain.

3.2.2 Concrete exposed to tensile stresses

As far as the author knows there is no work which deals with this subject, neither have any tests of his own been done within the field. Here are therefore chosen relations which have been considered to be reasonable and to have reasonable consequences at their application. If unloading occurs before maximum stress has been reached then the stress-strain relation is assumed to follow a straight line which has the same slope as the modulus of elasticity at the origin. At renewed loading the same line is followed until the original curve is reached and then this curve is followed. If the peak point has been passed, then at unloading a reversal takes place along a line that intersects the abscissa in the same point as if unloading had happened from the peak point. At renewed loading the same line is followed until the original curve is reached and then this is followed. The principle is shown in Fig. 3.8 and is expressed analytically through

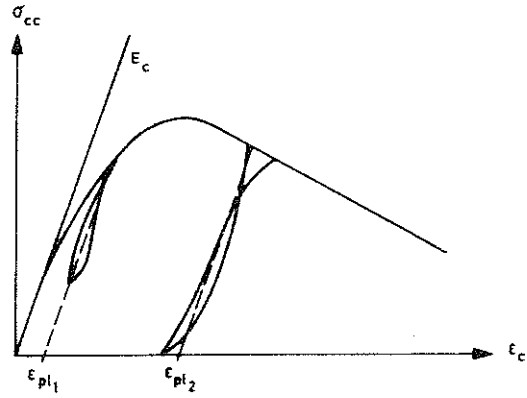

Figure 3.7 Stress-strain relation for concrete in compression at strain changes.

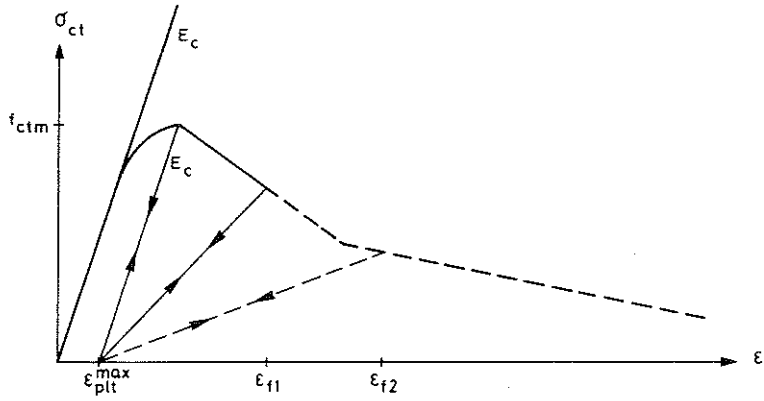

Figure 3.8 Stress-strain relation for concrete in tension at strain changes.

$$\sigma_{ct} = \min \begin{cases} f_t(\varepsilon_c) \\ E_c \cdot (\varepsilon_c - \varepsilon_{p\ell}) \\ \sigma_f(\varepsilon_c - \varepsilon_{p\ell})/(\varepsilon_f - \varepsilon_{p\ell}) \end{cases}$$

where f_t denotes the curve of the stress-strain relation for concrete in tension, $\varepsilon_{p\ell}$ the plastic strain, and ε_f the preceding strain where the peak point has been passed, and σ_f the stress belonging to ε_f.

The last assumption of reversal after the peak point has been passed is doubtful. If the local strain increment is wholly elastic then the assumption is correct, but if it is plastic the assumption is wrong, and at unloading a line that is parallell to the slope of the modulus of elasticity should be followed. In reality the strain increment has probably both an elastic and a plastic component. The error brings about a simplification and has probably no great significance, and it also makes the treatment easier in those cases when unloading is followed by compressive stresses.

3.2.3 Stresses change signs

Knowledge is lacking as to how concrete behaves in this case. An assumption about the behaviour which is estimated to be relatively realistic and which at the same time is relatively simple is presented. This is based on the following principles, where tensile strains and tensile stresses are assumed positive and compressive stresses and strains are assumed negative.

The starting point of the curve which constitutes the stress-strain relation for compressed concrete can only be displaced in a positive direction. The displacement is the same as the maximum plastic tensile strain that has occurred ($\varepsilon_{p\ell t}^{max}$). The maximum displacement is the same as the maximum plastic strain that may develop on the tension side. Similarly, the starting point for the curve for concrete in tension can only be displaced in a negative direction. The displacement is the same as the maximum plastic compressive strain that has occurred ($\varepsilon_{p\ell c}^{max}$). The model covers all conceivable

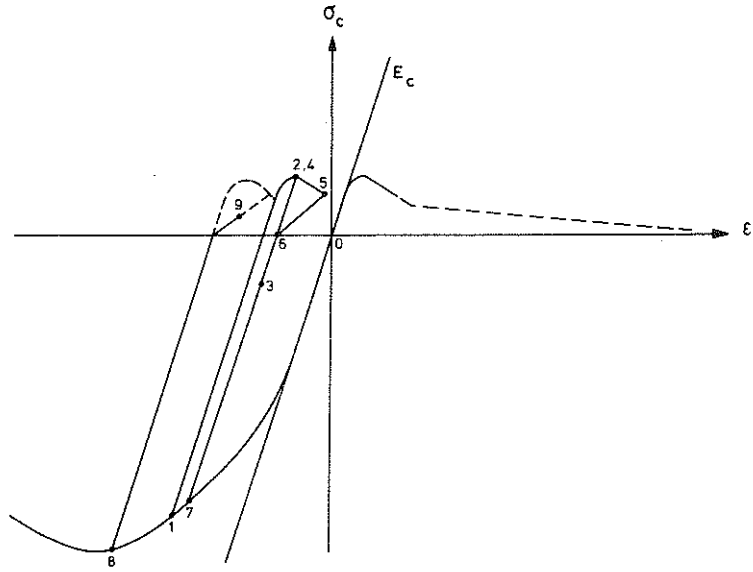

Figure 3.9 Stresses according to the stress-strain relation assumed, when the strains vary according to the order indicated by the numerals.

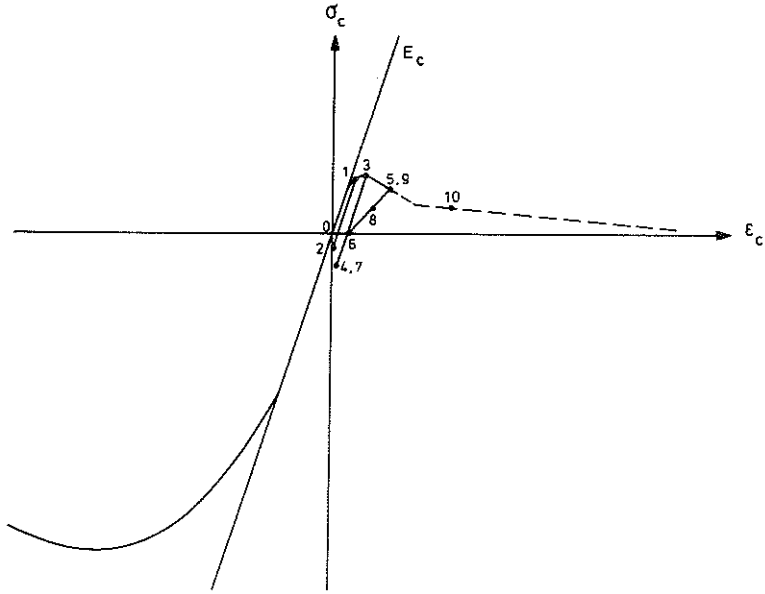

Figure 3.10 Stresses according to the stress-strain relation assumed when the strains vary according to the order indicated by the numerals.

stress variations and is analytically expressed through

$$\varepsilon_c > \varepsilon_{p\ell}: \quad \varepsilon_\ell = \varepsilon_c - \varepsilon_{p\ell c}^{max} \qquad \varepsilon_{\ell p\ell} = \varepsilon_{p\ell} - \varepsilon_{p\ell c}^{max} \qquad \varepsilon_{\ell f} = \varepsilon_f - \varepsilon_{p\ell c}^{max}$$

$$\sigma_{cf} = \min \left\{ f_t(\varepsilon_\ell),\ E_c \cdot (\varepsilon_\ell - \varepsilon_{\ell p\ell}),\ \sigma_f(\varepsilon_\ell - \varepsilon_{\ell p\ell})/(\varepsilon_{\ell f} - \varepsilon_{\ell p\ell}) \right\}$$

$$\varepsilon_c \leq \varepsilon_{p\ell}: \quad \sigma_{cc} = \max \left\{ f_c(\varepsilon_c - \varepsilon_{p\ell t}^{max}),\ E_c \cdot (\varepsilon_c - \varepsilon_{p\ell}) \right\}$$

where $\varepsilon_{p\ell}$ denotes the latest plastic strain and the other terms are explained earlier. The assumption is exemplified by Fig. 3.9 and Fig. 3.10. The numerals of the figures state the order according to which the points are reached at the assumed stress variations. The strong stress variations that are shown particularly in Fig. 3.9 probably seldom happen in reality. If such strong stress variation should occur, then the assumptions are probably not totally satisfactory.

3.3 The growth of compressive strength with time

Ching Fung Kee /71KE/ has proposed a formula for the growth of the compressive strength with time. It is valid for ordinary and rapid hardening Portland cement for periods from 1 day to 1 year. The temperature may vary during the process of maturing. The formula has proved to agree well with the tests that have been accounted for and is therefore used here

$$f_{ccm} = \frac{M}{m \cdot M + D} \tag{3.1}$$

The maturity is determined by $M = \Sigma \Delta t\ (11.7 + T)^{\circ}C$ days where Δt denotes the number of days during which the concrete has hardened at the temperature $T^{\circ}C$. The final strength of concrete is according to the formula $1/m$. If the compressive strength of concrete has been determined with two different degrees of maturity then m and D may be determined from

$$D = \frac{M_1(1 - f_{ccm1}/f_{ccm2})}{f_{ccm1}(1 - M_1/M_2)}$$

$$m = \frac{f_{ccm1}/f_{ccm2} - M_1/M_2)}{f_{ccm1}(1 - M_1/M_2)}$$

where indices 1 and 2 denote terms at the time 1 and 2 respectively. The compressive strength at other times can then be calculated by interpolation or extrapolation. The formula disregards the moisture content which must be an important factor since the hydration rate is depending on this.

For normal concrete, with Portland cement as a binder, /70CEB/ has suggested that the compressive strength in relation to the compressive strength at an age of 28 days varies with the time at normal temperature (15-20^{o}C) according to the following table

Age (days)	3	7	28	90	360
normal	0.40	0.65	1.00	1.20	1.35
fast hardening	0.55	0.75	1.00	1.15	1.20

If the temperature diverges from 20^{o}C then the age is calculated by the formula

$$t = \Sigma\Delta t(10 + T)/30$$

With the values of /70CEB/ for 28 and 7 days as starting point the equation 3.1 above gives a slower growth of strength with time than /70CEB/, a fact which appears at a comparison between the above table and the following one

Age (days)	3	7	28	90	360
normal	0.40	0.65	1.00	1.14	1.20
fast hardening	0.52	0.75	1.00	1.08	1.11

3.4 The drying process of concrete

The equation for transient two-dimensional moisture conduction at varying diffusivity can be written /72BA/

$$\frac{\delta(C\,\frac{\delta H}{\delta x})}{\delta x} + \frac{\delta(C\,\frac{\delta H}{\delta y})}{\delta y} - \frac{\delta H}{\delta t} = 0$$

where H denotes the relative air humidity of the pores of the concrete which from now on will be called pore humidity and C denotes the diffusivity. The equation is analogous to that for heat conduction and is solved by making an element approximation of the differential equation and describing the time variation approximately with a forward difference procedure. The following equation is used to obtain an acceptable approximation of the diffusivity (which is strongly non-linear)

$$C = \frac{1}{H_2 - H_1} \cdot \int_{H_1}^{H_2} D(H) \cdot dH$$

where indices 1 and 2 signify the points between which the diffusivity is calculated. The diffusivity has been chosen to vary with the pore humidity (H) according to Fig. 3.11. The full line in the figure is the variation assumed by Bazant /72BA/, which has shown good agreement with tests, whereas the dashed line, which connects well with the full line, is the one here assumed. The parameter C_1 denotes the diffusivity for H = 1 and $\alpha_0 \cdot C_1$ the diffusivity for H = 0. At the calculations made by Bazant in order to get a good agreement with the tests reported by him the value of C_1 has been varying between $14 \cdot 10^{-6}$ and $40 \cdot 10^{-6}$ m^2/day with one occasional value of $193 \cdot 10^{-6}$ m^2/day. For concrete with an unknown value of C_1 Bazant states that as a rough approximation $C_1 = 25 \cdot 10^{-6}$ m^2/day may be chosen. This is the average value of his comparisons between calculations and tests. The parameter α_0 has been varying between 0.024 and 0.1, and when its magnitude is unknown it has been put equal to 0.05. The great difference of the diffusivity for high and low pore humidity depends on capillary transport at high pore humidity. The difference causes great gradients in the pore humidity during a drying process.

At present there is no reliable correlation between the diffusivities and the composition of the concrete. However, generally it can be stated that C_1 increases with the water-cement ratio of the concrete /72BA, 76NI/, and that the opposite is valid for α_0 /76NI/.

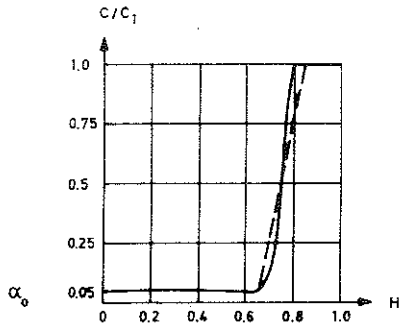

Figure 3.11 Diffussivity as a function of pore humidity, where the full line is the one stated by /72BA/ and the dashed line is the one here assumed.

The coefficient of moisture transfer quoted by /73SA/ is so big in relation to the diffusivity of concrete that, with good accuracy, the surface layer of concrete may be considered to have the same relative humidity as the surrounding air.

It is doubtful whether Bazant's moisture transfer model describes the drying process in a phenomenologically correct way. The model should, however, give results that are realistic at the right choice of C_1 and α_0.

The calculation method used here has been established and programmed by Ulf Wickström and Sven Strandberg at the Division of Structural Mechanics and Concrete Construction, Lund Institute of Technology, Lund, Sweden.

3.5 Shrinkage of concrete

Two phenomena cause shrinkage, viz. drying and carbonization. The carbonization means that the carbon dioxide of the air reacts with certain constituents of the cement. The carbonization does not occur when the concrete is almost dry. The most advantageous condition for carbonization appears when the pore humidity is about 50 % /72KE/. For very porous concrete the carbonization shrinkage may then come close to half of the total shrinkage. For ordinary concrete the carbonization, however, penetrates only a few centimeters into the surface layer.

The drying shrinkage is the greatest part of the shrinkage of concrete and in this work shrinkage will be treated as if it consisted only of drying shrinkage. This is caused by the fact that the calcium silicate gel contracts when the moisture content decreases. Shrinkage starts at the transition from the capillary area to the hygroscopic one which occurs at about 98 % pore humidity. The magnitude of the drying shrinkage for ordinary concrete qualities varies between 400 and 800 microstrain for drying to about 40 % pore humidity.

3.5.1 Effect of the material properties on shrinkage

The drying shrinkage of the cement paste is 5-15 times larger than that of concrete /72KE/. The aggregate counteracts the shrinkage. The more thickly packed the aggregate is and the higher its modulus of elasticity the less will be the shrinkage. Outside Sweden are sometimes used aggregates that are affected by moisture and they may cause a considerable increase in shrinkage. Also some Swedish aggregate materials such as sandstone and slate are affected by moisture.

The water content of the concrete mixture has a great influence on the magnitude of the shrinkage. This depends, among other things, on the fact that when the water leaves the concrete there remains a pore which does not counteract the development of the shrinkage in the same way as the aggregate material would have done. The shrinkage for concrete which contains 270 kg water per cubic meter is more than twice as big as for concrete containing 150 kg/m^3.

An increase of the air content does not involve a great increase of shrinkage since a decrease of the water content may be done in order to obtain the same consistency.

An increase of the cement content and its fineness is by many considered to cause a greater shrinkage. The composition of the cement affects the shrinkage. An addition of calcium chloride may cause an increase of shrinkage by up to 50 % /72KE/.

3.5.2 Effect of the environment on shrinkage

Both the time function and the magnitude of shrinkage are ruled by the relative humidity of the environment. The final shrinkage is reached at the same time as the moisture content of the concrete is in equilibrium with that of the environment. In Fig. 3.12 the final shrinkage is shown as a function of the relative humidity of the environment in relation to the final shrinkage at

50 % relative humidity according to /70BE, 70CEB, 70ACI/. The difference between the curves is relatively small. In this paper the CEB suggestion is followed. The shrinkage is not totally reversible which means that the concrete does not swell in the same degree when the pore humidity increases as the first shrinkage at the corresponding decrease.

For indoor structures it may be assumed that the average value of the relative humidity during one year is about 40 %, the value being somewhat lower during heating season and higher during summer. For outdoor structures or structures in spaces not being heated the average value per year may be assumed to be about 80 %.

3.5.3 Magnitude of the final shrinkage

This chapter is based on an investigation performed by Hillerborg /74HI/ concerning the magnitude of the final shrinkage. This investigation will be the basis for the treatment of shrinkage in future Swedish codes.

Hillerborg starts from a simple model according to Fig. 3.13, where the aggregate counteracts the contraction of the cement paste. With the aid of equilibrium and compatibility equations the final shrinkage of concrete may be expressed as a function of the final shrinkage and modulus of elasticity of the cement paste and the amount and modulus of elasticity of the aggregate. The final shrinkage and modulus of elasticity of the cement paste are determined by the water-cement ratio, and the aggregate volume is determined by the water content and water-cement ratio. This means that the final shrinkage becomes a function of the water content and the water-cement ratio. The cement content has a minor importance compared to the water content and a simplification may therefore be done by expressing the final shrinkage in water content only. Hillerborg has suggested, within the appropriate variation limits of concrete mixtures, that the final shrinkage at 50 % relative humidity is

$$\varepsilon_{css} = 3.75 \quad (W_o - 50) \qquad \text{microstrain}$$

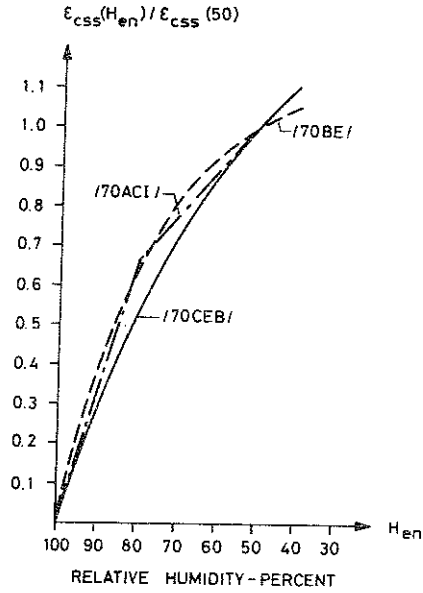

Figure 3.12 Final shrinkage as a function of the relative humidity of the environment according to different sources, where the final shrinkage at 50 % relative humidity is chosen equal to 1.

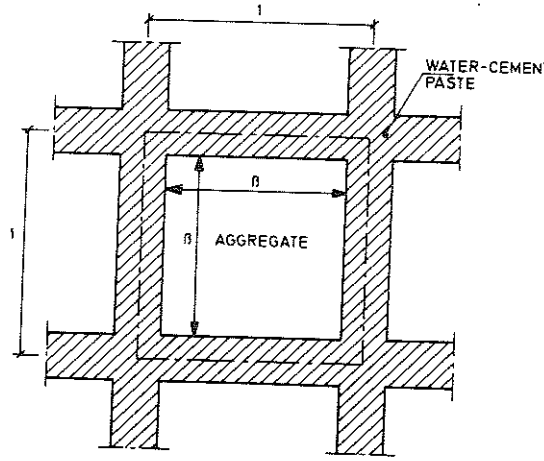

Figure 3.13 Model for calculation of the influence of aggregate on shrinkage.

where W_o denotes the original water content in ℓ/m^3.

Hansen and Mattoch /66HA/ have performed tests which indicate that the final shrinkage is dimension dependent, whereas tests by Mamillan /68MA, 69MA/ contradict this. CEB /73CEB/ has suggested a dimension dependence which is somewhere inbetween. In this work any possible dimension dependence of the final shrinkage is disregarded.

The designer does not usually know the water content of concrete, whereas, however, the consistency is known since it is stated on the drawings. Consequently, Hillerborg has transformed the parameter water content into consistency and maximum aggregate size for normally graded aggregate. As a function of these two parameters the final shrinkage may be determined from Fig. 3.14 at 50 % relative humidity. At a different relative humidity Fig. 3.12 should be taken into consideration.

3.5.4 Time function of shrinkage

Shrinkage, measured in tests consists of the overall deformations of the test specimen, which is an integrated effect of pure shrinkage, creep and stress at every particular point.

In order to determine the pure shrinkage at a certain time in one point of the structure the following method is used. The final shrinkage is determined by the relative humidity of the surrounding air. The pore humidity of the point, at the moment concerned, is calculated. The shrinkage is then determined as the final shrinkage multiplied by the present decrease and divided by the final decrease of pore humidity. The method is based on the assumption of linearity between shrinkage and decrease of pore humidity, and implies that the shrinkage will be governed by the same time function as the drying expressed as change in pore humidity.

The relation between final shrinkage and relative air humidity (Fig. 3.12) is not linear but the deviation is moderate. The drying to equilibrium moisture condition theoretically takes an infinite

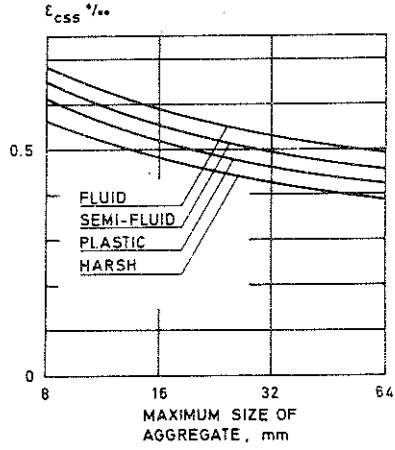

Figure 3.14 Relation between final shrinkage, consistency and the maximum size of aggregate at 50 % relative humidity.

time. A certain amount of time is probably needed for shrinkage to develop in one point. A certain pore humidity is reached faster if drying is to happen at a lower equilibrium state. This may imply that the deviation from a rectilinear relation between shrinkage and decrease becomes even smaller than what may be expected when regarding Fig. 3.12.

3.6 Creep of concrete

Creep is a function of several different parameters such as the composition of concrete, the properties and amount of materials included, the temperature and pore humidity of concrete before as well as during the loading process, the maturity of concrete at loading, and the state and magnitude of loading. Humidity and temperature changes have a great influence on the magnitude of creep. Creep has not yet been completely surveyed. Lots of tests have been performed within this field. However, many times the tests are not particularly well-defined as concerns all parameters, and sometimes the results are contradictory.

With the present knowledge it should be possible to split up creep into basic creep, occurring at equilibrium state of humidity and temperature, sorption creep, occurring at changes of humidity, and creep that occurs at temperature changes.

Basic creep may be divided into an irrecoverable, viscous component and a recoverable, delayed elastic component /68IL/. The recoverable component is assumed to be larger than the irrecoverable one at the beginning of the loading process and soon reaches a limiting value. The irrecoverable component is assumed to grow continuously with a decreasing rate or possibly reach a limiting value asymptotically after a very long time.

Sorption creep occurs both at drying and wetting. The concrete generally contains more moisture shortly after concreting than later when the moisture is in equilibrium with the humidity of the environment, and therefore sorption creep is often called drying creep. Depending on the degree of drying, it is in many cases larger than basic creep and is considered fully developed when the equilibrium state of

moisture is reached. It is assumed to have the same time function as drying and shrinkage.

When temperature increases a special kind of creep occurs. This is relatively large compared to basic creep even at moderate temperature increases and many times larger at big temperature increases. It is considered to have the same time function as the temperature increase of concrete and to be proportional to this. At temperature decreases this creep does not occur. If the temperature varies in cycles it is insignificant except on the first temperature increase. This type of creep will not be treated here, but is described in /66HAN,74TH/. All creep is a function of stress.

3.6.1 Basic creep of concrete

By basic creep is meant the recoverable and irrecoverable creep, which occur when the concrete is in temperature and humidity equilibrium with the environment. For simplifying purposes it has here been chosen not to separate the recoverable and irrecoverable components from each other, but to treat basic creep as a whole. This is partly due to the difficulties in choosing the correct values of the parameters governing the two components of creep. The magnitude of basic creep is dependent on the creep of cement-paste, the quantity and properties of the aggregates, the pore humidity, the temperature and the time under load, and the age at loading, and may be expressed as

$$\varepsilon_{cc} = f_1(\sigma)\cdot f_2(t)\cdot f_3(t_o)\cdot f_4(H)\cdot f_5(T)\cdot f_6(\alpha)\cdot \varepsilon'_{mc} \cdot f_7(\varepsilon_{cc})$$

where

f_1 = function of stress
f_2 = function of time under load
f_3 = function of age at loading
f_4 = function of pore humidity
f_5 = function of temperature
f_6 = function of the composition of concrete
ε'_{mc} = specific creep of the cement paste
f_7 = function of previous creep

3.6.1.1 Influence of stress on basic creep

Most creep tests are performed on concrete in compression. The relation between creep at compression and stress is linear when the ratio between stress and strength is low. When this ratio exceeds 0.3 to 0.6 then creep increases more than stress /70NE/. At a low water-cement ratio the deviation from the rectilinear relation occurs earlier than at a high water-cement ratio /66RU/. The ratio between stress and strength is generally not higher for concrete in compression at serviceability limit state than to make it possible, as a reasonable approximation, to assume a linear relation between creep and stress.

It is more difficult to determine creep in tension since the stresses must be kept relatively low because of the low tensile strength of concrete. Opinions vary as to whether there is any difference between the influence on creep of tensile and compressive stress /70NE/. In serviceability limit state the tensile strength is often exceeded. This implies that the stress-strength ratio is often high. In order to simplify and because of lack of knowledge the same linear relations have been assumed between tensile stress and creep as between compressive stress and creep.

3.6.1.2 Time function of basic creep

It is difficult to find a time function which shows good agreement with the development of creep at any time. Different creep tests give different time functions and it is also difficult to be totally assured that the tests accounted for are free from drying creep. The tensile and the compressive creep are considered to have the same time function. It has here been chosen to let creep vary with time according to

$$\varepsilon_{cc} = \sigma \cdot \alpha_c \cdot t^{\beta_c}$$

Ruetz /66RU/ relates tests where a 6 day creep constitutes 31 % of the 2 year creep if the age of loading is 28 days. (At a lower age of loading the 6 day creep constitutes a higher percentage). This

gives β_c the value 0.244. The term β_c has been chosen equal to 0.24. Possibly this value is somewhat high when the time under load surpasses 2 years.

Neville /70Ne/ has stated creep values that correspond to considerably lower values of the term β_c particularly upon longer times under load. At these tests there is probably a drying creep simultaneously. The value 0.24 of the constant implies that the creep is doubled when time under load is multiplied 18 times.

3.6.1.3 Influence of age at loading on basic creep

The dependence of creep upon age at loading is assumed to vary according to

$$f_3(t_o) = \alpha_{ct} \cdot t_o^{-\beta ct}$$

where t_o denotes the age of loading in days and the term α_{ct} is determined so that f_3 will be equal to 1 when t_o = 28 days. According to /70NE/, where /59HE/ is accounted for, the terms α_{ct} and β_{ct} may be estimated to 1.95 and 0.2 respectively. These values are valid for test specimens that have been stored in about 75 % relative humidity of air and where t_o varies from 7 to 300 days. Since the test specimens have probably not been in equilibrium state of moisture with the environment there is a risk that this has influenced the results. Ruetz /66RU/ has performed tests where the test specimens have not had any moisture exchange with the environment. From the results related by him it is possible to estimate roughly the constants α_{ct} and β_{ct} to 2.54 and 0.28 respectively ($14 \leq t_o \leq 365$). Ruetz's tests indicate that the constants are dependent on the water-cement ratio of concrete. Here, however, this fact is neglected and the function is chosen

$$f_3(t_o) = 2.54 \cdot t_o^{-0.28}$$

If the temperature deviates much from 20°C then time should be adjusted in the same way as is done upon the growth of strength with time. The influence of age at loading is given in the table below for both /70NE/ and the alternative chosen

t_o days	14	28	90	180	360
$f_3(t_o)$ chosen	1.21	1.00	0.72	0.59	0.51
$f_3(t_o)$ /70NE/	1.15	1.00	0.79	0.69	0.62

As can be seen the time function chosen here varies more with time than the one from /70NE/.

3.6.1.4 Influence of pore humidity on basic creep

Relations measured between the magnitude of basic creep upon equilibrium relative humidity at lower pore humidity than 100 % and the magnitude at 100 % are given in Fig. 3.15 /66RU/ for two different water-cement ratios. The simplified relation assumed here, which is independent of the water-cement ratio, is shown by the dashed line. This relation which, on the whole, follows the curve for the water-cement ratio 0.65, is assumed to be the one that corresponds most to normal concrete, and may at the the same time be assumed as a reasonable approximation, since the basic creep upon heavy drying merely constitutes a minor part of the total creep. Consequently, the relation may be expressed

$$\eta = 1 \qquad H \geq 0.80$$
$$\eta = H \cdot 2 - 0.6 \qquad 0.35 \leq H \leq 0.80$$
$$\eta = 0.1 \qquad H \leq 0.35$$

where H = the pore humidity of concrete.

3.6.1.5 Influence of temperature on basic creep

The rate of creep increases with the temperature. If the test specimen is saturated, however, the velocity of hydration also increases. In Fig. 3.16 is shown how these two factors co-operate /66RU/. If the concrete is dried before loading there is no further hydration and the creep increases continuously with temperature (Fig. 3.17 /66RU/). The velocity of hydration decreases when the pore humidity drops below about 80 % and it ceases at about 30 % /70NE/.

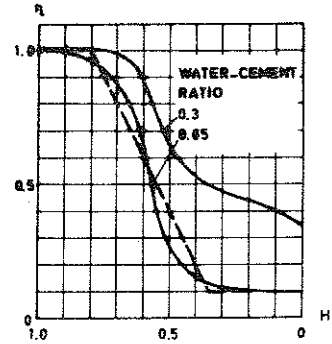

Figure 3.15 Basic creep as a function of pore humidity at equilibrium state of moisture /66RU/. The dashed curve is assumed to be valid in this paper regardless of the water - cement ratio.

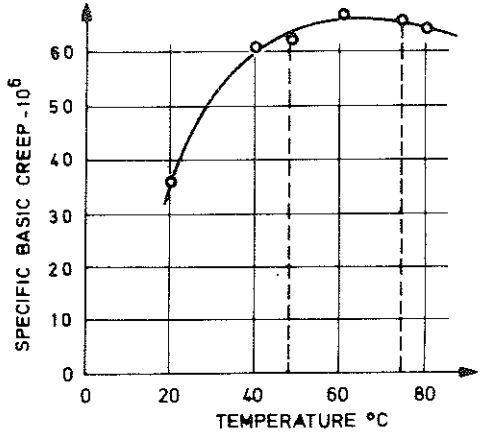

Figure 3.16 6-day creep strain measured on sealed specimens at different temperatures after storing in a sealed state for 28 days. Water-cement ratio = 0.3. /66RU/.

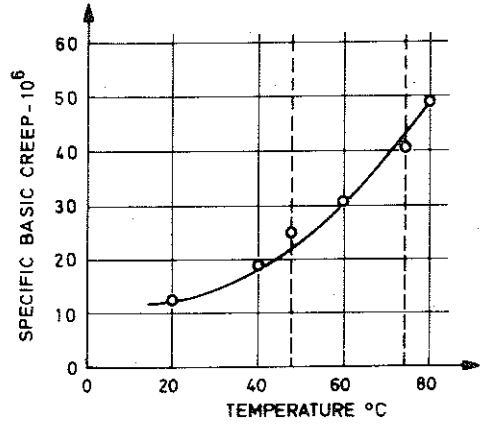

Figure 3.17 6-day creep strain at different temperatures after removal of approx. 70 % of the evaporable water content at 20°C. Age of specimens 28 days, water-cement ratio = = 0.3. /66RU/.

3.6.1.6 Relation between creep of cement paste and concrete

The same model that was used to determine the relation between the shrinkage of concrete and cement paste can be used. Assuming that the aggregates do not creep or affect the creep of cement paste through chemical processes, the following equations may be established at elastic conditions at an exterior stress equal to 1 (Fig. 3.18)

The initial state

$$1 = \sigma_{m1}(1 - \beta^2) + \sigma_{a1}\cdot\beta^2 \qquad \text{equilibrium equation}$$

$$\frac{\sigma_{m1}}{E_m} = \frac{\sigma_{a1}}{E_a} \qquad \text{compatibility equation}$$

$$\frac{1-\beta}{E_m} + \frac{\sigma_{a1}}{E_a}\cdot\beta = \varepsilon_e \qquad \text{total deformation}$$

later

$$1 = \sigma_{m2}(1 - \beta^2) + \sigma_{a2}\cdot\beta^2 \qquad \text{equilibrium equation}$$

$$\frac{\sigma_{m2}}{E_m} + \sigma_{m3}\cdot\varepsilon'_{mc} = \frac{\sigma_{a2}}{E_a} \qquad \sigma_{m1} \geq \sigma_{m3} \geq \sigma_{m2}$$
compatibility equation

$$\frac{1-\beta}{E_m} + \varepsilon'_{mc}(1-\beta) + \frac{\sigma_{a2}}{E_a}\cdot\beta = \varepsilon_e + \varepsilon'_{cc}$$
total deformation

From these equations follows

$$\varepsilon'_{cc} = \varepsilon'_{mc}\,(1-\beta)(1+k_p)$$

where

$$\frac{\beta(1+\beta)}{(1+\beta^2(\alpha-1))^2} \geq k_p \geq \frac{\beta(1+\beta)}{(1+\beta^2(\alpha-1))(1+\beta^2(\alpha-1+\varepsilon'_{mc}\cdot E_a))}$$

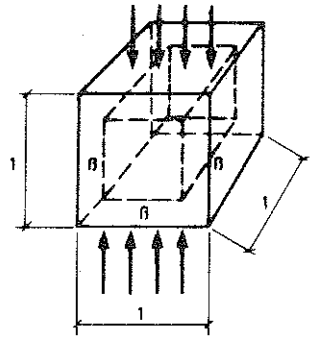

Figure 3.18 Model for the calculation of the relation between the creep of concrete and cement-paste.

for

$$\sigma_{m1} \geq \sigma_{m3} \geq \sigma_{m2} \quad \text{and}$$

where $\alpha = E_a/E_m$ and β^3 = volume share of aggregate.

Theoretically k_p is situated in the interval $0.14 \geq k_p \geq 0.064$ at a reasonable variation of the parameters encircling k_p. At a test accounted for by /66RU/ $k_p = 0.16$. Since k_p for normal concrete is relatively small, its variation has little influence, and therefore the value of k_p is assumed to be 0.16.

Neville /70NE/ has assumed that an equation established by Pickett concerning shrinkage may also be used for creep

$$\varepsilon'_{cc} = \varepsilon'_{mc} \, (1 - \beta^3)^k$$

where k theoretically is about 1.4 whereas values between 1 and 2 have been determined on comparisons with tests. At shrinkage the shrinkage of cement paste is not affected by the fact that forces are transferred to the aggregates. This is, however, the case at creep, which means that the equations for shrinkage and creep should not have the same structure.

The ratio between creep of cement paste and concrete has therefore been chosen

$$\varepsilon'_{cc} = 1.16 \cdot \varepsilon'_{mc}(1 - \beta) \qquad (3.2)$$

where β^3 = volume share of aggregate and is equal to the total volume minus the volume of water and cement.

$$\beta^3 = 1 - \frac{W_o}{1000} \, (0.32/vct + 1) \qquad (3.3)$$

where W_o is the original water contents of concrete in ℓ/m^3 and vct the water-cement ratio. At air-entraining regard is taken to this in a corresponding manner.

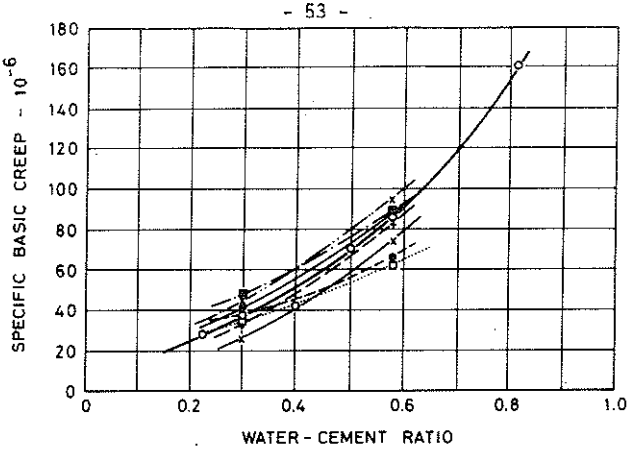

Figure 3.19 6-day creep strain of 28-day old specimens of different water - cement ratio when stored in a sealed state. Measured values for 8 different kinds of cement. /66RU/.

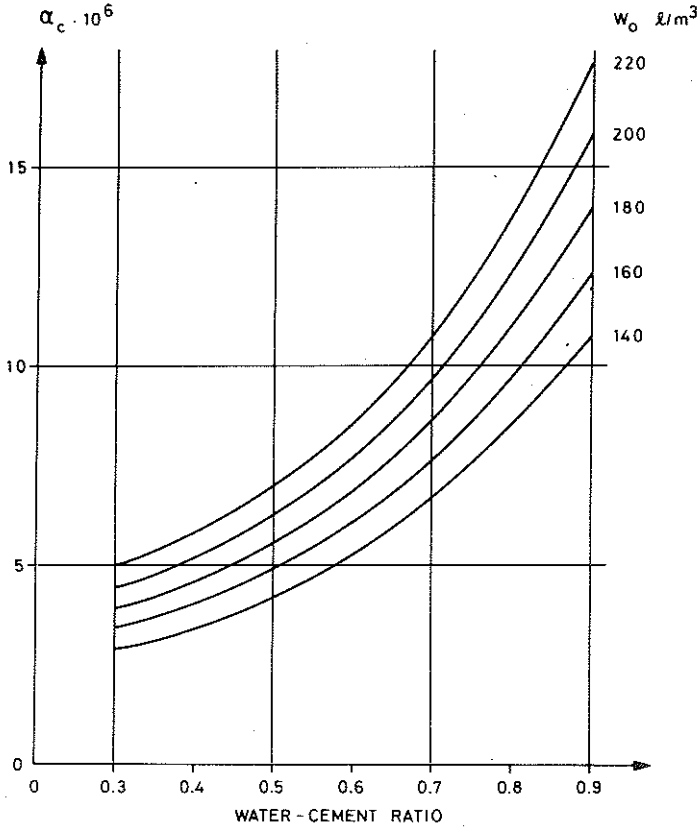

Figure 3.20 Diagram for the determination of α_c in Eq. 3.4 as a function of the water - cement ratio and the original water content (W_o).

3.6.1.7 Basic creep for different concrete mixtures

The mineralogical composition of the aggregates may have great influence on creep /69BE, 70NE/. Somewhat diverging opinions exist as to how different aggregate materials behave in concrete. Here it is assumed that the aggregate material consists of granite which is the most common in Sweden, and which does not react with the other materials in the mixture.

The specific basic creep is here described by the formula

$$\varepsilon'_{cc} = \alpha_c \cdot t^{\beta_c}$$

where t denotes the time under load in days, and the term β_c, as described earlier, has been given the value 0.24. Fig. 3.19 /66RU/ shows the specific basic creep of the cement paste after 6 days at 100 % relative humidity, the age of loading is 28 days. By using the equations 3.2, 3.3 and 3.4 and Fig. 3.19 it is possible to determine α_c as a function of the water-cement ratio of concrete and its original water contents W_0. This relation is shown in Fig. 3.20.

At a different age of loading and pore humidity, α_c may be corrected according to sections 3.6.1.3 and 3.6.1.4 respectively.

3.6.1.8 Basic creep at varying stresses

Basic creep is assumed to be proportional to stress i.e. concrete is supposed to be linearly visco-elastic. At least five generally established models are available for the determination of the creep of concrete at varying stresses.

The most simple and maybe most used design method consists of counting with a fictitious modulus of elasticity. This method totally neglects the stress history, it gives a complete and immediate creep recovery at unloading and underestimates the creep at decrease of stress. Other methods for a determination of creep are one that is valid for time hardening materials /71CE/, rate of creep, and one that is valid for strain hardening materials. To a

certain degree, these two methods take into consideration the stress history, but they assume that the whole creep is irreversible and consequently no creep recovery may occur at unloading. The superposition method /58RO/ normally presupposes that the whole creep is reversible. This means that creep is underestimated at a decreasing stress. The method rate of flow /65EN/ distinguishes two components of creep, an irreversible and a recoverable delayed elastic component. This means that in order to use it the magnitude of each creep component and their time functions must be known.

At an assumed stress variation according to Fig. 3.21, where also the curve for the specific creep is shown, creep will be calculated according to a model valid for time hardening materials (TH) as

$$\text{TH} \quad \varepsilon_{cc2} = \varepsilon_{cc1} + (\sigma_1 + \Delta\sigma)\cdot\left[\varepsilon'_{cc}(t_1 + \Delta t) - \varepsilon'_{cc}(t_1)\right]$$

and according to the superposition method (SP) where creep is assumed totally recoverable

$$\text{SP} \quad \varepsilon_{cc2} = \sigma_1\cdot\varepsilon'_{cc}(t_1 + \Delta t) + \Delta\sigma\cdot\varepsilon'_{cc}(\Delta t)$$

and for a strain hardening material (SH)

$$\text{SH} \quad \varepsilon_{cc2} = \varepsilon_{cc1} + (\sigma_1 + \Delta\sigma)\cdot\left[\varepsilon'_{cc}(t'_1 + \Delta t) - \varepsilon'_{cc}(t'_1)\right]$$

where t'_1 is determined from the relation $(\sigma_1 + \Delta\sigma)\cdot\varepsilon'_{cc}(t') = \varepsilon_{cc1}$.

The TH method is simple to use. However, it does not take into consideration the previous stresses at calculation of the change of creep during the next time step. No creep recovery occurs at the decrease of stress, but the creep continuously increases at loading.

The SP method is very laborious to use and is not suitable for computer calculations since it requires that the whole stress history is used for a calculation of creep under a new time step. Its advantage is that a creep recovery takes place at decreases of stress. The method may be improved by using a new specific creep for every new time step which takes into consideration the age of loading for the stress changes.

The SH method is almost as simple to deal with as the TH method. In this method regard is taken to previous creep at a calculation of the creep changes. No creep recovery occurs at decreases of stresses.

At a comparison between experimentally measured and calculated values for creep with the TH and SP methods /58RO/ it appears that the TH method gives too small creep at increase of stress and too large at decrease of stress. For the SP method the opposite condition is valid. It may be shown that the SH method gives creep values between the calculated ones according to the TH and SP methods for both increase and decrease of stress. It has here been chosen to use the SH method, which is considered to give reasonable creep values in relation to the calculation work as well as to the insecurity at a determination of the parameter values which govern the creep.

During a drying process it may occur that the stresses change signs more than once in certain parts of a structure. The SH method established does not work when creep and stress have different signs. In order to be able to determine unequivocally the creep in these cases, a modification of the creep model has been done. With this creep is determined by

$$\varepsilon_{cc} = \varepsilon_{ccac} + \sigma \cdot \left[\varepsilon'_{cc}(t' + \Delta t) - \varepsilon'_{cc}(t')\right]$$

where σ is the stress during the time step Δt, $\varepsilon'_{cc}(t)$ the specific creep at time t, and ε_{ccac} the creep accumulated before. The time t' is determined by

$$\sigma \cdot \varepsilon'_{cc}(t') = \varepsilon_{ccac} - A$$

where A is equal to the maximum creep reached before, with the sign opposite to σ.

In order to simplify the understanding of the model and to describe its behaviour, a calculation is made for a stress process according to Fig. 3.22 where also the calculated creep process is shown.

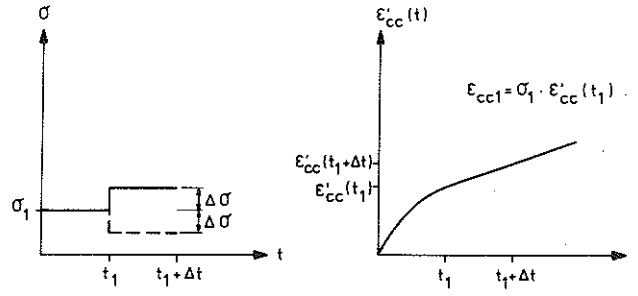

Figure 3.21 The assumed stress variation and the specific basic creep used in the calculation of the effects of stress variation on creep according to different models.

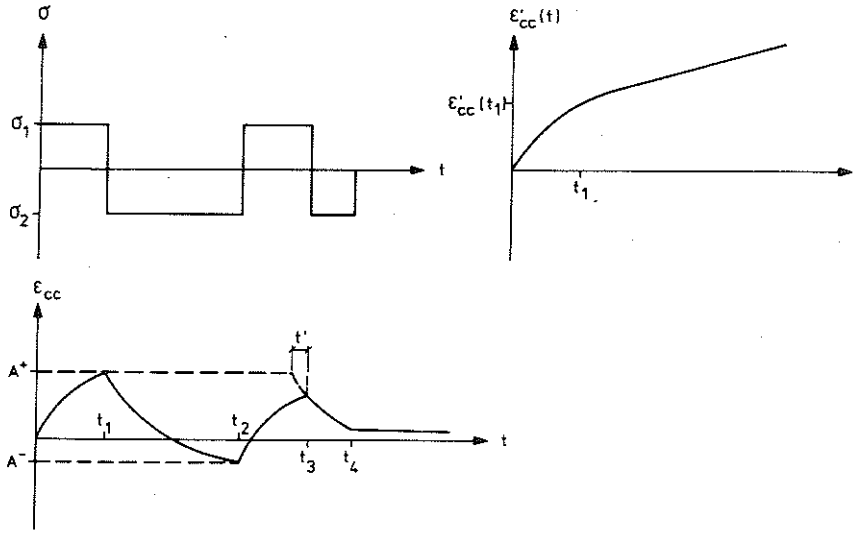

Figure 3.22 Creep according to the SH-method when stresses change signs.

t_1: $\varepsilon_{cc} = \sigma_1 \cdot \varepsilon'_{cc}(t_1)$ $\quad \varepsilon_{ccac1} = A^+ = \varepsilon_{cc}$

t_2: $\sigma_2 \cdot \varepsilon'_{cc}(t') = \varepsilon_{ccac1} - A^+ = 0 \Rightarrow t' = 0$

$$\varepsilon_{cc} = \varepsilon_{ccac1} + \sigma_2 \cdot \left[\varepsilon'_{cs}(t_2 - t_1) - 0\right]$$

$$\varepsilon_{ccac2} = A^- = \sigma_1 \cdot \varepsilon'_{cc}(t_1) + \sigma_2 \cdot \varepsilon'_{cc}(t_2 - t_1)$$

t_3: $\sigma_1 \cdot \varepsilon'_{cc}(t') = \varepsilon_{ccac2} - A^- = 0 \quad t' = 0$

$$\varepsilon_{cc} = \varepsilon_{ccac2} + \sigma_1 \cdot \left[\varepsilon'_{cc}(t_3 - t_2) - 0\right]$$

$$\varepsilon_{ccac3} = \sigma_1 \cdot (\varepsilon'_{cc}(t_1) + \varepsilon'_{cc}(t_3 - t_2)) + \sigma_2 \cdot \varepsilon'_{cc}(t_2 - t_1)$$

t_4: $\sigma_2 \cdot \varepsilon'_{cc}(t') = \varepsilon_{ccac3} - A^+ = \sigma_1 \cdot \varepsilon'_{cc}(t_3 - t_2) + \sigma_2 \cdot \varepsilon'_{cc}(t_2 - t_1)$

$$\varepsilon_{cc} = \varepsilon_{ccac3} + \sigma_2 \cdot \left[\varepsilon'_{cc}(t' + t_4 - t_3) - \varepsilon'_{cc}(t')\right] = \sigma_1 \cdot \varepsilon'_{cc}(t_1) +$$

$$+ \sigma_2 \varepsilon'_{cc} \cdot (t' + t_4 - t_3)$$

At a computer calculation, two values of A as well as the accumulated creep must be stored for each concrete element. If the values of A are not stored in the model, but only accumulated creep is used and t' is given the value zero when accumulated creep and stress have opposite signs, the calculation of creep will not be unequivocal, which is shown in Fig. 3.23, where the calculation of a time step is alternatively done by dividing it into two time steps.

In appendix A2 equations have been derived for a determination of creep and relaxation with the SH method at continuous stress changes.

The creep model here assumed, which is based on the assumption that concrete is strain hardening, does not imply a linear relation between creep and stress, so that, if another relation is assumed to prevail, σ may be exchanged by this relation.

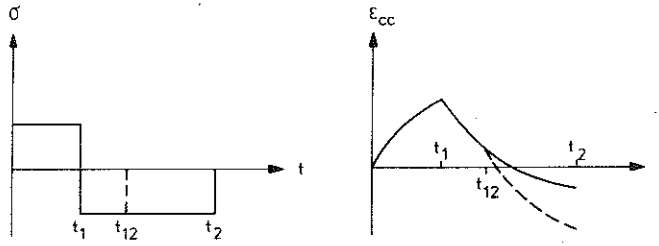

Figure 3.23 If the accumulated creep is used as a basic for the determination of 't' the model will not be unequivocal at stress changes.

3.6.1.9 Basic creep at varying pore humidity and temperature

Concrete generally contains more moisture at an early age than at its future equilibrium state of humidity with the environment. The pore humidity will therefore vary with time. Basic creep is a function of the pore humidity according to section 3.6.1.4.

Upon calculating basic creep at varying pore humidity, the same model as is used at varying stress, based on the assumption that concrete is strain hardening, may be used. The stress must then be multiplied with the value from the function governing the relation between pore humidity and basic creep. In the model the pore humidity as well as the stress may vary at the same time.

If temperature varies the same procedure may be used, and since it may be assumed that the functions governing the relations between basic creep and stress, pore humidity and temperature are independent of each other, σ in the model in section 3.6.1.8 may be exchanged by the values of the functions multiplied with each other.

3.6.2 Sorption creep of concrete

That part of creep which can be assigned to changes in the pore humidity of concrete is called sorption creep. Here it will be called drying creep, since it is the most frequent one as the pore humidity of concrete normally is higher shortly after concreting than at a later equilibrium state of moisture with the environment. Generally, drying creep is larger than basic creep. This is particularly conspicuous for slender structures, subject to heavy and fast drying. The creep which occurs at wetting is analogous to the drying creep. Ruetz /66RU/ has performed very well-defined tests which describe the behaviour qualitatively.

There are difficulties in finding reliable experimental data within this field in literature which can be the basis for establishing a quantitative model. The statement of results and the

testing conditions may be vague and simultaneously it may be difficult to know whether equilibrium state of moisture has been reached during the time lapse of the tests. At an estimate of the reliability of the model assumed here, the small basis of tests must be taken into consideration which, at an extention, should make possible a safer judgement of the drying creep. The tests should preferably be performed with slender test specimens arriving at equilibrium state of moisture relatively fast.

The model established here is based on tests accounted for by /59PE/ and /65HE/. Furthermore, efforts have been made to design the model in such a way that other known concrete behaviours are represented. De la Peñas' /59PE/ tests were performed with cement mortar pipes with a wall thickness of 2 mm. After being stored for seven days in water the test specimens were loaded in compression at 50 and 10% relative humidity for seven days, whereupon it was estimated that equilibrium state of moisture was reached. L'Hermite's /65HE, 68HE/ tests were performed with test specimens of concrete with a 7·7 cm cross-section. After 28 days storage in water, these were loaded for five years at 50 and 75% relative humidity.

The model for drying creep is built up in such a way that the additional drying creep, at the stress σ and the time t days after the beginning of drying and when shrinkage of concrete is changed by $\Delta\varepsilon_{cs}$, may be expressed

$$\Delta\varepsilon_{ccs} = \sigma \cdot \varepsilon'_{cc}(7) \cdot f_{ccs}(H_{en}) \cdot \frac{\Delta\varepsilon_{cs}}{\varepsilon_{ccs}} \cdot f_{ccs}(t)$$

where the different terms will be explained below and compared to the corresponding terms for basic creep.

At a higher stress level the drying creep increases more than linearly with stress /65HE, 59PE/, but not as much as the basic creep. Therefore a linear relation between drying creep and stress has been assumed here as for basic creep.

According to de la Peñas' tests the relation between the total

creep after seven days, when equilibrium state of moisture is reached, and the basic creep at 100% relative humidity after seven days is the same for different compositions of mortar. This implies that the same material parameters which govern basic creep also govern the drying creep. The influence of the age of loading may also be assumed to be the same for the two types of creep. Since the specific basic creep at a certain time, e.g. seven days, is a funciton of the material parameters and the age of loading, the assumptions made above justify a linking between drying and basic creep with the aid of the specific basic creep at seven days ($\varepsilon'_{cc}(7)$).

If the total creep in de la Peñas' tests is reduced by the basic creep occurring during drying, calculated according to the model previously described for basic creep, then the relation between drying creep at drying up to equilibrium state of moisture and basic creep at seven days in 100% relative humidity respectively will be 7.4 and 5.55 respectively at 10 and 50% relative humidity respectively. If it is assumed that drying creep may be linked to basic creep thorugh the specific basic creep after seven days ε'_{cc} (7) then $f_{ccs}(H_{en})$ may be determined. According to /68HE/ the drying creep at 75% relative humidity will be about half of the one at 50% relative humidity. In Fig. 3.24 the assumed rectilinear relation between $f_{css}(H_{en})$ and the surrounding relative humidity is shown ($40\% \leq H_{en} \leq 100\%$), as well as de la Peñas' values indicated with circles. The magnitude of drying creep at drying to equilibrium state of moisture has here been linked to basic creep after seven days. However, it might be linked to basic creep at any time if the function $f_{css}(H_{en})$ had been changed correspondingly.

The time function for the development of drying creep is assumed to be the same as for the drying process expressed as a reduction of pore humidity or a change of shrinkage. Since drying creep is fully developed at the same time as shrinkage (ε_{css}) the time function may be expressed as $\Delta\varepsilon_{cs}/\varepsilon_{css}$.

At drying a slender structure reaches equilibrium state of moi-

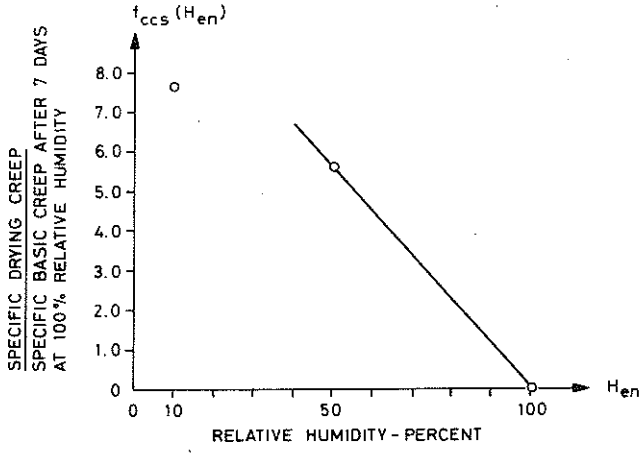

Figure 3.24 The ratio between the specific drying creep at drying to equilibrium state of moisture and the specific basic creep after seven days at 100 % relative humidity as a function of the relative humidity of the environment.

sture faster than a thick one. Since basic creep is smaller at a lower pore humidity, the basic creep will be smaller for the slender structure at the time when the thick one has reached equilibrium state of moisture. Therefore drying creep must be smaller for the thick structure since total creep must not be larger. This is fulfilled if the drying creep, due to a reduction of pore humidity, is smaller if the reduction occurs at a later event. A correction factor producing this has therefore been inserted

$$f_{ccs}(t) = \max\begin{cases} 1 - 0.15 \cdot \ln\,(1 + t/28) \\ 0 \end{cases}$$

where t is equal to time under load in days. To a certain extent, this time function may also be seen as a parallell to the time function of basic creep, which has the effect that the basic creep decreases with time.

The model for drying creep as well as the other models previously described concerning the behaviour of concrete give reasonable agreement with the tests referred by L'Hermite.

The largest part of the drying creep as well as the drying process occurs during a relatively short period since the gradient in the pore humidity and the coefficient of moisture diffusivity are at their largest at the beginning of the drying process.

At varying relative humidity of the environment the creep will be larger than the one corresponding to a drying to average moisture. /70NE/ states values at a varation between two relative humidities which correspond to a drying to the lower relative humidity. /68HE/ states results where variations of relative humidity between 60 and 90% in the open air, but with the test specimens sheltered from rain, correspond to creeps measured at a constant climate with 50% relative humidity in a laboratory. This implies that drying creep might be estimated at varying relative humidity by using a lower but constant relative humidity of the environment when calculating.

At a judgement of the reliability of the model for drying creep, regard must be taken to the small basis of tests, which at an extension should make possible a safer estimate of the drying creep.

4 THE MATERIAL PROPERTIES OF THE REINFORCEMENT

The reinforcement is assumed ideally elasto-plastic with the modulus of elasticity equal to $2.0 \cdot 10^5$ MN/m^2 and the yield stress equal to the strength f_{st}. Creep that may occur in the reinforcement is neglected.

5 FORCE - DEFORMATION RELATIONS OF THE SEGMENT

In this chapter the tensile and compressive strains caused by normal force, curvature caused by moment and moment plus normal force, and curvature and shear deformation caused by shear force will be treated. Simplified force - deformation relations are established, where creep and shrinkage are considered. The reliability of these relations is verified by calculations according to method A (Fig. 2.1) where regard is taken to the drying process and the load history.

5.1 Deformations of concentric normal force

For non-reinforced segments the initial deformation is easily determined by using the stress-strain relation of concrete according to section 3.1 or, at low stress levels, with the aid of the modulus of elasticity for concrete. The long-term deformation on account of creep without simultaneous drying may be calculated according to section 3.6.

During a drying process generally great stress changes take place in a specimen. In the separate parts of the specimen there is not only deformation on account of shrinkage but also of drying creep, basic creep and stresses during the time lapse. In Fig. 5.1 is an example of the different components of deformation and the stresses for one-dimensional drying calculated according to method A (Fig. 2.1) at different times, where regard has been taken to the drying process and the stress history of the different elements.

In order to determine the deformation of normal force at simultaneous drying, the above-mentioned calculation has been performed for square cross-sections where drying occurs in two directions, as well as for cross-sections with one-dimensional drying. The calculations have been made for several different stress levels and at different combinations of material parameters (α_{cref}, ε_{cssref}) which govern shrinkage and creep. The relative humidity of the environment (H_{en}) has been 40 and 70%. From the calcula-

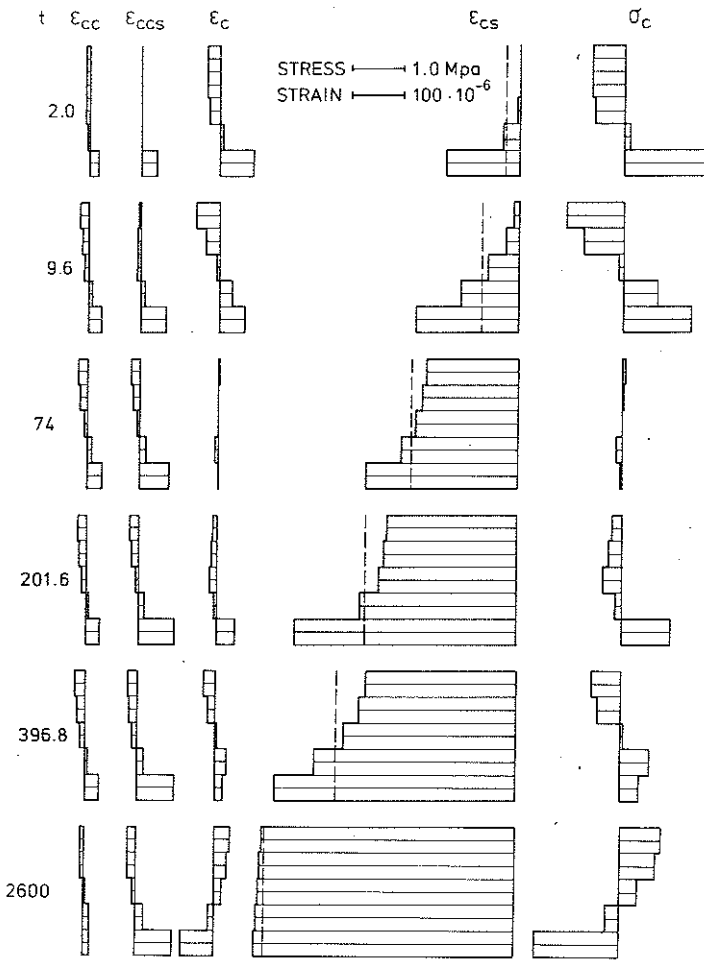

Figure 5.1 Strains and stresses calculated according to method A, for a non-loaded and non-reinforced plate segment with a thickness of 100 mm during a drying process at an ambient RH of 40%. The top faces of the diagrams coincide with the plane of symmetry of the plate. From the left is indicated the time from the beginning of the drying t in days, the basic creep ε_{cc}, the drying creep ε_{ccs}, the stress-related strain ε_c, the shrinkage ε_{cs} and the stress σ_c. The dashed line in the shrinkage strain diagram indicates the total strain. The figures show that the stress in the lower edge of the plate, which at the beginning of the drying process is positive (tensile stress), after three sign changes becomes negative at the end of the drying process. The same is valid for the stress in the plane of symmetry with the exception that the stress has opposite sign. $\alpha_c = 10 \cdot 10^{-6}$, $\varepsilon_{ccs} = 500 \cdot 10^{-6}$.

tion results it appears that the total deformation can be determined almost exactly by the formula

$$\varepsilon_{ctot} = \varepsilon_{ci} + \frac{\alpha_c}{\alpha_{cref}} \cdot \varepsilon'_{cc} \cdot \sigma_c + \frac{\varepsilon_{css}}{\varepsilon_{cssref}} \cdot \varepsilon_{cs} \qquad (5.1)$$

where ε_{cs} and ε'_{cc}, which also include the drying creep, can be determined from Figs 5.2 - 5.5 as a function of time, and ε_{cssref} = 500 · 10^{-6} and 300 · 10^{-6} for an ambient RH of 40 and 70% respectively, and α_{cref} = 10 · 10^{-6}. The term α_c may be calculated according to section 3.6 for the current composition of concrete and ε_{css} according to section 3.5. In the calculations diffusivity is assumed to vary according to section 3.4. At a different variation the time function does not agree but the final values are about the same.

The same calculations as above have been made for symmetrically reinforced cross-sections, and it appears that the deformation is best calculated with a formula, derived under the assumption that creep is proportional to the average stress during the time step, and that plane cross-sections remain plane.

$$\varepsilon_{tot} = \frac{\sigma_o}{E_c} \cdot \frac{1 + \phi + \psi}{1 + \psi} + \frac{\varepsilon_{cs}}{1 + \psi} \qquad (5.2)$$

where $\sigma_o = N/(b \cdot h \cdot (1 + \alpha \cdot \rho))$, $\alpha = E_s/E_c$, $\rho = (A_s + A'_s)/(b \cdot h)$, $\psi = \rho \cdot \alpha \cdot (2 + \phi)/2$, $\phi = \varepsilon'_{cc} \cdot E_c$, and ε'_{cc} and ε_{cs}, the total specific creep and shrinkage can be taken from Figs 5.2 - 5.5 at the time in question and at other values of ε_{cssref} and α_{cref} they may be modified in the same way as in Eq. 5.1.

In spite of the large stress variations that occur during a drying process, the above formulae (5.1, 5.2) show that the total deformation can easily be determined by superposing the influence of the initial deformation, creep and shrinkage.

5.2 Deformations of moment

Simplified relations between moment and curvature have been established. With these relations the curvature may be determined at short-time load without previous drying for first-time loadings

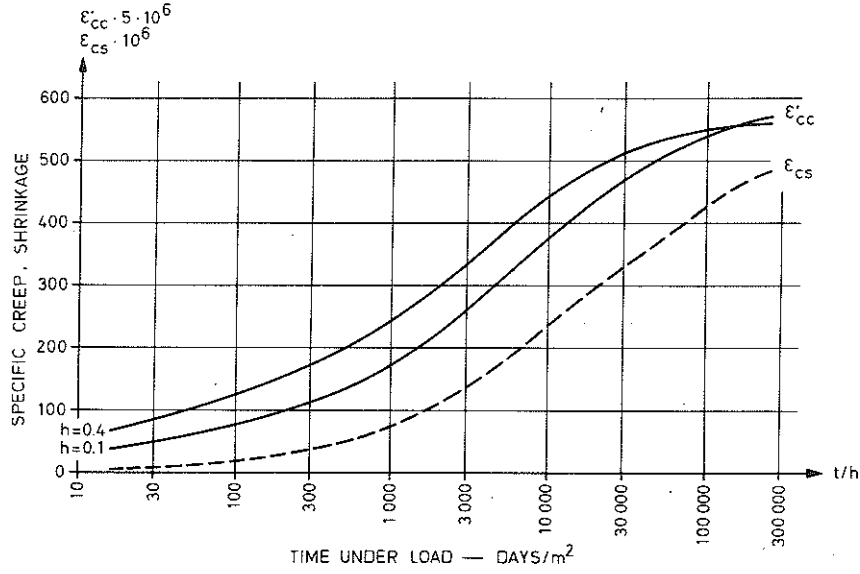

Figure 5.2 One-dimensional drying of a plate with a thickness of h m at an ambient RH of 40%. The values of specific creep and shrinkage, to be inserted into Eq. 5.1 are given as a function of t/h^2. $\alpha_{cref} = 10 \cdot 10^{-6}$, $\varepsilon_{sccref} = 500 \cdot 10^{-6}$.

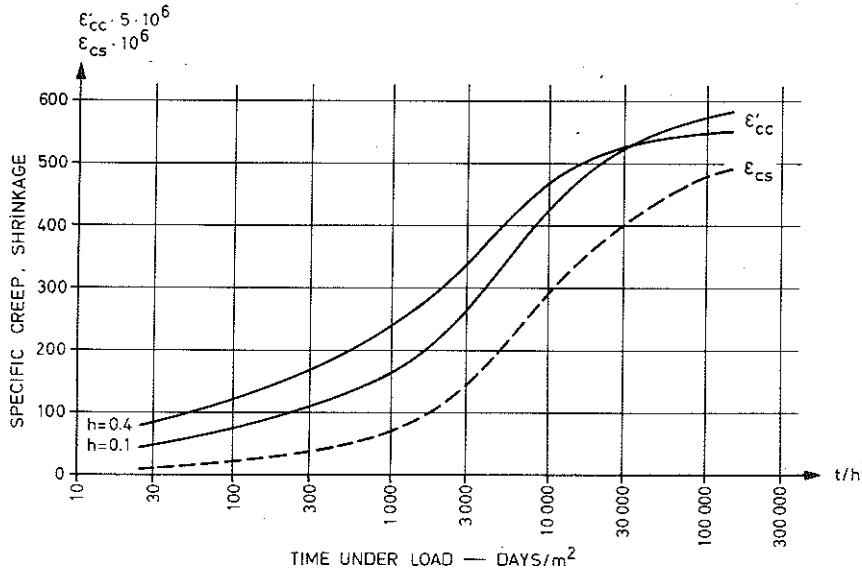

Figure 5.3 Two-dimensional drying of a square prism with the side h m at an ambient RH of 40%. The values of specific creep and shrinkage to be inserted into Eq. 5.1, are given as a function of t/h^2. $\alpha_{cref} = 10 \cdot 10^{-6}$, $\varepsilon_{sccref} = 500 \cdot 10^{-6}$.

and moment changes, appearing at momentaneous support movements. Simplified relations have also been established for a determination of the curvature at constant moment under the influence of creep, non-uniform shrinkage and simultaneous normal force. The derivations of these bilinear relations are given in Appendix A3, and are based on the assumptions that plane cross-sections remain plane, that a linear relation is prevailing between stresses and strains, that the creep is governed by the final stress at the current time, that the possible shrinkage is fully developed, and that the cross-sections are rectangular. These simplified relations, which form the basis of calculation method B, are controlled against a calculation model (method A) where regard is taken to the drying process and the load history of the elements. With the latter method calculations also are made to estimate on the one hand the influence of a certain drying before loading and on the other hand the relation between moment and curvature at relaxation.

5.2.1 Moment-curvature relations at short-term loading

In Fig. 5.6 and Fig. 5.7 the calculations of the moment-curvature relation are accounted for two different cross-sections. The calculations have been performed according to method A by dividing the segments into elements and regard has been taken to the load history of the elements. No drying or creep has occurred neither before nor after the loading. In the figures also simplified bilinear moment-curvature relations are shown according to Monnier /69MO/. A slight deviation from the straight lines happens near the cracking moment as well as shortly after the cracking moment. The latest deviation is largest for lightly reinforced segments.

The flexural rigidity of the uncracked segment $(EI)_o$ is in good agreement with the rigidity, calculated with the consideration of the reinforcement, and may, according to equation A3.16 be expressed

$$(EI)_o = \frac{b \cdot h^3 \cdot E_c}{12} \cdot \beta_1 \qquad (5.3)$$

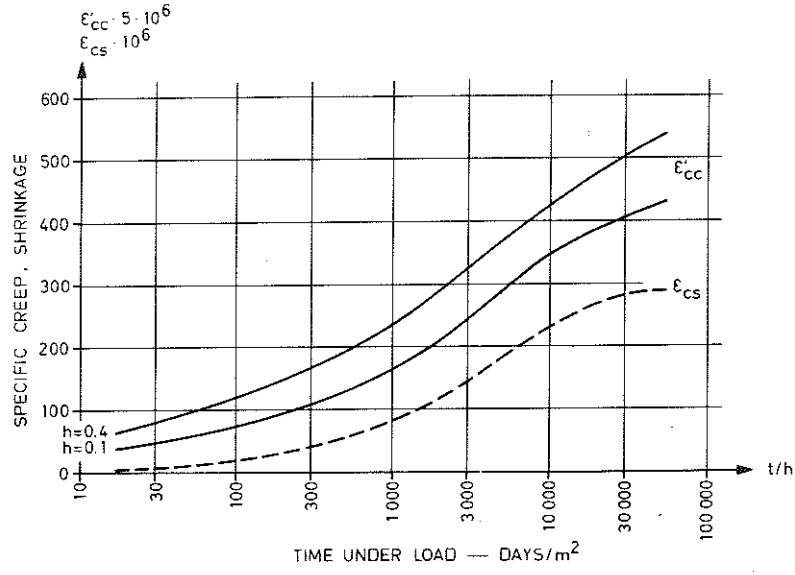

Figure 5.4 One-dimensional drying of a plate with a thickness of h m at an ambient RH of 70%. The values of specific creep and shrinkage, to be inserted into Eq. 5.1, are given as a function of t/h^2. $\alpha_{cref} = 10 \cdot 10^{-6}$, $\varepsilon_{cssref} = 300 \cdot 10^{-6}$.

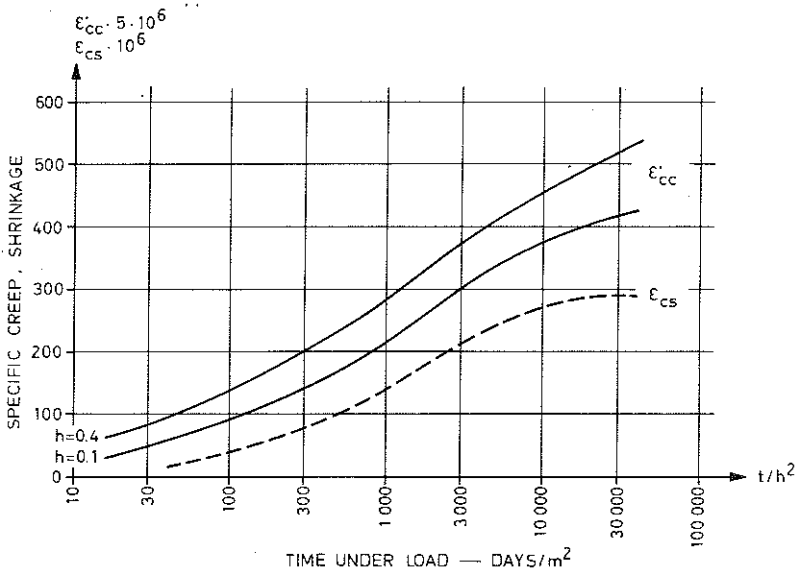

Figure 5.5 Two-dimensional drying of a square prisma with the side h m at an ambient RH of 70%. The values of specific creep and shrinkage, to be inserted into Eq. 5.1, are given as a function of t/h^2. $\alpha_{cref} = 10 \cdot 10^{-6}$, $\varepsilon_{cssref} = 300 \cdot 10^{-6}$.

where $\beta_1 = 1 + 3\,(1 - 2c/h)^2 \cdot (\psi + \psi' + 4\psi \cdot \psi')/(1 + \psi + \psi')$, $\psi = \alpha \cdot A_s/(b \cdot h)$; $\psi' = \alpha \cdot A_s'/(b \cdot h)$, $\alpha = E_s/E_c$ and c = the distance from the centroid of the tensile reinforcement to the edge in tension, which is supposed to be equal to the distance from the centroid of the compressive reinforcement to the edge in compression. The coefficient β_1 is shown in Fig. 5.8 for c/h = 0.1.

The flexural rigidity in cracked state has by Monnier empirically been determined to

$$(EI)_r = d^2 \cdot A_s \cdot 10^5 \qquad (5.4)$$

for percentages of tensile reinforcement below 1.5%. The discrepancy between this rigidity and the rigidities calculated here by the use of the above-mentioned method A is less than 10%. The bilinear relation has a breaking point at the moment (Eq. A3.20)

$$M_r = \frac{f_{cbm} \cdot b \cdot h^2}{6} \cdot \beta_2 \qquad (5.5)$$

where $\beta_2 = \dfrac{1 + \psi + \psi' + 3(1 - 2\,c/h)^2 \cdot (\psi + \psi' + 4\psi \cdot \psi')}{1 + 2\psi \cdot c/h + 2\psi' \cdot (1 - c/h)}$

and may be seen from Fig. 5.9 for c/h = 0.1.

5.2.2 Moment-curvature relations at short-term loading and load changes

These relations are useful at the calculation of structures subjected to load changes or support movements. In section 6.3, simplified relations established by Monnier /69MON/ have been used for the calculation of beams, exposed to support movements at serviceability limit state and after that loaded until failure occurs. Below a comparison will be made between relations calculated according to method A and Monnier's method, as well as a short description of these.

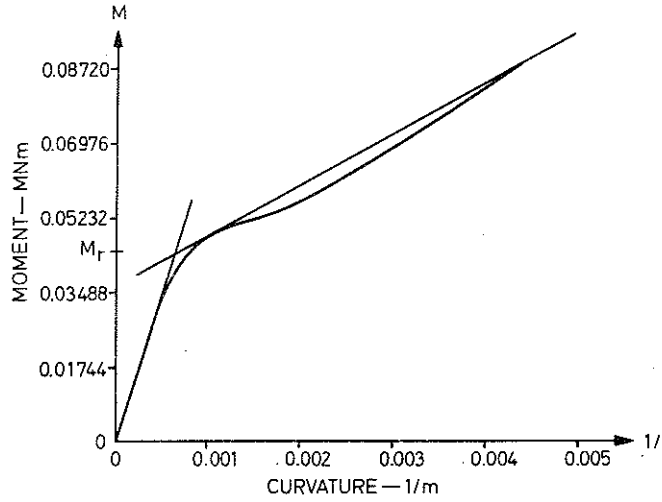

Figure 5.6 Simplified (straight lines) and according to method A (curved line) calculated moment-curvature relations. Section data: b = 0.25, h = 0.5, c/h = 0.1, A_s = 0.000625, A_s' = 0, f_{ccm} = 25 and f_{st} = 400.

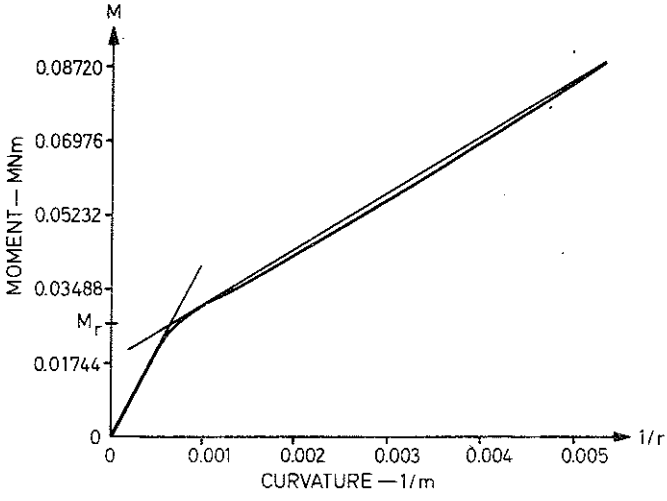

Figure 5.7 Simplified (straight lines) and according to method A (curved line) calculated moment-curvature relations. Section data: b = 0.125, h = 0.5, c/h = 0.1, A_s = A_s' = 0.000625, f_{ccm} = 25 and f_{st} = 400.

Moment-curvature relations calculated according to method A at load changes are accounted in Fig. 5.10, where a singly reinforced segment has been unloaded from two different moment levels and after that reloaded to the same levels, and in Figs 5.11 and 5.12 where a doubly reinforced segment after loading has been charged with negative moments and after that it has been reloaded with moments larger that the original ones.

Monnier /69MON/ has performed tests on beams exposed to moment changes, and on the basis of these he has developed simplified moment-curvature relations (Fig. 5.13), which partly diverge from those calculated here. Monnier has the opinion that, at unloading, a straight line should be followed which goes towards the cracking moment of opposite sign and the curvature belonging to this. For sections with higher percentages of reinforcement, the deviation is small, but somewhat larger at lower percentages of reinforcement. If the plastic strain for concrete in tension had been assumed somewhat larger than was done here, there would have been a better agreement with Monnier's assumption. The assumption, that a straight line should be followed towards the positive cracking moment after a reversal from a moment with the opposite sign, is more difficult to explain and does not occur with this calculation method. It is also difficult to prove the correctness of the assumption from the test results related by Monnier. Monnier's relations are relatively simple, their divergence from those calculated here has probably no practical significance at the calculation of a whole structure, and they might probably be used as a good approximation of the real relations.

5.2.3 Moment-curvature relations at short-time loading when a certain drying has taken place before loading

The drying of concrete takes place slowly. For normal sizes of cross-sections this means that the changes of the pore humidity are small for periods of a couple of weeks. Consequently, the influence of a shorter drying period on the moment-curvature relation is insignificant. The difference in percentage of the deformation between a non-dried beam and a partly dried one is

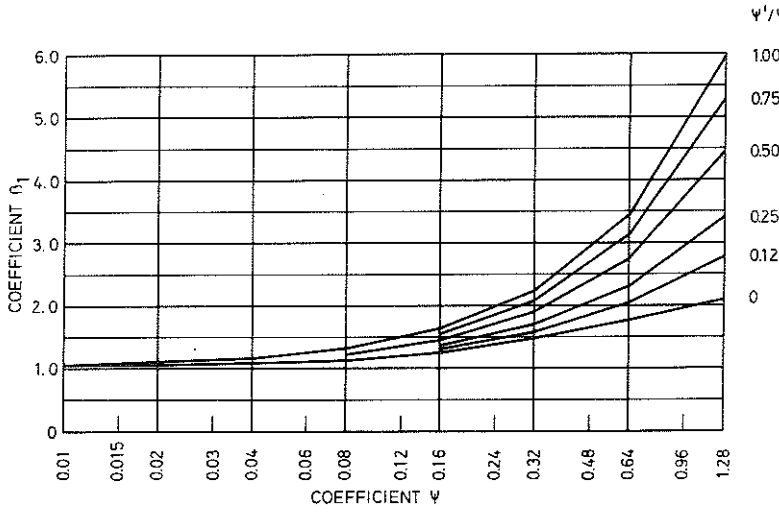

Figure 5.8 The coefficient β_1 for the determination of flexural rigidity at uncracked state according to Eqs. 5.3, 5.6 and 5.9. Valid for c/h = 0.1.

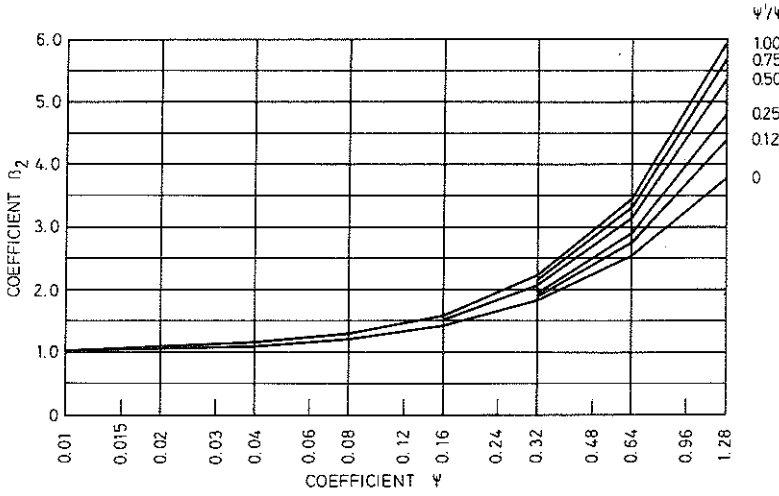

Figure 5.9 The coefficient β_2 for the determination of the cracking moment according to Eqs. 5.5 and 5.10. Valid for c/h = 0.1.

largest at moments of the same magnitude as the cracking moment of the non-dried beam, since drying somewhat lowers the cracking moment. As an example it may be mentioned, that for a beam with the same cross-section and material properties as the one in Fig. 5.7, exposed to drying during 32 days in a relative humidity of 40%, the curvature increases most, calculated as a percentage, with about 14% at moment loadings around the cracking moment for the non-dried beam, whereas the increases of deformation in percent are considerably smaller at the remaining load levels.

5.2.4 Influence of basic creep on curvature at constant moment

For a concrete segment loaded with a constant moment during a long period in a constant climate, where there is no drying, the curvature increases with time on account of creep. The additional curvature will be larger in percent for an uncracked segment, since the whole cross-section of the concrete is active in the first-mentioned case and since it is the concrete that creeps.

The calculations of the curvature at creep has been done with method A according to the following. The segment has been divided into elements and the creep at each element has been calculated with the aid of the average stress of the element in the time step. The duration of the first time step has been chosen to 24 hours, and the following time steps have been chosen so that there is a doubling of the time under load.

The relation calculated in this way (method A) between moment and curvature at different load levels, but for the same time under load, is illustrated for two different segments in Figs 5.14 and 5.15. In the figures also the moment-curvature relations for short-time loading are shown as a comparison. According to section 5.2.1 these may be described by two straight lines and a breaking point. From the figures it appears, that this can be done also when creep occurs.

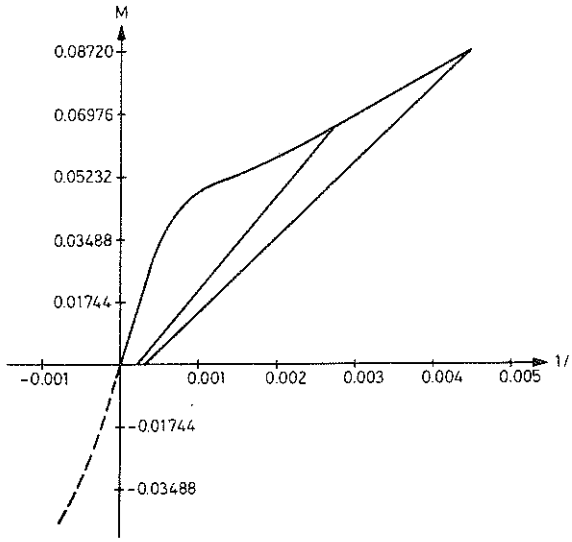

Figure 5.10 Moment-curvature relations calculated according to method A at unloading and reloading. Section data: b = 0.25, h = 0.5, c/h = 0.1, A_s = 0.000625, A_s' = 0, f_{ccm} = 25 and f_{st} = 400.

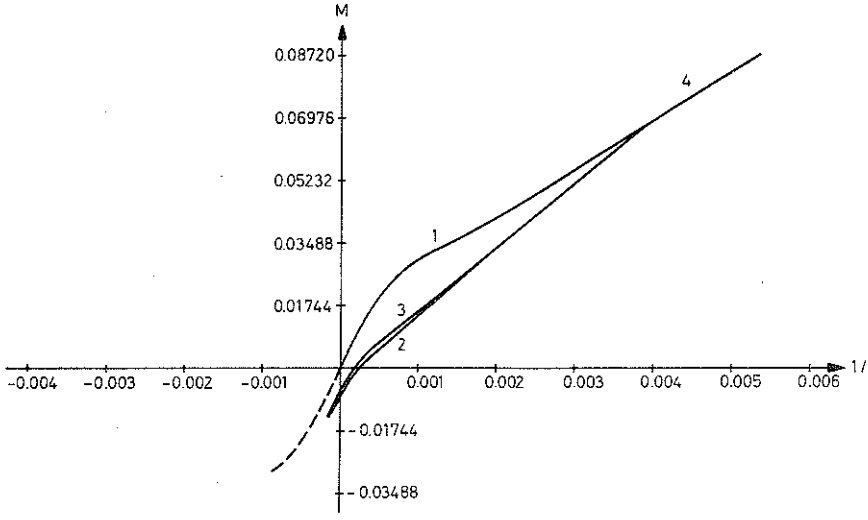

Figure 5.11 Moment-curvature relations calculated according to method A at moment alternations. The numerals denote the order according to which the branches of the curves are run through. Section data: b = 0.125, h = 0.5, c/h = 0.1, A_s = A_s' = 0.000625, f_{ccm} = 25 and f_{st} = 400.

In order to determine this simplified bilinear relation, a derivation of the flexural rigidities of the uncracked and cracked states respectively has been carried out (Appendix 3). The derivations can be done with the aid of two equilibrium equations and a compatibility equation, where plane cross-sections remain plane and the creep is assumed to be proportional to the final stress at the moment in question. For uncracked segments, the flexural rigidity according to Eq. A3.16 is

$$(EI)_{oc} = \frac{b \cdot h^3 \cdot E_c}{12(1 + \phi)} \cdot \beta_1 \qquad (5.6)$$

where $\beta_1 = 1 + 3(1 - 2c/h)^2 \cdot (\psi + \psi' + 4\psi \cdot \psi)/(1 + \psi + \psi')$, $\psi = \alpha \cdot (1 + \phi) \cdot A_s/(b \cdot h)$, $\psi' = \alpha \cdot (1 + \phi) \cdot A_s'/(b \cdot h)$, $\alpha = E_s/E_c$, ϕ = the creep coefficient and c is the distance from the centroid of the tensile reinforcement to the edge in tension, which has been assumed to be equal to the distance from the centroid of the compressive reinforcement to the edge in compression. For $c/h = 0.1$ β_1 may be determined from Fig. 5.8.

The flexural rigidity at cracked state, derived in the same way, gets too large, since it does not take into consideration the uncracked concrete between the cracks. This can be compensated by dividing the flexural rigidity of the segment, subjected to creep with the rigidity likewise derived when creep does not occur, and by multiplying it with the flexural rigidity according to section 5.2.1 which takes into consideration the influence of the concrete between the cracks.

$$(EI)_{rc} = \frac{(EI)_{rcf}}{(EI)_{rf}} \cdot A_s \cdot d^2 \cdot 10^5 \qquad (5.7)$$

where, according to Eq. A3.38

$$\beta_3 = \frac{(EI)_{rcf}}{(EI)_{rf}} = \frac{(1 - c/h - x/h) \cdot (3 - 3c/h - x/h) + (x/h - c/h) \cdot (x/h - 3c/h) \cdot \psi'/\psi}{(1 - c/h - y/h) \cdot (3 - 3c/h - y/h) + (y/h - c/h) \cdot (y/h - 3c/h) \cdot \psi'/\psi}$$

where

$$x/h = [(\psi + \psi')^2 + 2\psi \cdot (1 - c/h) + 2\psi' \cdot c/h]^{1/2} - (\psi + \psi')$$

$$y/h = [(\alpha \cdot \rho + \alpha \cdot \rho')^2 + 2\alpha \cdot \rho \cdot (1 - c/h) + 2\alpha \cdot \rho' \cdot c/h)]^{1/2} - (\alpha \cdot \rho + \alpha \cdot \rho')$$

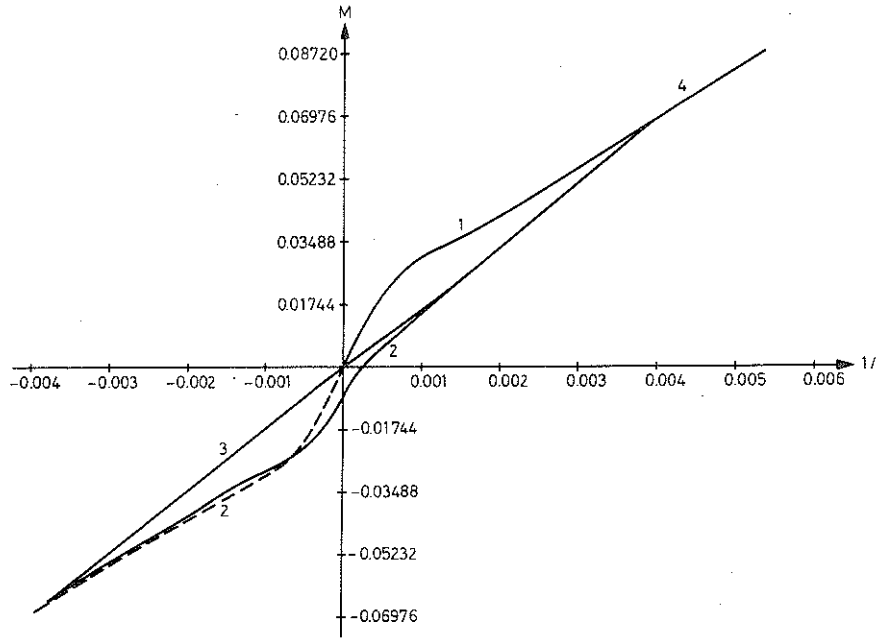

Figure 5.12 Moment-curvature relations calculated according to method A at moment alternations. The numerals denote the order according to which the branches of the curves are run through. Section data: b = 0.125, h = 0.5, c/h = 0.1, $A_s = A'_s = 0.000625$, $f_{ccm} = 25$ and $f_{st} = 400$.

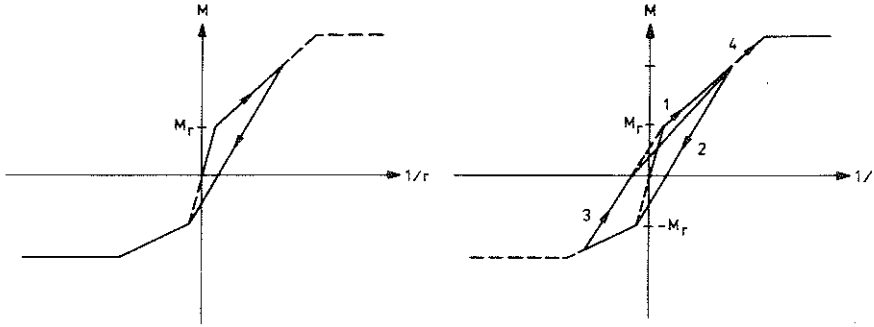

Figure 5.13 Simplified assumption of the moment-curvature relations at moment alternations according to /69MON/.

$\rho = A_s/(b \cdot h)$, $\rho' = A'_s/(b \cdot h)$, $\psi = (1 + \phi) \cdot \alpha \cdot \rho$ and $\psi' = (1 + \phi) \cdot \alpha \cdot \rho'$

The coefficient β_3 may be determined from Fig. 5.16 for c/h = 0.1.

The breaking point occurs at the same magnitude of moment as upon short-time load. The moment cannot be larger since the creep cannot heal already cracked concrete. It should not be smaller, since the creep transfers forces from the concrete in tension to the reinforcement, and simultaneously there is a growth of strength in concrete, and these two factors might counteract the smaller long-term strength of concrete.

The relations determined with the simplified model show good agreement with those more accurately calculated according to method A.

5.2.5 Influence of creep and shrinkage on curvature at constant moment

During long-term loading , a structure is normally exposed to drying, which means that, except being influenced by basic creep according to the previous section, it is also influenced by shrinkage and drying creep. The increase of the curvature at constant moment upon simultaneous drying and creep is considerably larger than the one upon creep alone. The larger the drying is, the larger will be the difference. The drying up to almost equilibrium state of moisture between concrete and the environment takes very long time for ordinary structures. However, most of the increase of deformation takes place during a relatively short period. The shrinkage involves a decrease of the cracking moment.

The calculation of the curvature according to method A has been done by dividing the segment into elements. For each element, regard has been taken to the drying process and the influence of the varying stress history, on shrinkage, drying and basic creep, and elastic and plastic strains, upon the calculation of its deformation. The calculation has been done with about 30 time steps

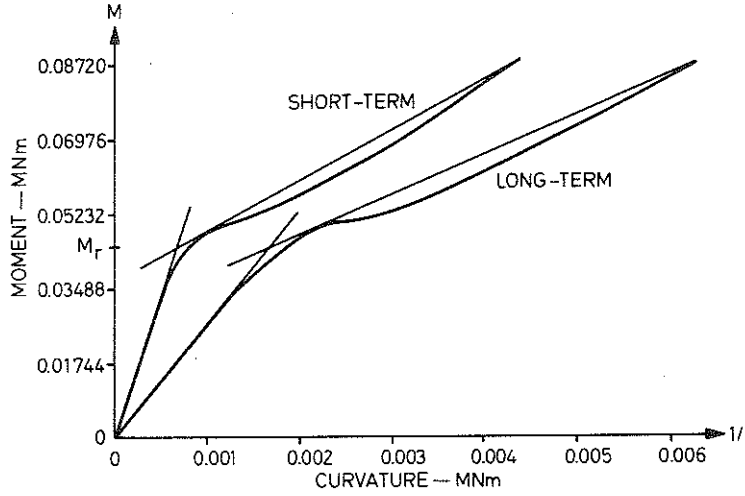

Figure 5.14 The moment-curvature relations at short-term load and long-term load (basic creep) calculated according to method A. In the figure the simplified bilinear relations are also shown. Section data: b = 0.25, h = 0.5, c/h = 0.1, A_s = 0.000625, A'_s = 0, f_{ccm} = 25 and f_{st} = 400. Creep data: t = 4096 days and ϕ = 1.92.

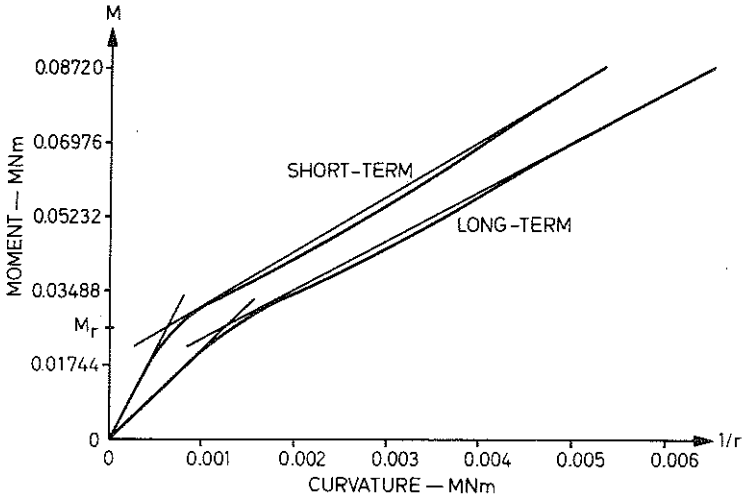

Figure 5.15 The moment-curvature relations at short-term load and long-term load (basic creep) calculated according to method A. In the figure the simplified bilinear relations are also shown. Section data: b = 0.125, h = 0.5, c/h = 0.1, A_s = A'_s = 0.000625, f_{ccm} = 25 and f_{st} = 400. Creep data: t = 4096 days and ϕ = 1.92.

up to the final moment, and within each time step, the average value of the stresses in each element at the beginning and end of the time step has determined the creep. The drying and loading have started simultaneously at the age of 28 days, and the relative humidity of the environment has been 40%. The final shrinkage has been assumed to be uniformly distributed over the whole cross-section.

In Fig. 5.17 is a statement of calculated relations between curvature and moment for short-time loading (A), for basic creep during 7 years (B), and for simultaneous drying and creep during 100 days (C) and during 7 years (D). It takes about seven years before the slab reaches almost equilibrium state of moisture with the environment. From the figure it appears that the largest part of the increase of curvature on account of drying takes place at the beginning. In Figs 5.18 and 5.19 the corresponding curvatures for beams subjected to two-dimensional drying are shown. From the firgures it appears that it is possible to describe the moment-curvature relation with two straight lines also for segments, subjected to shrinkage. At different amounts of compressive and tensile reinforcement, a curvature is received also for an unloaded segment.

In order to determine the simplified bilinear relation the flexural rigidities at uncracked and cracked stages have been derived in Appendix A3. The derivation has been done with the aid of two equilibrium equations and a compatibility equation, where plane cross-sections remain plane. The derivation is valid when shrinkage is fully developed over the whole cross-section, and creep has been assumed proportional to the final stress at the point of time in question.

According to this derivation, the curvature at zero moment according to Eq. A3.17 is

$$\frac{1}{r_o} = \frac{\epsilon_{css}}{h} \cdot \beta_4 \qquad (5.8)$$

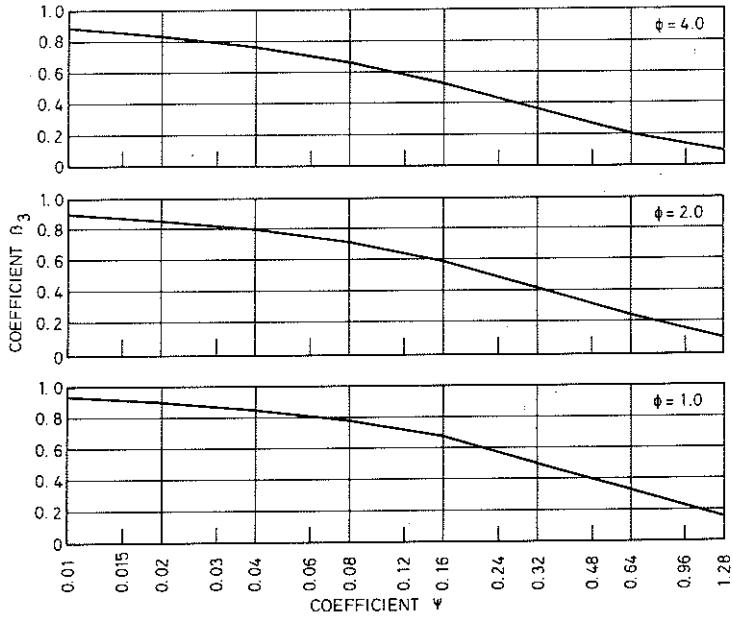

Figure 5.16 The coefficient β_3 for the determination of the flexural rigidity at cracked state according to Eq. 5.7 for a segment subjected to creep or creep and shrinkage. Valid for c/h = 0.1. The slight difference between the different values of ϕ is illusory since ψ increases with ϕ.

where $\beta_4 = \dfrac{(\gamma - 1)\cdot(1 + \psi + \psi') + (\gamma + 1)\cdot 3\cdot(1 - 2c/h)(\psi - \psi')}{1 + \psi + \psi' + 3(1 - 2c/h)^2\cdot(\psi + \psi' + 4\psi\cdot\psi')}$

and the flexural rigidity for the uncracked segment according to Eq. A3.16 is

$$(EI)_{ocs} = \frac{b\cdot h^3\cdot E_c}{12(1 + \phi)}\cdot\beta_1 \qquad (5.9)$$

where $\beta_1 = 1 + 3(1 - 2c/h)^2\cdot(\psi + \psi' + 4\psi\cdot\psi')/(1 + \psi + \psi')$

and ε_{css} denotes the final shrinkage at the edge in tension and $\gamma\cdot\varepsilon_{css}$ is the final shrinkage at the edge in compression. $\psi = (1 + \phi)\cdot\alpha\cdot A_s/(b\cdot h)$ and $\psi' = (1 + \phi)\cdot\alpha\cdot A_s'/(b\cdot h)$, $\alpha = E_s/E_c$; ϕ = the creep coefficient in which drying creep is included, and c is the distance from the centroid of the tensile reinforcement to the edge in tension and the same is assumed to be valid for the compression reinforcement. The coefficient β_4 and β_1 are shown in Figs 5.20 and 5.8 respectively for c/h = 0.1.

For segments with the same compressive and tensile reinforcement the curvature $1/r_0$ and the flexural rigidity $(EI)_{ocs}$ are in good agreement with the result given at a calculation with the more accurate method (method A). At tensile reinforcement exclusively the curvature $1/r_0$ may give a result at uniform shrinkage which exceeds the one of the accurate calculation by up to 30%. For this case also the flexural rigidity $(EI)_{ocs}$ is about 20% too large. A more correct value of the curvature $1/r_0$ is received if the term $(\gamma + 1)\cdot 3\cdot(1 - 2c/h)\cdot(\psi - \psi')$ is multiplied by 0.7. The errors of the curvature $1/r_0$ and the flexural rigidity $(EI)_{ocs}$ at tensile reinforcement exclusively counteract each other with the effect that, upon the calculation of a beam where the moment varies along the longitudinal axis of the beam, the errors have no practical significance. Consequently, the equations for the rigidity $(EI)_{ocs}$ and the curvature $1/r_0$ together result in good accuracy, despite the larger approximation made that the final stress governs creep. This is a large approximation since, at the small influence of the moment on the stresses, the variation of stresses becomes very large during the drying process.

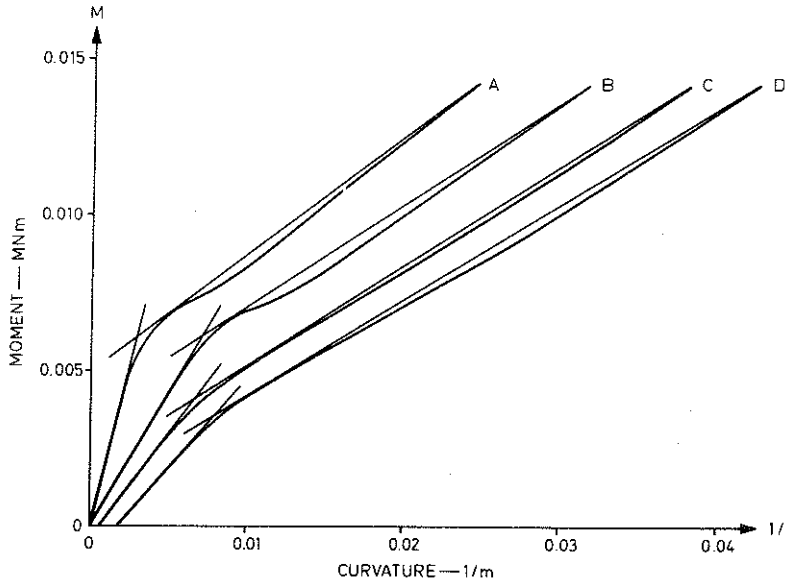

Figure 5.17 The moment-curvature relations for a plate segment calculated according to method A and the simplified relations. A = short-term load, B = basic creep at 100% RH during seven years, C = drying at 40 % RH during 100 days, D = drying at 40% RH during seven years. Section data: b = 1.0, h = 0.1, c/h = 0.1, $A_s = 0.0005$, $A_s' = 0$, $f_{ccm} = 20$ and $f_{st} = 400$. $\alpha_c = 10 \cdot 10^{-6}$ and $\epsilon_{css} = 500 \cdot 10^{-6}$.

The flexural rigidity at cracked state may be determined with the aid of equations A3.32 and A3.33 in Appendix A3. However, the flexural rigidity becomes somewhat large, since the derivation is based on the assumption that the tensile stresses of concrete are neglected. However, this condition may be evaded by a procedure similar to the one used for the determination of the rigidity for segments subjected to pure creep, i.e. by dividing the rigidity derived by a rigidity derived similarly with neither creep nor shrinkage, and then multiply with the flexural rigidity $(EI)_r$ according to section 5.2.1 (Eq. 5.4) which takes the tensile stresses of concrete into consideration. Eqs. A3.32 and A3.33 are very laborious to use for the calculation of the flexural rigidity. However, by numerical calculations it is possible to show that at the same creep coefficient ϕ the same flexural rigidity is received as upon a calculation according to Eq. A3.38, where the influence of shrinkage is disregarded. This implies that the flexural rigidity may be determined in the same way as according to section 5.2.4 (Eq. 5.7), if the influence of drying creep is included in the creep coefficient. Shrinkage, uniformly or non-uniformly distributed over the cross-section, consequently does not affect the rigidity in cracked state. The flexural rigidity, calculated according to this simplified method agrees well with the one received by the more accurate calculation (method A).

$$(EI)_{rcs} = (EI)_{rc} \tag{5.10}$$

Shrinkage causes a decrease of the cracking moment, which is derived in Appendix A3 and may be calculated according to Eq. A3.20.

$$M_{rcs} = \frac{\sigma_r \cdot b \cdot h^2}{6} \cdot \beta_2 - \frac{b \cdot h^2 \cdot \varepsilon_{css} \cdot E_c}{3(1 + \phi)} \cdot \beta_5 \tag{5.11}$$

where $\beta_2 = \dfrac{1 + \psi + \psi' + 3(1 - 2c/h)^2 \cdot (\psi + \psi' + 4\psi \cdot \psi')}{1 + 2\psi \cdot c/h + 2\psi' \cdot (1 - c/h)}$

is shown in Fig. 5.9 for c/h = 0.1 and where

$$\beta_5 = \frac{(\gamma - 1) \cdot (\psi \cdot (2 - 3c/h) \cdot c/h - \psi' \cdot (1 - c/h) \cdot (1 - 3c/h))}{1 + 2\Psi \cdot c/h + 2\Psi' \cdot (1 - c/h)} +$$

$$+ \frac{\psi \cdot (2 - 3c/h) - \psi' \cdot (1 - 3c/h) + 6\psi \cdot \psi' \cdot (1 - 2c/h)^2}{1 + 2\psi \cdot c/h + 2\psi' \cdot (1 - c/h)}$$

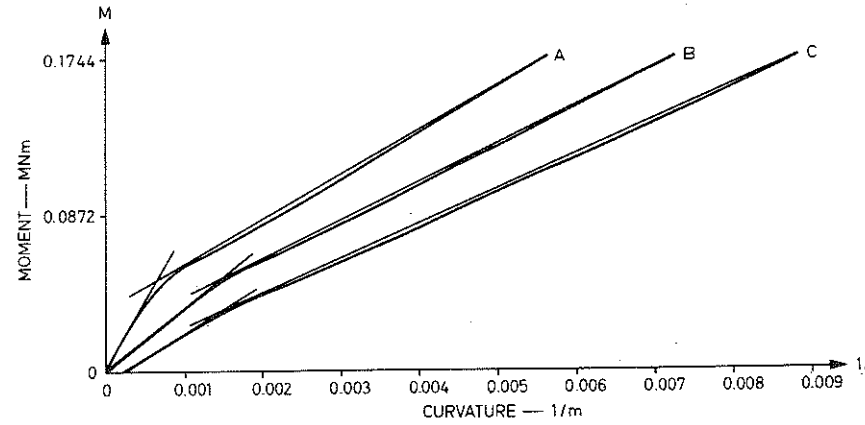

Figure 5.18 The moment-curvature relations calculated according to method A for a beam segment. A = short- term load, B = basic creep at 100% RH during 45 years, C = drying at 40% RH during 45 years. Section data: b = 0.25, h = 0.5, c/h = 0.1, A_s = 0.00125, $A_s' = A_s/2$, f_{ccm} = 25 and f_{st} = 400. $\alpha_c = 10 \cdot 10^{-6}$ and $\varepsilon_{css} = 500 \cdot 10^{-6}$.

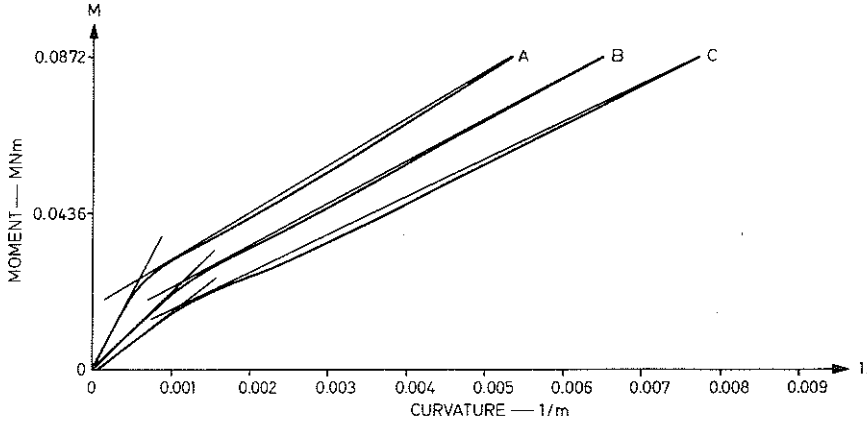

Figure 5.19 The moment-curvature relations calculated according to method A for a beam segment. A = short-term load, B = basic creep at 100% RH during 11 years, C = drying at 40% RH during 11 years. Section data: b = 0.125, h = 0.5, c/h = 0.1, $A_s = A_s' = 0.000625$, f_{ccm} = 25 and f_{st} = 400. $\alpha_c = 10 \cdot 10^{-6}$ and $\varepsilon_{css} = 500 \cdot 10^{-6}$.

is shown in Fig. 5.21 for c/h = 0.1.

The fictitious tensile strength σ_r becomes less than f_{cbm} owing to the non-linear shrinkage over the cross-section during the drying process. If it is chosen to vary with shrinkage according to

$$\sigma_r = f_{cbm} \cdot (1 - 500 \cdot \varepsilon_{css}) \tag{5.12}$$

the agreement between the simplified calculation of the cracking moment according to Eq. 5.11 and the more accurate one according to method A will be satisfying.

5.2.6 Influence of creep, shrinkage and normal force on curvature at constant moment and normal force

Except creep and shrinkage, also a normal force often exists, which may be assumed to act in the centroid of the cross-section of the concrete. The curvature at zero moment, cracking moment and the flexural rigidities at uncracked and crakced states may be calculated according to Appendix A3.

According to Eq. A3.17 we get

$$\frac{1}{r_o} = \frac{\varepsilon_{css}}{h} \cdot \beta_4 - \frac{N \cdot (1 + \phi)}{b \cdot h^2 \cdot E_c} \cdot \beta_6 \tag{5.13}$$

where the normal force N is positive in tension, β_4 is shown by Eq. 5.8 and

$$\beta_6 = \frac{6\,(1 - 2c/h) \cdot (\psi - \psi')}{1 + \psi + \psi' + 3(1 - 2c/h)^2 \cdot (\psi + \psi' + 4\psi \cdot \psi')}$$

is shown by Fig. 5.22 for c/h = 0.1.

The flexural rigidity at uncracked state is not affected by the normal force and may be determined according to Eq. 5.9

$$(EI)_{ocsN} = (EI)_{ocs} \tag{5.14}$$

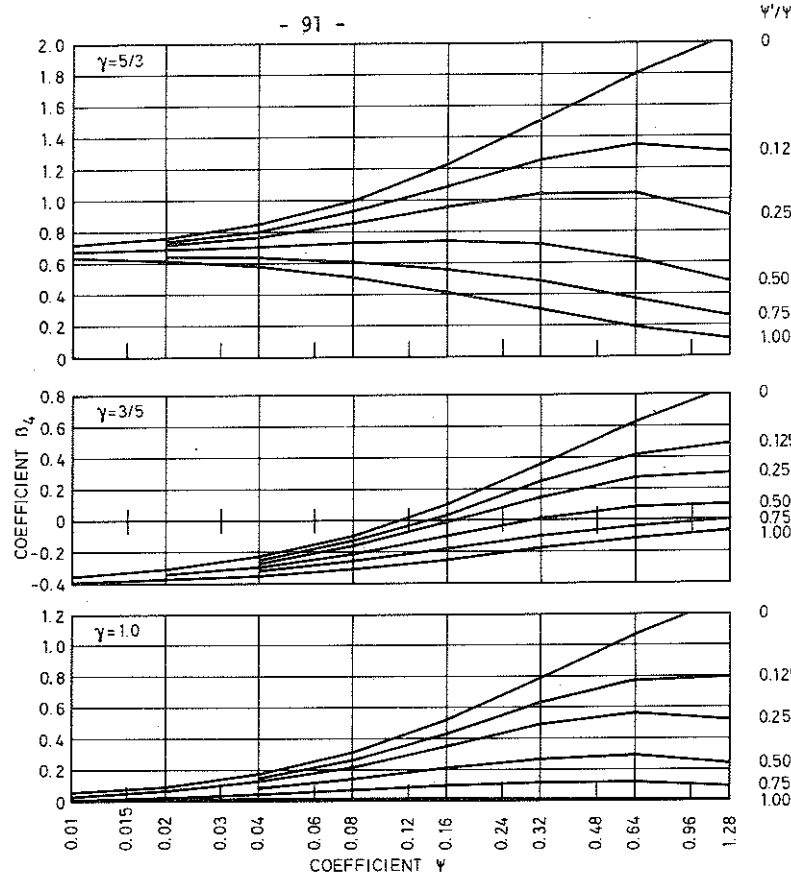

Figure 5.20 The coefficient β_4 for the calculation of $1/r_0$ according to Eqs. 5.8 and 5.13. Valid for c/h = 0.1.

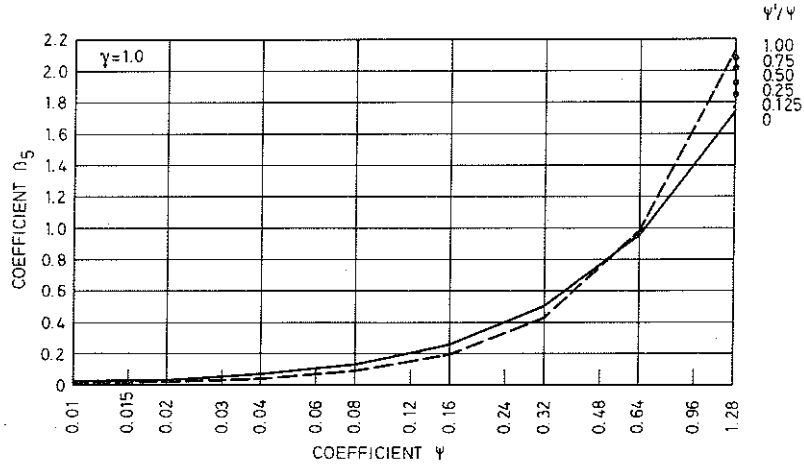

Figure 5.21 The coefficient β_5 for the calculation of the cracking moment according to Eqs. 5.11 and 5.16. Valid for c/h = 0.1. For $3/5 \leq \gamma \leq 5/3$ the deviation is less than 10% of the value for $\gamma = 1$.

It is very laborious to determine the flexural rigidity at cracked state according to Appendix A3, and then besides take into consideration the influence of the tension zone of concrete according to section 5.2.4. Numerical calculations of the flexural rigidity according to these relations have therefore been performed where the parameters M, N, Ψ, Ψ', ϕ and ε_{css} are varied within their current ranges, and the results from these calculations show that the flexural rigidity, may be determined by the following equation, if shrinkage does not exist

$$(EI)_{rcN} = (EI)_{rc} \cdot \beta_7 \qquad (5.15)$$

where $(EI)_{rc}$ is flexural rigidity in cracked state at basic creep according to Eq. 5.7 (in ϕ the influence of drying creep will be included), and β_7 is shown in Table 5.1. At a large shrinkage β_7 decreases by up to 20% of the difference between 1 and the value of β_7, when shrinkage is lacking. An eventual non-uniformity of shrinkage does not involve any change.

The cracking moment is determined according to Eq. A3.26.

$$M_{rcsN} = \frac{b \cdot h^2 \cdot \sigma_r}{6} \cdot \beta_2 - \frac{b \cdot h^2 \cdot \varepsilon_{css} \cdot E_c}{3(1 + \phi)} \cdot \beta_5 - \frac{N \cdot h}{6} \cdot \beta_8 \qquad (5.16)$$

where $\beta_8 = \dfrac{1 - 6(1 - 2c/h) \cdot (\psi \cdot c/h - \psi' \cdot (1 - c/h))}{1 + 2\psi \cdot c/h + 2\psi' \cdot (1 - c/h)}$

is shown by Fig. 5.23 for c/h = 0.1 and σ_r is determined according to Eq. 5.12 and β_2 and β_5 according to Eq. 5.11.

5.2.7 Relaxation of moment caused by creep and shrinkage at constant curvature

In the previous sections moment-curvature relations have been established under the assumption of a constant moment during time under load. If, instead, a constant curvature is imposed, and the corresponding moment is calculated (relaxation) the result will be different. The relations in Fig. 5.24, calculated according to method A show that the curves at relaxation (C, E)

Table 5.1 The coefficient β_7 for a determination of rigidity at cracked state according to Eq. 5.15.

$\frac{N \cdot h}{M}$	ψ'/ψ	$\psi = (1 + \phi) \cdot \alpha \cdot A_s/(b \cdot h)$			
		0.04	0.15	0.60	2.0
-4	0		1.30	1.04	1.00
-4	1		1.57	1.20	1.06
-3	0	1.51	1.15	1.03	1.00
-3	1	1.62	1.26	1.11	1.05
-2	0-1	1.12	1.06	1.02	1.01
-1	0-1	1.01	1.01	1.00	1.00
0	0-1	1.00	1.00	1.00	1.00
1	0-1	0.99	0.99	0.99	1.00
2	0-1	0.93	0.91	0.92	0.96

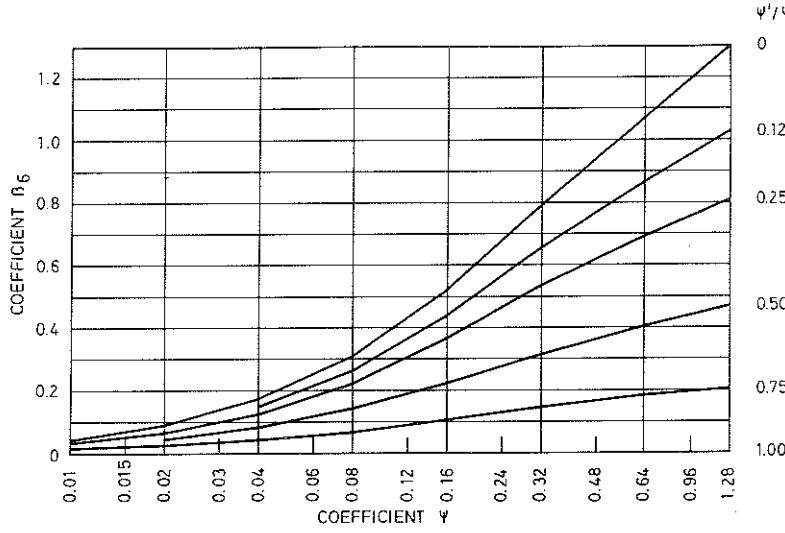

Figure 5.22 The coefficient β_6 for the calculation of the curvature $1/r_o$ according to Eq. 5.13. Valid for c/h = 0.1.

are rather much below the corresponding curves (B, D) calculated for constant load.

The relaxation relations would be appropriate to use for, for example, built in unloaded concrete beams, subjected to support movements. For concrete structures however, the dead load constitutes a large part of the loading, and therefore combinations of the relations for constant moment and relaxation are probably more current. This will be further dealt with in chapter 6.

5.3 Deformations caused by shear force

The shear deformation is calculated by the formula

$$\beta = V/GA \tag{5.17}$$

where V denotes the shear force and GA the shear rigidity.

At uncracked state shear rigidity approximately may be put equal to the area of the cross-section multiplied by the elastic modulus of concrete divided by 2. The deformation of shear force is normally negligible for an uncracked segment.

At cracked state the shear force may be assumed to be carried according to the lattice analogy /66DI/ and its deformation may be calculated with the aid of this. The concrete compression zone then works as a compression flange and the tensile reinforcement as a tension flange. The shear reinforcement then works as tension rods and the inclined lattices of concrete between the cracks as compression rods. Simultaneously as the shear deformation takes place, the concrete compression zone will be unloaded and an additional tensile force of the same magnitude will be charged to the tensile reinforcement, causing an additional curvature.

If the cracks are assumed to form an angle of 45^{0} with the longitudinal axis of the beam, the shear rigidity may be calculated with the formula /66DI/

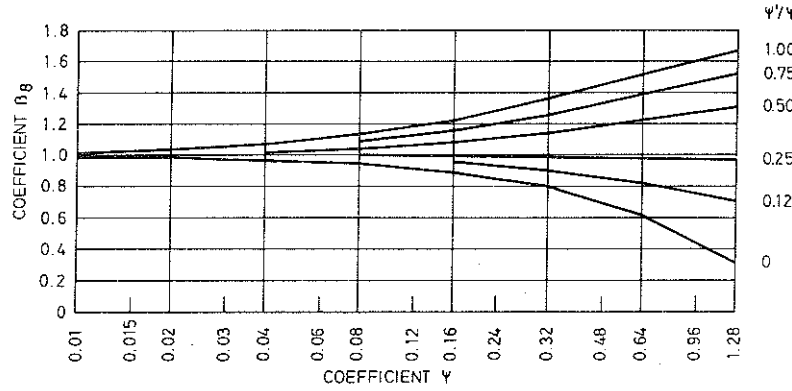

Figure 5.23 The coefficient β_8 for the calculation of the cracking moment according to Eq. 5.16. Valid for c/h = 0.1.

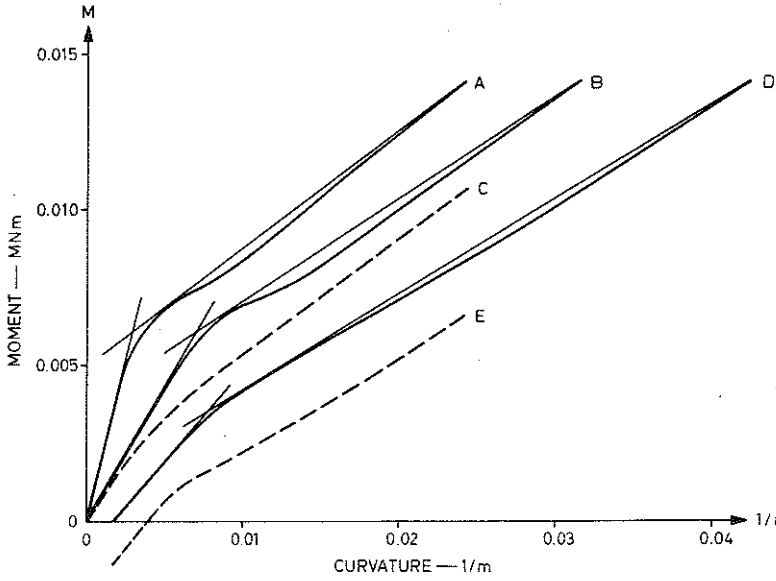

Figure 5.24 The moment-curvature relations calculated according to method A for a plate segment. A = short-term load, B = basic creep at 100% RH during seven years, C = relaxation at 100% RH during seven years, D = drying at 40% RH during seven years, E = relaxation at 40% RH during seven years. Section data: b = 1.0, h = 0.1, c/h = 0.1, $A_s = 0.0005$, $A'_s = 0$, $f_{cbm} = 20$ and $f_{st} = 400$. $\alpha_c = 10 \cdot 10^{-6}$ and $\varepsilon_{css} = 500 \cdot 10^{-6}$.

$$GA = \frac{\rho_v \cdot E_s \cdot b \cdot z}{k_1 + k_2 \cdot \alpha \cdot \rho_v} \qquad (5.18)$$

where $\rho_v = \frac{A_b}{t \cdot \sin v \cdot b}$

A_b = cross-section area of the stirrup

t = horizontal center to center distance of the stirrups

v = the angel of the stirrup with respect to the axis of the beam

z = distance from tensile reinforcement to the centroid of the resultant compressive force of concrete

k_2 = 4, when the stirrups form a 45^o angle with the axis of the beam

k_2 = 1, when the stirrups form a 90^o angle with the axis of the beam

$k_1 = \frac{\tau - \tau_o}{\tau}$

τ = current shear stress

τ_o = shear stress required for a shear crack to occur

Theoretically, the constant k_1 should have had the value 1. However, at tests it has been observed that the stress in the shear reinforcement is lower than the one theoretically calculated by the lattice analogy. Consequently, Dilger /66DI/ has given k_1 the above mentioned value in order to take this into consideration and to obtain a better agreement between measured and calculated shear rigidity.

The additional force of tensile reinforcement at vertical stirrups is equal to half the shear force, and at 45^o inclined stirrups equal to zero. For vertical stirrups the additional curvature may be calculated to

$$\Delta(1/r) = \frac{\varepsilon_s - \varepsilon_c}{z} = \frac{V}{2z}\left(\frac{1}{E_s \cdot A_s} - \frac{1}{b \cdot x \cdot E_c}\right)$$

Since the concrete strain normally is small in comparison to the reinforcement tensile strains we may write approximately

$$\Delta(1/r) = \frac{V}{2\ E_s \cdot A_s \cdot d} \qquad (5.19)$$

The additional curvature is assumed to be zero until cracks occur and then it increases linearly and reaches its full value at the double stress. This is due to the fact that there must be several cracks of a certain length before the deformation can be assumed to be fully developed. Technical difficulties in calculation may also appear if curvature is changed stepwise.

Since the same criteria must be used for the case when carrying according to the lattice analogy starts to function for the two deformations, τ_0 is replaced in the constant k_1 by the shear stress which prevails at cracking if this is caused by moment stresses.

At shrinkage and creep α in Eq. 5.18 might be replaced by $(1+\phi)\cdot\alpha$, as a rough approximation and β in Eq. 5.17 is multiplied with $(1+\phi)$. These deformation models have been used in calculations in section 6.3.

6 BEAMS AT SERVICEABILITY LIMIT STATE

Simply supported beams, supported cantilever beams and beams clamped at both ends are studied. They are subjected to uniform lateral load. Deflection, moment distribution and coefficients for the determination of moment redistribution at support displacements are calculated and accounted for as figures or tables. These are given as functions of material parameters, geometric parameters, safety against failure and the ratio between the areas of support and span tensile reinforcement, at both short-term load, creep and simultaneous creep and shrinkage. An approximate formula is established for the determination of moment redistribution at support displacements for non-loaded supported cantilever beams and beams clamped at both ends. In Appendix A4 a calculation method with aid formulae for the determination of the moment distribution at other load and end conditions is accounted for. In section 6.3 calculated and measured moment distributons are compared for supported cantilever beams, which under loading up to failure are subjected to support displacements. In Appendix A5 a formula is established for the determination of the reinforcement stress in a crack for a segment subjected to pure bending.

6.1 Theoretical analysis of moment distribution and deflection for beams subjected to uniform lateral load

At first the calculation assumptions and notations used in the following are described. Only bending deformations have been taken into account. Simplified moment-curvature relations according to chapter 5 have been used. The calculation has been performed by integration of the curvature along the beam with regard to the boundary conditions. Consideration has not been taken to the effects of possible moment redistributions on the moment-curvature relations, i.e. the moment-curvature established for constant moment has been used. Yielding is not assumed to take place in any cross-section. The magnitude of the load is such that safety

against bending failure according to a plastic theory analysis is equal to s. In the determination of the safety against failure the yielding moment has been assumed equal to

$$M_y = 0.82 \cdot h \cdot A_s \cdot f_{st} \tag{6.1}$$

The members are assumed to be beams with rectangular cross-section or to be one-way slabs and to have constant concrete cross-section along their whole length. They are assumed to be reinforced in such a way that the ultimate resisting moment of the cracked section is greater than the cracking moment, and furthermore to have such a design that the deformation caused by shear forces is small and that the safety against shear failure is larger than safety against bending failure.

The effects of the terminations of the reinforcement are neglected, and at positive moment the area of the tensile reinforcement is assumed to be equal to A_{sf} and at negative moment equal to A_{ss}. At negative moment there is also a compressive reinforcement equal to $A_{sf}/4$. The distance from the centroid of the tensile reinforcement to the edge in tension has been assumed one tenth of the total depth of the beam. The same condition is valid for the compressive reinforcement.

In the presentation of the results from the calculations it has appeared advantageous to use a parameter ζ which mainly governs the degree of cracking for the beams, and where a large value of ζ means small cracking and a small value means large cracking. The parameter ζ is defined by the equation

$$\zeta = \frac{f_{cbm} \cdot s}{\rho_{tot} \cdot f_{st}} \tag{6.2}$$

where f_{cbm} denotes the flexural strength of concrete, s the safety against bending failure for the beam, f_{st} the tensile strength of the reinforcement, and ρ_{tot} is the total share of reinforcement. For simply supported beams ρ_{tot} is defined as $\frac{A_{sf}}{b \cdot h}$, for beams clamped at both ends as $\frac{A_{ss} + A_{sf}}{b \cdot h}$, and for supported cantilever beams as

$\frac{n \cdot A_{sf}}{b \cdot h}$ with n given by

$$n = \frac{2 + A_{ss}/A_{sf} + 2\sqrt{1 + A_{ss}/A_{sf}}}{4} \approx 1 + 0.43\ A_{ss}/A_{sf} \qquad (6.3)$$

or

A_{ss}/A_{sf}	1	2	3	4	5	6
n	1.46	1.87	2.25	2.62	2.97	3.32

The definition of ρ_{tot} implies that the load-carrying capacity of the beams is not changed at a redistribution of the reinforcement between support and span as long as ρ_{tot} is constant.

6.1.1 Moment distribution and deflection at short-term load

The support moment at short-term load is shown in Fig 6.1 for beams clamped at both ends and in Fig 6.2 for supported cantilever beams. It is given as a function of the ratio of the areas of support and span tensile reinforcement (A_{ss}/A_{sf}), ζ (Eq. 6.2) and the reinforcement strength divided by the safety against failure (f_{st}/s). For a beam clamped at both ends and with constant flexural rigidity along its length the support moment will be equal to $2/3 \cdot ql^2/8$ and the maximum deviation from this value in the figure is about $\pm$ 15 per cent. For $\zeta = 4$ the beam is uncracked. The great variation for $\zeta = 2$ depends on the fact that the span moment and span cracking moment have almost the same magnitude. For a supported cantilever beam with constant flexural rigidity along its length the support moment will be equal to $ql^2/8$ and the maximum deviation from this value in the figure is about + 28 per cent and - 19 per cent. For $\zeta = 6$ the beam is uncracked. The vertical lines in Figs. 6.1 and 6.2 show the scatter when the strength of concrete f_{ccm} varies between 15 - 60 MPa and f_{st}/s between 229 - 457 MPa. The figures are valid only as long as yielding does not take place in any section, which limits the permissible value of the support moment to

$$1 - s/(1 + n) \leq \frac{M_s}{ql^2/8} \leq s \cdot n/(1 + n) \qquad (6.4)$$

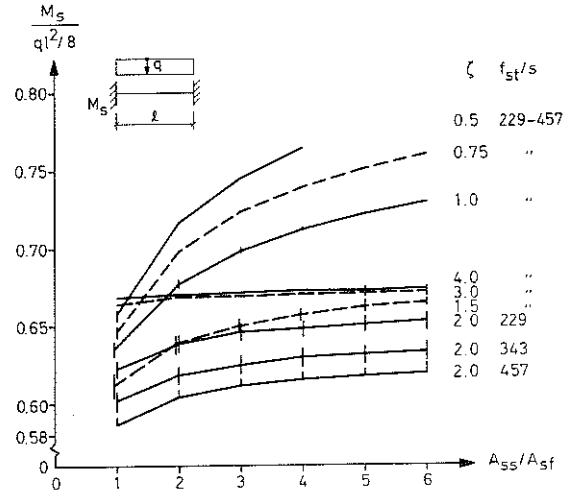

Figure 6.1 The support moment for a beam clamped at both ends subjected to uniform lateral load as a function of the reinforcement distribution (A_{ss}/A_{sf}), ζ (Eq. 6.2) and f_{st}/s. The vertical lines show the scatter when f_{ccm} varies between 15-60 Mpa and f_{st}/s between 229-459 Mpa.

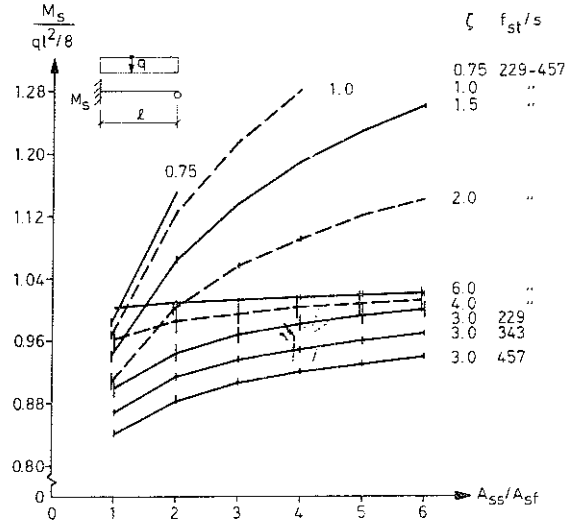

Figure 6.2 The support moment for a supported cantilever beam subjected to uniform lateral load as a function of the reinforcement distribution (A_{ss}/A_{sf}), ζ (Eq. 6.2) and f_{st}/s. The vertical lines show the scatter when f_{ccm} varies between 15-60 Mpa and f_{st}/s between 229-459 Mpa.

for the beam clamped at both ends, and to

$$4 - 8\sqrt{s}\cdot(\sqrt{1+\eta}-1)/\eta \leq \frac{M_s}{q\cdot\ell^2/8} \leq 4s\cdot(\sqrt{1+\eta}-1)^2/\eta \qquad (6.5)$$

for the supported cantilever beam where $\eta = A_{ss}/A_{sf}$

The maximum span moment is determined by the equation

$$\frac{M_f}{q\cdot\ell^2/8} = 1 - \frac{M_s}{q\cdot\ell^2/8} \qquad (6.6)$$

for the beam clamped at both ends and by

$$\frac{M_f}{q\cdot\ell^2/8} = (1 - \frac{M_s}{q\cdot\ell^2/2})^2 \qquad (6.7)$$

for the supported cantilever beam.

From Fig. 6.3 the maximum deflection may be determined for the beam clamped at both ends at short-term load. The deflection diagram is constructed so that for each line the load-carrying capacity is constant if only redistribution of reinforcement between support and span takes place with a preservation of the same value of ρ_{tot}. The figure shows that a redistribution of the reinforcement has little influence on the magnitude of the deflection. The lines are drawn for the strength of concrete f_{ccm} = 35 MPa. The upper limits of the vertical lines are valid for f_{ccm} = 60 MPa and the lower limits for f_{ccm} = 15 MPa. Similarly, the influence of the reinforcement distribution on the deflection at the location of the maximum span moment is small for the supported cantilever beam. The maximum deflection is only slightly larger than the deflection at the location of the maximum span moment. In Figs. 6.4 and 6.5 the deflection at the location of the maximum span moment is shown as a function of ζ and f_{st}/s, for the supported cantilever beam and the beam clamped at both ends. The figures are drawn for f_{ccm} = 35 MPa and A_{ss}/A_{st} = 2 but are valid, with satisfactory accuracy, also for other concrete qualities and reinforcement distributions. In Fig. 6.6 the deflection at the centre for a simply supported beam is shown (f_{ccm} = 35 MPa).

6.1.2 Moment distribution and deflection at basic creep

The moment changes due to basic creep are relatively small which implies that the used moment-curvature relations for constant mo-

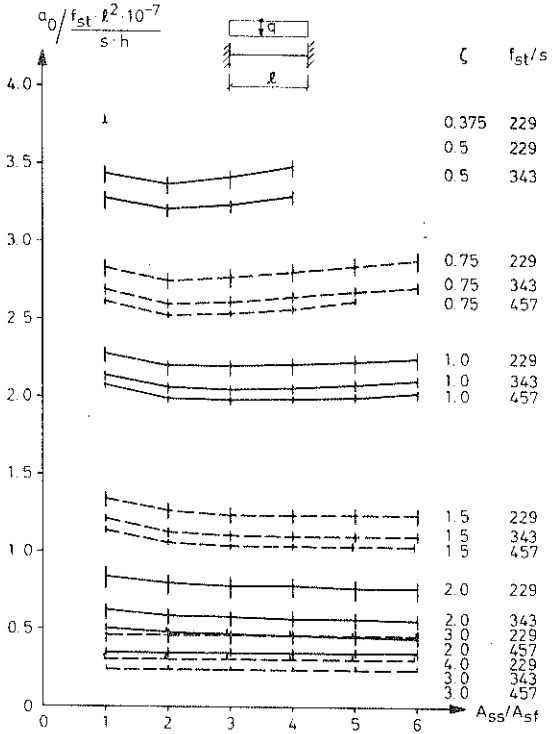

Figure 6.3 The maximum deflection for a beam clamped at both ends subjected to uniform lateral load as a function of the reinforcement distribution (A_{ss}/A_{sf}), ζ (Eq. 6.2) and f_{st}/s. f_{ccm} = 35 Mpa. The vertical lines show the scatter when f_{ccm} varies between 15-60 Mpa. Only bending deformations are considered.

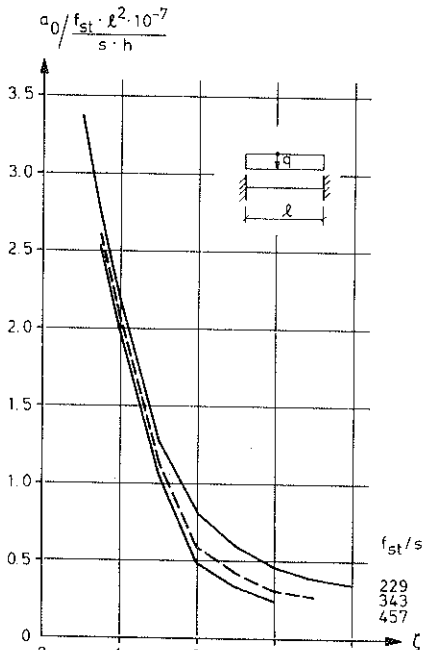

Figure 6.4 The maximum deflection a_0 for a beam clamped at both ends subjected to uniform lateral load as a function of ζ (Eq. 6.2) and f_{st}/s. Only bending deformations are considered.

ments are adequate. Generally, there is a slight increase of the support moment in relation to the one at short-term load, which is shown by the following table

support moment increase, per cent

ζ	6	4	3	2.5	2	1.5	1	0.5	0.375
supported cantilever beam		1-2	1-3		6-8	2-4	0-4	0-5	4-5
beam clamped at both ends	1-5	4-8	8-11	4-7	0-5		-2-5	6-9	

where the variations of the moment increase depend on the variations in f_{ccm} ($15 \leq f_{ccm} \leq 60$) and f_{st}/s ($229 \leq f_{st}/s \leq 457$).

The deflection at the location of the maximum span moment at basic creep is denoted with a_c and the corresponding deflection at short-term load with a_0 (Figs. 6.4 - 6.6). The ratio between the deflections is represented by $\frac{a_c}{a_0(1+\phi)}$ as a function of ζ and f_{st}/s, and is accounted for in Fig. 6.7 for the beam clamped at both ends, in Fig. 6.8 for the supported cantilever beam and in Fig. 6.9 for the simply supported one. The diagrams are valid for f_{ccm} = 35 MPa and a ratio between the areas of support and span tensile reinforcement equal to 2 for the statically indeterminate beams. For other concrete qualities and reinforcement ratios $\frac{a_c}{a_0(1+\phi)}$ deviates not more than a few per cent at the most from the values stated in the figures.

6.1.3 Moment distribution and deflection at creep and final shrinkage

The moment changes due to simultaneous creep and shrinkage are relatively small, which means that the calculation conditions may be considered to be fulfilled. For an uncracked or slightly cracked supported cantilever beam or beam clamped at both ends, the shrinkage counteracts the increase of support moment on account of creep, whereas for more cracked beams the shrinkage coacts with the creep and increases the support moment in relation to the one at short-term

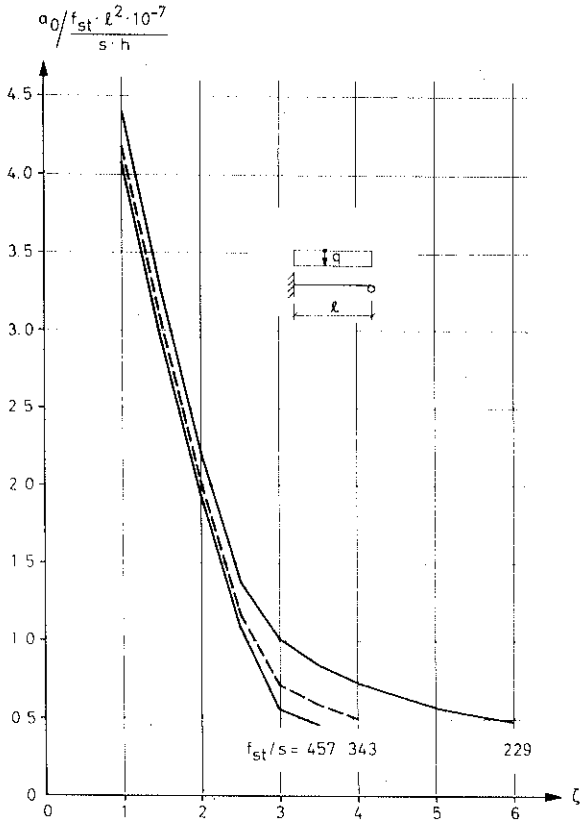

Figure 6.5 The deflection a_0 at the location of the maximum span moment for a supported cantilever beam subjected to uniform lateral load as a function of ζ (Eq. 6.2) and f_{st}/s. Only bending deformations are considered.

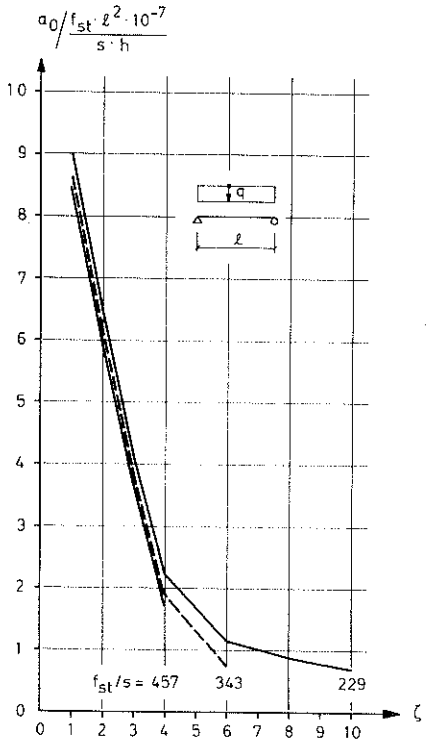

Figure 6.6 The maximum deflection a_0 for a simply supported beam subjected to uniform lateral load as a function of ζ (Eq. 6.2) and f_{st}/s. Only bending deformations are considered.

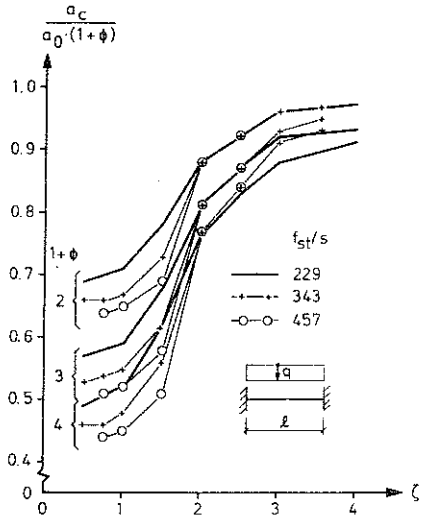

Figure 6.7 The maximum deflection a_c for a beam clamped at both ends subjected to uniform lateral load and basic creep as a function of ζ (Eq. 6.2), the creep coefficient ϕ, f_{st}/s and a_0 (Fig. 6.4). Only bending deformations are considered.

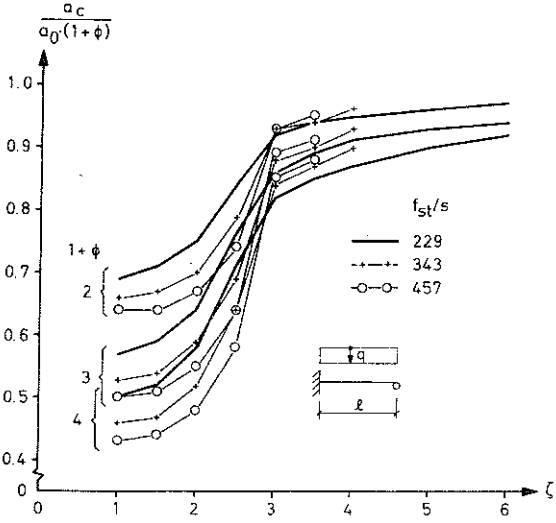

Figure 6.8 The deflection a_c at the location of the maximum span moment for a supported cantilever beam subjected to uniform lateral load and basic creep as a function of ζ (Eq. 6.2), the creep coefficient ϕ, f_{st}/s and a_0 (Fig. 6.5). Only bending deformations are considered.

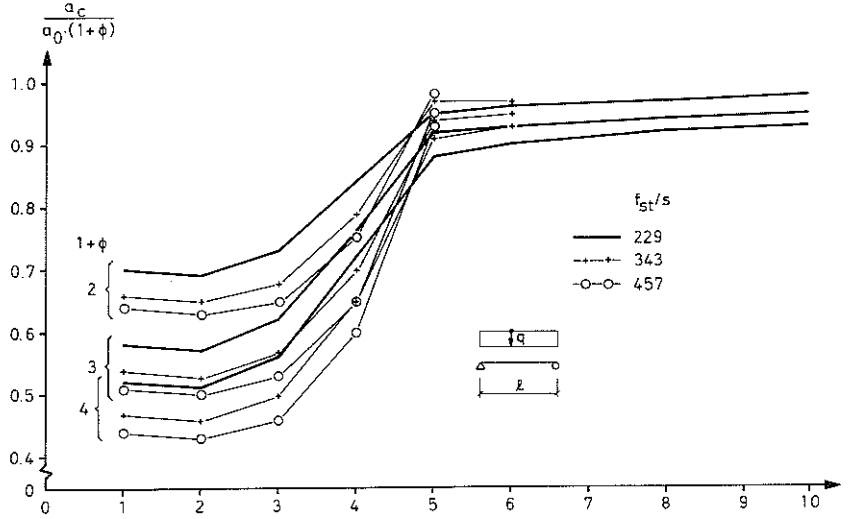

Figure 6.9 The maximum deflection a_c for a simply supported beam subjected to uniform lateral load and basic creep as a function of ζ (Eq. 6.2), the creep coefficient ϕ, f_{st}/s and a_0 (Fig. 6.6). Only bending deformations are considered.

load. For the supported cantilever beams the shrinkage decreases the support moment for $\zeta \geq 2.5$ so that it will be maximally 6% smaller than at short-term load. If $\zeta \leq 1.5$ the shrinkage and the creep increase the support moment so that it will be maximally 8% larger than at short-term load. For the beams clamped at both ends the shrinkage decreases the support moment for $\zeta \geq 4$ on account of cracking at support so that it will be maximally about 6 per cent smaller than at short-term load. If $\zeta < 2.5$ the shrinkage and the creep increase the support moment so that it will be maximally about 10% larger than the moment at short-term load due to heavier cracking in span.

The deflection at the location of the maximum span moment at creep and shrinkage is denoted by a_{cs} and the deflection for short-term load by a_0 (Figs. 6.4 - 6.6). The ratio between the deflections is represented by $\frac{a_{cs}}{a_0 \cdot (1 + \phi)}$ and is accounted for in Figs. 6.10 - 6.12. ϕ is the creep coefficient. The diagrams are valid for the concrete strength $f_{ccm} = 35$ MPa and $A_{ss}/A_{sf} = 2$. At other concrete strengths and ratios between the tensile reinforcement areas the deviation is at the most a few per cent when $\frac{a_{cs}}{a_0 \cdot (1 + \phi)}$ is smaller than 1 and up to about 10% when $\frac{a_{cs}}{a_0 \cdot (1 + \phi)}$ is larger than 1.5.

For a beam, which is uncracked or slightly cracked in the initial state, the deflection change will be larger at a great shrinkage combined with a small creep, since the shrinkage reduces the cracking moment and in this case the creep counteracts this reduction very little.

6.1.4 Moment redistribution at support displacement

The design of the beams, the load of the beams and the assumed positive direction of the support displacement as well as the formula for the determination of the support moment changes are shown in Fig. 6.13.

The same calculation conditions as in section 6.1 are valid. The

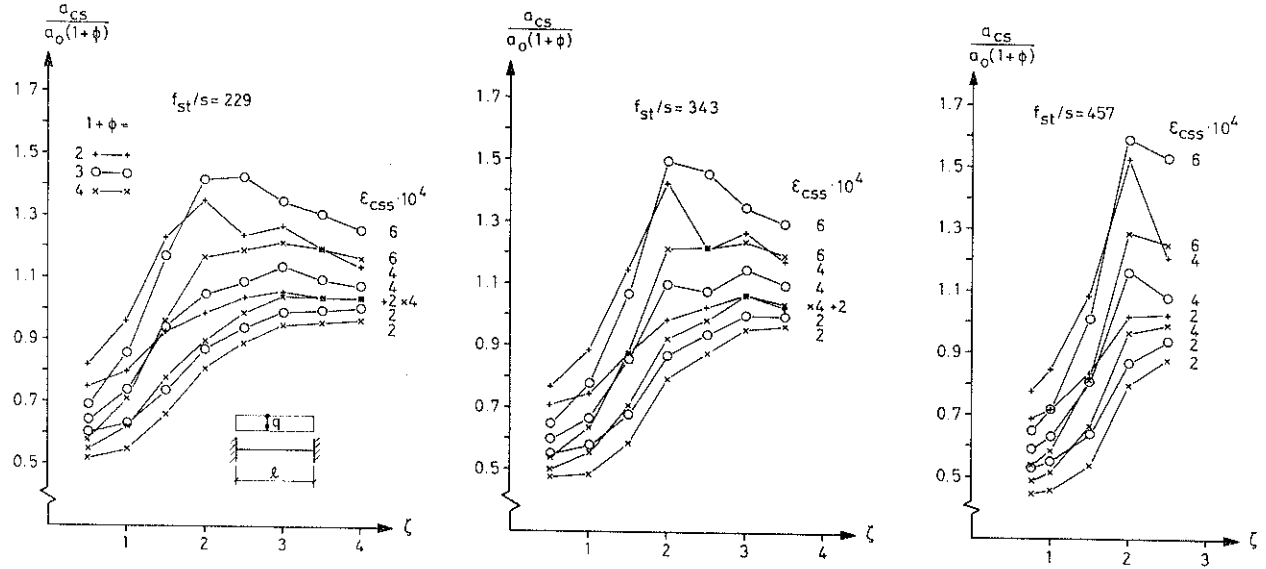

Figure 6.10 The maximum deflection a_{cs} for a beam clamped at both ends subjected to uniform lateral load, creep and final shrinkage as a function of ζ (Eq. 6.2), the creep coefficient ϕ, the final shrinkage ε_{css}, f_{st}/s and a_o (Fig. 6.4). Only bending deformations are considered.

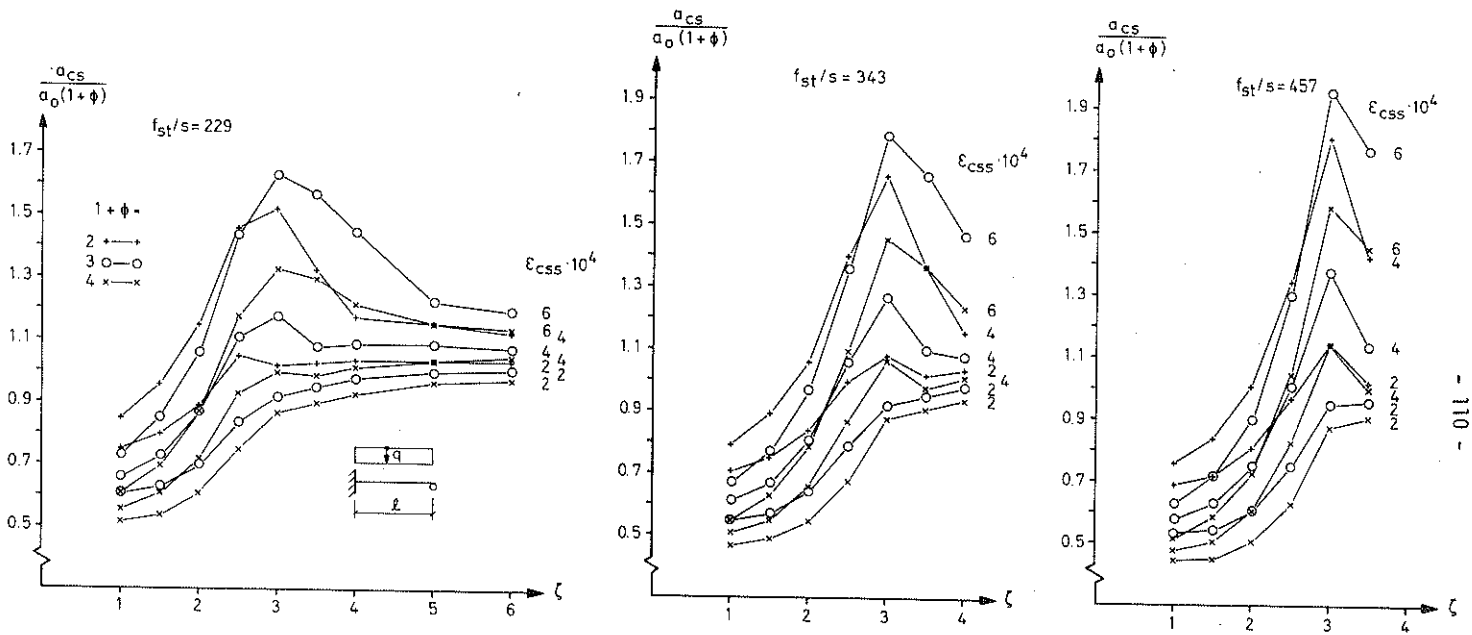

Figure 6.11 The deflection a_{cs} at the location of the maximum span moment for a supported cantilever beam subjected to uniform lateral load, creep and final shrinkage as a function of ζ (Eq. 6.2), the creep coefficient ϕ, the final shrinkage ε_{css}, f_{st}/s and a_0 (Fig. 6.5). Only bending deformations are considered.

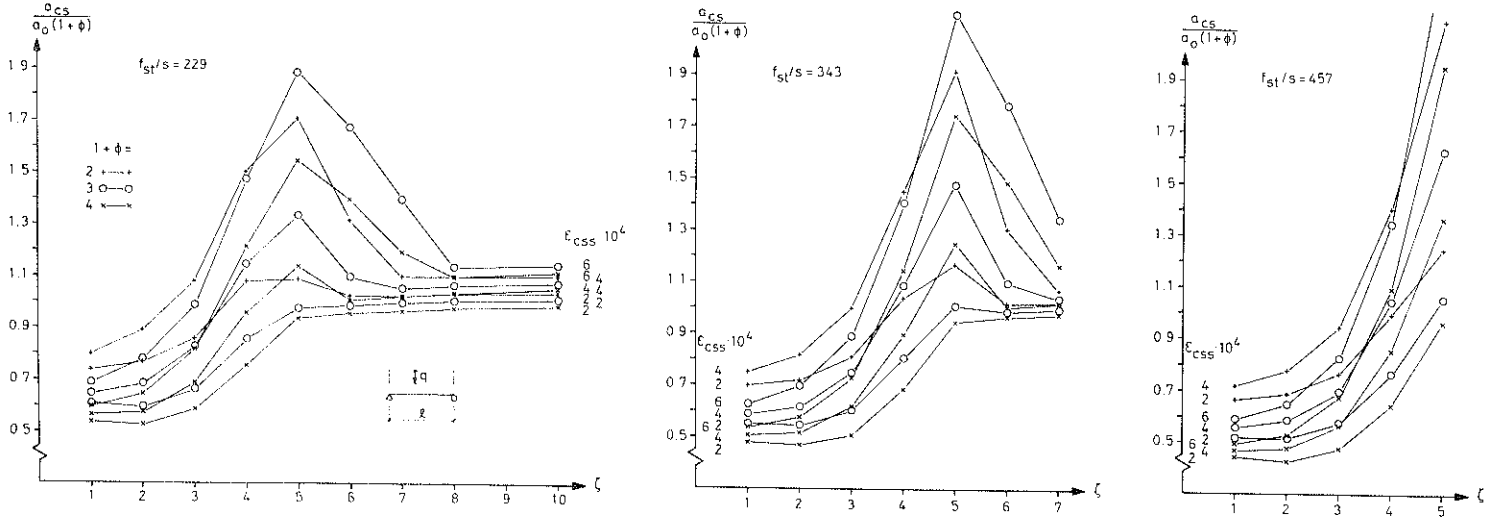

Figure 6.12 The maximum deflection a_{cs} for a simply supported beam subjected to uniform lateral load, creep and final shrinkage as a function of ζ (Eq. 6.2), the creep coefficient ϕ, the final shrinkage ε_{css}, f_{st}/s and a_o (Fig. 6.6). Only bending deformations are considered.

loading and the support displacement are assumed to take place simultaneously.

The factor ξ_s in Fig. 6.13 for the strength of concrete f_{ccm} = 35 MPa and at a support displacement a = $f_{st} \cdot \ell^2 \cdot 10^{-7}/(s \cdot h)$ for different magnitudes of creep and shrinkage is shown in Table 6.1 for supported cantilever beams and in Table 6.2 for beams clamped at both ends.

At short-term load and f_{ccm} = 60 ξ_s is increased by maximally 8 units and for f_{ccm} = 15 ξ_s is decreased by maximally 8 units. If creep and shrinkage take place, the change of ξ_s with the strength of concrete will be considerably smaller. For $\zeta \leq 2$ the rigidity for the determination of the moment change is relatively independent of the magnitude of the support displacement, which is due to the fact that the beams are rather heavily cracked from the load alone and that the magnitude of the support displacement has little influence on the cracking and does not cause any further cracking of significance.

For beams with a larger value of ζ the magnitude of the support displacement has a considerably larger influence, and this influence increases for higher values of ζ. For these beams the rigidity decreases with the magnitude of the support displacement, since the formation of cracks at support increases and hence the rigidity decreases. These beams are at the same time relatively lightly reinforced and therefore the difference between the rigidity at cracked and uncracked state is great.

For the beam clamped at both ends the moment reduction at the one end will be approximately the same as the moment increase at the other end for $\zeta \leq 2$, whereas it will be larger for higher values of ζ since the beam will be considerably less cracked or uncracked and consequently much more rigid at the support where the moment reduction takes place.

For beams with the same strength of concrete, (f_{ccm}) reinforement quality (f_{st}), safely against failure (s) and the same total percentage of reinforcement (ρ_{tot}) and the same ratio between the

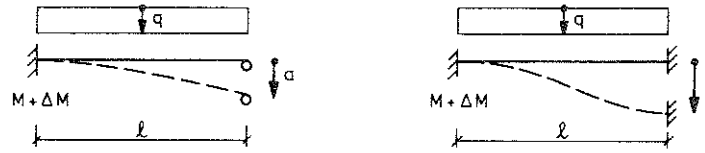

$$\Delta M = \frac{3 \cdot EI}{\ell^2} \cdot a \qquad \Delta M = \frac{6 \cdot EI}{\ell^2} \cdot a$$

$$EI = \frac{b \cdot h^3}{12} \cdot E_c \cdot \xi_s \cdot 10^{-2}$$

Figure 6.13 Notations and formulae for the determination of the change of the support moment at support displacement.

Table 6.1 The coefficient ξ_s defined according to Fig. 6.13 for the determination of rigidity upon the calculation of the changes of the support moment for a supported cantilever beam subjected to uniform lateral load as a function of ζ (Eq. 6.2), A_{ss}/A_{sf}, f_{st}/s, the creep coefficient ϕ and the final shrinkage ε_{css}.

$1+\phi$	1	2	3	2	3	3	4	4	f_{st}/s	$\frac{A_{ss}}{A_{sf}}$	a direction
$\varepsilon_{css}\cdot 10^6$	0	0	0	200	200	400	400	600			
ζ											
6	103	53	37	51	35	28	24	19	229	1	+ -
5	84	52	37	40	32	25	21	18			+
4	59	40	30	34	28	23	20	15			+
3	54	36	28	30	27	20	19	15			+
2.5	44	33	26	27	25	20	19	16			+ -
2	41	31	26	28	25	22	20	18			+ -
1.5	45	35	29	32	28	26	23	22			+ -
1	57	44	37	42	36	34	31	29			+ -
0.5	99	75	67	73	61	59	52	51			+ -
5	104	54	37	50	36	28	23	19			-
4	97	49	34	40	30	25	21	15			-
3	66	40	30	30	28	20	19	15			-
6	104	54	37	52	36	31	26	20		2	+ -
5	93	54	38	44	35	28	24	20			+
4	72	45	33	40	32	27	23	18			+
3	67	43	33	37	32	23	22	17			+
2.5	54	39	30	41	27	22	21	17			+
2	46	34	30	31	29	25	22	20			+ -
1.5	50	40	33	36	32	29	26	24			+ -
1	67	51	42	48	41	38	34	32			+ -
5	105	55	38	51	36	30	25	21			-
4	101	52	36	45	34	28	24	16			-
3	75	46	34	33	33	21	20	16			-
2.5	48	36	29	30	27	22	20	18			-
6	105	55	38	52	36	32	27	21		4	+ -
5	99	55	39	48	37	30	25	21			+
4	83	49	36	44	34	30	25	20			+
3	78	49	36	41	35	26	24	17			+
2.5	65	46	36	38	33	24	22	19			+
2	61	42	33	35	30	26	23	21			+
1.5	59	43	35	39	33	30	27	25			+
5	105	55	39	52	37	32	26	22			-
4	104	54	38	48	36	31	25	16			-
3	86	50	37	34	35	22	21	16			-
2.5	49	38	31	30	27	23	21	17			-
2	46	36	29	31	27	24	22	20			-
1.5	51	39	33	37	31	29	26	24			-
4	46	32	25	28	23	20	17	12	343	1	+
3	43	29	23	22	22	15	14	12			+
2.5	30	24	20	20	18	15	14	12			+ -
2	28	22	19	21	19	16	15	14			+ -
1.5	30	25	21	23	21	19	17	16			+ -
1	39	31	27	30	26	25	23	21			+ -
0.5	68	53	45	51	44	43	38	37			+ -
4	94	47	32	38	28	22	19	12			-
3	49	33	25	22	21	15	14	12			-

$1+\phi$	1	2	3	2	3	3	4	4	f_{st}/s	$\frac{A_{ss}}{A_{sf}}$	a direction
$\varepsilon_{css} \cdot 10^6$	0	0	0	200	200	400	400	600			
ζ											
4	57	38	29	33	27	23	20	14	343	2	+
3	53	35	27	27	26	18	17	13			+
2.5	38	29	24	25	22	17	16	14			+
2	35	27	22	24	21	19	17	15			+
1.5	36	28	24	27	24	22	20	18			+ -
1	46	36	30	35	30	28	25	24			+ -
4	98	50	34	43	31	26	21	13			-
3	59	38	29	24	25	16	15	13			-
2.5	33	26	22	21	20	17	16	14			-
2	31	25	21	23	20	18	17	15			-
4	67	43	31	38	30	26	22	17		4	+
3	63	41	31	32	30	21	19	14			+
2.5	46	35	28	29	25	19	17	14			+
2	43	31	25	26	23	20	18	16			+
1.5	41	31	26	29	25	23	20	19			+
4	100	51	35	46	33	28	23	13			-
3	65	43	32	24	26	17	16	13			-
2.5	33	27	23	22	21	17	16	13			-
2	32	25	22	24	20	18	17	15			-
1.5	35	28	24	26	23	21	19	18			-
3	36	25	20	18	17	12	12	10	457	1	+ -
2.5	23	19	16	16	15	12	12	10			+ -
2	21	18	15	16	15	13	12	11			+ -
1.5	23	19	17	18	16	15	14	13			+ -
1	29	24	21	23	21	20	18	17			+ -
3	45	31	24	21	21	15	14	11		2	+ -
2.5	29	23	20	20	18	14	13	11			+ -
2	27	21	18	19	17	15	14	12			+ -
1.5	28	22	19	21	19	17	16	15			+ -
1	35	28	24	27	24	23	20	19			+ -
2.5	25	20	17	17	16	13	13	11			-
2	23	19	17	18	16	15	14	12			-
3	53	35	27	26	25	18	16	12	457	4	+
2.5	36	28	23	23	21	15	14	12			+
2	33	25	20	21	18	16	15	13			+
1.5	31	24	21	23	20	18	17	15			+
3	46	39	29	19	19	13	13	10			-
2.5	25	21	18	18	16	13	13	11			-
2	24	20	18	19	17	15	13	12			-
1.5	27	22	19	21	19	17	16	15			

areas of the tensile reinforcement at support and in span (A_{ss}/A_{sf}) we get the same moment change in percentage if the expression $a \cdot h/\ell^2$ is constant. For low values of ζ we get the same total moment change if the parameters in the expression $a \cdot h^3/\ell^2$ are changed in such a way that the value of the expression is not changed.

In order to examine the influence of the loading history on the moment change, refined calculations (method A) have been performed for a supported cantilever beam. The beam has been divided longitudinally into 9 segments and each segment has been divided into ten concrete elements and two reinforcement elements, and consideration has been taken to the load history, the drying and creep process of each element. The magnitude of the support displacement, the design and the load intensity of the beam have been chosen so that as great differences as possible are obtained between the cracking patterns and hence the moment distribution at the different loading histories. The quantities have been chosen so that if the support displacement takes place first or at the same time as the loading, cracking occurs only at the support, whereas if the loading takes place first cracking is also developed in the span. ($b=1.0$, $h=0.2$, $d=0.18$, $\ell=4.0$, $A_{sf}=0.000944$, $A_{ss}/A_{sf}=2.06$, $f_{ccm}=35$, $f_{st}=400$, $\alpha_c=10 \cdot 10^{-6}$, $\varepsilon_{css}=500 \cdot 10^{-6}$, $H_{en}=40\%$, $q=0.03513$, $a=0.009$). The ratio between the rigidities at support and in span has its smallest value if the support displacement takes place first, since the cracking zone at support gets larger in this case than if the loading takes place first or at the same time as the support displacement when there is no cracking in span. If the loading takes place first, the ratio between the rigidities has its largest value and we get the largest support moment at this loading history. The maximum difference between the largest and the smallest support moments at the different loading histories is below 5% at short-term load. At long-term load the difference decreases due to creep and if there is shrinkage at the same time the difference decreases further since the cracking moment is reduced, and we get the same cracking patterns independently of the loading history. This means that the moment change at support displacements in normally valid independently of the loading history at long-term load and with satisfactory accuracy at short-term load.

Table 6.2 The coefficient ξ_s defined according to Fig. 6.13 for the determination of the rigidity upon the calculation of the increase of the support moment for a beam clamped at both ends subjected to uniform lateral load as a function of ζ (Eq. 6.2), A_{ss}/A_{sf}, f_{st}/s, the creep coefficient ϕ and the final shrinkage ε_{css}.

$1+\phi$	1	2	3	2	3	3	4	4	f_{st}/s	$\frac{A_{ss}}{A_{sf}}$
ε_{css}	0	0	0	200	200	400	400	600		
ζ										
4	84	54	36	46	36	27	24	16	229	1
3	59	41	32	32	28	20	19	15		
2.5	49	34	27	28	25	20	18	15		
2	43	31	25	28	24	21	19	16		
1.5	43	32	27	29	26	22	21	18		
1	49	37	31	35	31	28	26	24		
0.5	77	59	50	57	49	47	42	40		
4	89	54	37	48	36	29	25	18		2
3	67	45	34	36	31	23	21	17		
2.5	58	38	30	33	28	23	20	17		
2	52	36	29	33	28	24	21	18		
1.5	52	38	31	34	30	26	23	21		
1	58	43	36	41	35	32	29	26		
0.5	91	68	56	65	55	53	46	45		
4	91	55	37	49	36	30	26	19		4
3	73	47	35	39	33	25	22	18		
2.5	64	42	32	36	30	25	22	19		
2	58	40	31	36	36	26	23	20		
1.5	59	42	33	37	32	28	25	22		
1	64	48	39	44	37	34	30	28		
3	43	32	26	25	22	17	15	12		1
2.5	36	26	21	22	19	16	14	12		
2	32	24	20	22	19	16	15	13		
1.5	30	24	20	22	19	17	16	14		
1	33	27	23	25	22	21	19	18		
0.5	53	42	36	40	35	34	31	29		
3	50	36	28	29	25	19	17	14		2
2.5	43	30	24	26	22	19	17	14		
2	39	28	23	26	22	19	17	14		
1.5	37	28	23	25	22	20	18	16		
1	40	31	27	30	26	24	21	20		
0.5	63	49	41	47	40	38	34	33		
3	55	39	30	32	27	21	19	15		4
2.5	48	33	26	29	24	20	18	14		
2	44	31	25	20	24	20	18	16		
1.5	42	31	26	28	24	21	19	17		
1	45	34	29	32	28	25	23	21		
2.5	30	22	18	18	16	13	12	10	457	1
2	27	20	16	18	15	13	12	10		
1.5	23	19	16	17	15	14	13	11		
1	25	21	18	20	18	16	15	14		
0.5	40	32	28	32	28	27	24	23		
2.5	35	25	20	22	19	16	14	12		2
2	32	23	19	21	18	15	14	12		
1.5	29	23	19	20	18	16	15	13		
1	31	25	21	23	21	19	17	16		
2.5	39	28	22	24	21	17	15	13		4
2	36	26	21	24	20	17	15	13		
1.5	32	25	21	22	20	17	16	14		
1	34	27	23	25	22	21	19	17		

The moment change following an instantaneous support displacement decreases considerably with time on account of creep and shrinkage. If the support displacement takes place successively, the decrease will not be as large, due to the fact that the relaxation on account of creep and shrinkage is not acting upon the total support displacement during the whole process. The later the support displacement takes place the smaller will be the decrease. If the support displacement takes place successively at a rate which approximately corresponds to that of the creep and drying processes of the beam, the decrease may be roughly estimated to about 2/3 of the decrease at an instantaneous support displacement.

At the determination of the values of the tables (Tables 6.1 and 6.2) the moment-curvature relation for constant moment has been used for long-term load. The curves for the moment-curvature relations at constant curvature (relaxation) lie below these (Fig. 5.22). In the calculations there is a combination of relaxation and curvature change at constant moment. A more accurate calculation (method A) gives rigidities insignificantly below those that we get with the more simple calculation method used here.

At the determination of the total moment at long-term load and support displacement, regard must be taken to the possible moment change that is caused by creep and shrinkage on the beam subjected to load alone (sections 6.1.2, 6.1.3).

From the tables is shown that the rigidity upon the calculation of moment changes on account of support displacements normally becomes much smaller than according to the present Swedish codes, where the rigidity of the uncracked cross-section is to be used with consideration to the reinforcement.

Neglecting the influence of reinforcement at creep and calculating the rigidity by dividing E_c with $1 + \phi$ may, at a high steel ratio (ζ small) have the effect of an underestimation of the rigidity.

6.2 Support moment due to support displacement for nonloaded concrete beams

An approximate equation is derived for the determination of the support moment for nonloaded supported cantilever beams and beams clamped at both ends. The derivation proceeds from the bilinear moment-curvature relation, but disregards the influence of the curvatures $1/r_0$. These are small at uniform shrinkage and counteract each other at support and span, and therefore the error arising from this approximation is insignificant. The equation is valid when cracking takes place at support and is expressed for the supported cantilever beam by

$$a = \frac{M_r \cdot \ell^2}{6 \cdot (EI)_r} \cdot \frac{1}{n^2} \cdot [(n - 1) \cdot (2n + 1) + \frac{(EI)_r}{(EI)_0} \cdot (3n^2 - 1)] \qquad (6.7)$$

where $n = M_s/M_r$ and M_s denotes the support moment of the support displacement a. The cracking moment M_r and the flexural rigidities $(EI)_0$ and $(EI)_r$ may be calculated according to chapter 5 for the reinforcement at support. At creep and shrinkage the support moment may be determined by inserting the cracking moment and rigidities then valid. In this case the moment change is overestimated since the curve for the moment-curvature relation at relaxation is below the curve for the relation at constant moment for which the flexural rigidities are stated. The coefficient n is solved from the equation by a trial and error calculation.

For the beam clamped at both ends a and ℓ in Eq. 6.7 are exchanged for a/2 and $\ell/2$ respectively.

If the curvature at zero moment $(1/r_0)$ is significant for example at heavy non-uniform shrinkage, or the flexural rigidities at cracked state are different at the two supports for the beam clamped at both ends, or if the restraints are elastic, then the aid formulae of Appendix A4 may be used.

6.3 Comparison between measured and calculated moment redistributions at support displacement

This section is mainly based on a paper by the author /72AL/ which deals with an experimental and theoretical investigation of the effect of support displacements on loaded supported cantilever beams. The experimental part of the investigation was made by pupils, who were untrained for this type of work, as a part of their education under the supervision of the author.

The supported cantilever beams were loaded by concentrated loads at their third points and the support displacement of the clamped end was simulated by a slope change there. The loading was made by about fifteen load steps up to the collapse load. For most of the beams a support displacement was performed at a load corresponding to the load at serviceability limit state.

Seventeen beams were tested of which eleven were subjected to support raisings or lowerings at the clamped end by one hundredth or one two hundredth of the span. The A- and B-beams had the width b = 150 mm, the depth h = 180 mm, d = 156 mm and the span ℓ = 2100 mm while for the C-beams b = 300, h = 100, d = 81 and ℓ = 2700 mm. All the beams had the same longitudinal reinforcement and the tensile reinforcement consisted of 6ϕ8 at the clamped end and 4ϕ8 in the span, and the cutoff of the reinforcement was made according to the Swedish concrete regulations. The beams had different kinds of shear reinforcement. The A-beams had vertical stirrups and the B-beams had stirrups which formed a 45^0 angle with the beam axis between the concentrated loads and the ends of the beam and vertical stirrups between the concentrated loads. The C-beams had no stirrups. The stirrups (ϕ6) were designed to carry the whole shear force. The strength of the concrete f_{ccm} was about 20 MPa and the strength of the reinforcement f_{st} = 435 MPa.

In /72AL/ calculations have been performed according to method B (Fig. 2.1) by dividing the beams into 16 segments. Regard was taken to the moment-curvature relations at moment alternations according to Monnier (section 5.2.2), to the deformations on account of shear

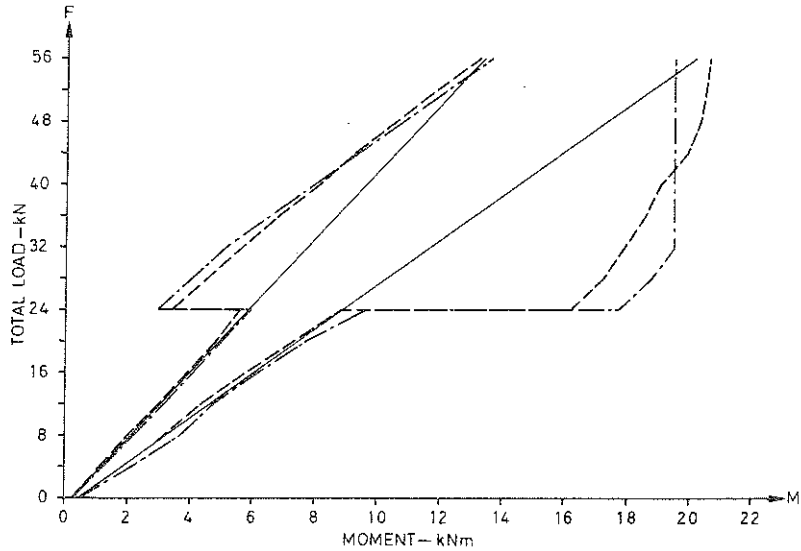

Figure 6.14 The measured and calculated moments at the clamped end and at the location of the concentrated load nearest the supported end for beam AR1 as a function of the total load and a raising of the clamped end by ℓ/100. Measured moments —·— . Calculated moments — — — . Moments for a beam which has constant flexural rigidity along its length and no support displacement ——. /72AL/.

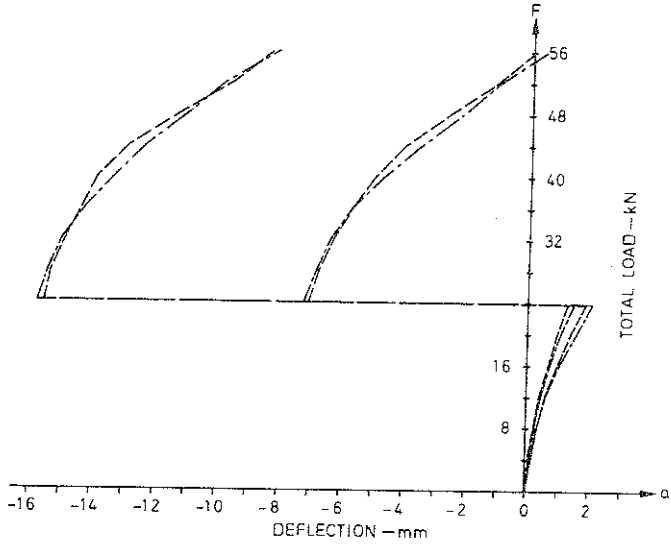

Figure 6.15 The measured and calculated deflections at the location of the two concentrated loads for beam AR1 as a function of the total load and a raising of the clamped end by ℓ/100. The deflections are given in relation to the supported end and a negative value indicates a deflection upwards. Measured deflection —·—. Calculated deflections — — — . /72AL/.

forces (section 5.3) and to the fact that plastic hinges might be developed. In the calculations considerations have also been taken to the real dimensions of the beam, the real placing of the reinforcement and the measured strength of the concrete. Small differences exist between the moment-curvature relations used in these calculations and the relations stated in this paper as well as between the modulus of elasticity and the flexural strength as a function of the concrete strength (f_{ccm}). In Figs 6.14-6.17 are shown the measured and calculated moments and deflections for two of the beams as a function of the total load and the support displacement. In /72AL/ a theoretical investigation of the influence of the deformations on account of shear forces has been performed for the A- and B-beams which are not subjected to support displacements. The investigation shows that this influence on the moment distribution is insignificant and that it increases the deflection at service load with about 7 percent for the A-beams and 2,5 percent for the B-beams and at the dubble service load with about 15 and 9 percent respectively.

Calculations have also been performed according to method C (Fig. 2.3) with the use of the moment-curvature relations and the relations between the material parameters stated in this paper. The same systematized calculation model has been used as the one which is described for frames at the beginning of chapter 8. The beams have been divided into three members of equal length, which means that the concentrated loads are applied at the joints. In the calculations the real quantities of the beams have been used.

In Table 6.3 are shown the measured moment changes at the clamped end together with the calculated ones according to the two calculation models described above. The moment changes determined according to the Swedish regulations are also shown and it can be seen that they are 2 - 3 times too large. For most of the beams there is good agreement between the calculated and the measured values. The agreement between the two calculation methods is also good which implies that the more simple calculation model (method C) could be used at a determination of the moment changes at support displacements. For the

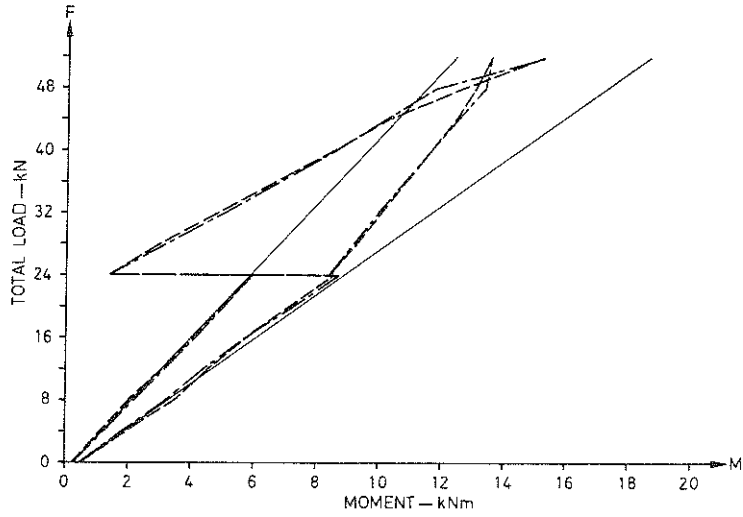

Figure 6.16 The measured and calculated moments at the clamped end and at the location of the concentrated load nearest the supported end for beam AL1 as a function of the total load and a lowering of the clamped end by ℓ/115. Measured moments ——·——. Calculated moments — — — . Moments for a beam which has constant flexural rigidity along its length and no support displacement ——. /72AL/.

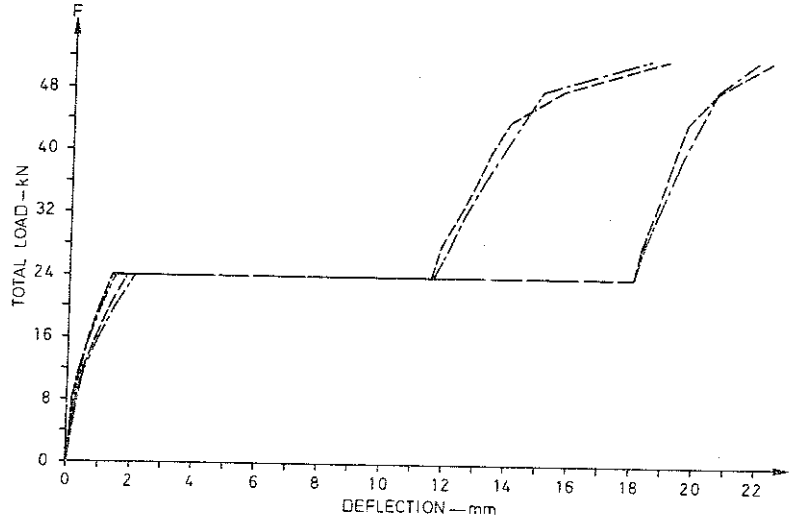

Figure 6.17 The measured and calculated deflections at the location of the two concentrated loads for beam AL1 as a function of the total load and a lowering of the clamped end by ℓ/115. The deflections are given in relation to the supported end and a negative value indicates a deflection upwards. Measured deflection ——·——. Calculated deflections — — —. /72AL/.

C-beams the difference between the two methods is largest, which is natural since the C-beams have no stirrups and the deformations on account of shear forces will be largest for these.

Table 6.3 The measured and calculated moment changes at the clamped end at support displacements for supported cantilever beams at service load.

beam	support movement		moment change of the clamped end						
			measured	Swedish regulations	theoretical /72AL/	theoretical method C	measured / theoretical /72AL/	measured / theoretical method C	theoretical /72AL/ / theoretical method C
	mm		kNm	kNm	kNm	kNm			
AR1	-21.0	℄/100	6.46	25.70	8.87	8.90	0.73	0.73	1.00
AR2	-10.5	℄/200	4.49	12.85	5.06	4.81	0.89	0.93	1.05
AL1	18.6	℄/115	-7.13	-22.80	-7.40	-7.82	0.96	0.91	0.95
AL2	10.5	℄/200	-7.00	-12.85	-5.02	-5.28	1.39	1.33	0.95
BR1	-21.0	℄/100	8.06	25.70	9.46	9.19	0.85	0.88	1.03
BR2	-10.5	℄/200	5.47	12.85	5.20	4.70	1.05	1.16	1.11
BL2	10.5	℄/200	-5.57	-12.85	-4.70	-4.64	1.19	1.20	1.01
CR1	-27.0	℄/100	2.24	6.50	2.98	2.63	0.75	0.85	1.13
CR2	-13.5	℄/200	1.48	3.25	1.40	1.16	1.06	1.28	1.21
CL1	27.0	℄/100	-2.47	-6.50	-2.49	-2.67	0.99	0.92	0.93
CL2	13.5	℄/200	-1.51	-3.25	-1.51	-1.14	1.00	1.32	1.32

7 COLUMNS

Formulae have been derived for the determination of the deflection and the restraint moment for a laterally loaded cantilever column. Furthermore directions are given for the determination of inter-action diagrams for the buckling load.

The column is assumed to have a cracked zone near the support and to be uncracked in the other parts. Its load together with the notations used in the formulae are shown in Fig. 7.1. The formulae derived may also be used for columns fixed at both ends according to Fig. 7.2. For columns with other loadings, cracking, or end conditions, calculations may be performed according to the first order theory by the aid of Appendix A4.

In the derivation a bilinear moment-curvature relation is assumed. This may be determined according to chapter 5, which implies that regard may be taken to the influence of the tensile zone of concrete, nonsymmetrical reinforcement, creep and non-uniform shrinkage.

7.1 Calculation according to first order theory

The deflection a_o at the top of the column may be determined by the equation

$$a_o = \frac{1}{(EI)_r} \cdot \left[\frac{V_o \cdot \ell^3}{3} \cdot (1-\beta^3 \cdot \alpha_1) + \frac{M_o \cdot \ell^2}{2} \cdot (1-\beta^2 \cdot \alpha_1) + \right.$$
$$\left. + \frac{q \cdot \ell^4}{8} \cdot (1-\beta^4 \cdot \alpha_1) - \frac{M_r \cdot \ell^2}{2} \cdot \alpha_1 \cdot (1-\beta^2) \right] + \frac{\ell^2 \cdot 1/r_o}{2} \qquad (7.1)$$

where $\alpha_1 = 1 - (EI)_r/(EI)_o$ and $\beta\ell$, which constitutes the distance from the top of the column to the cracking zone, is determined by

$$M_r = V_o \cdot \beta\ell + M_o + q \cdot (\beta\ell)^2/2 \qquad (7.2)$$

The parameters M_r, $1/r_o$, $(EI)_o$ and $(EI)_r$ may be determined according to chapter 5 with consideration of normal force and possible non-uniform shrinkage and creep.

The restraint moment will be equal to

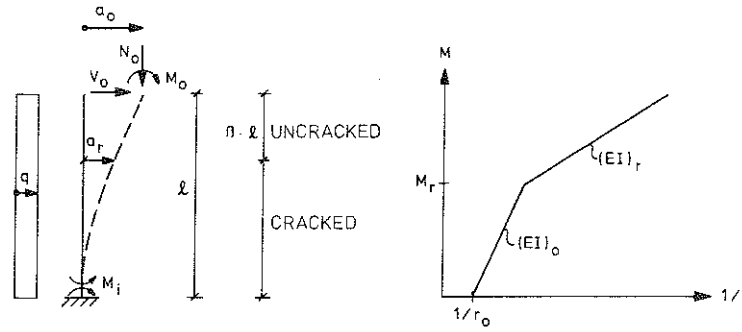

Figure 7.1 The notations and moment-curvature relation used in the evaluation and the loads and deflection of the column

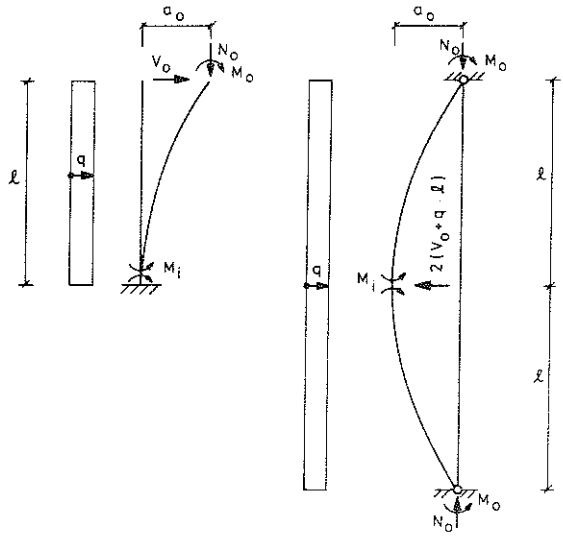

Figure 7.2 The conditions for which the formulae derived are valid for a column hinged at both ends

$$M_s = V_o \cdot \ell + M_o + q \cdot \ell^2/2 \qquad (7.3)$$

and an improved value may be calculated by adding the moment of the deflection and normal force.

$$M_s = V_o \cdot \ell + M_o + q \cdot \ell^2/2 + N_o \cdot a_o \qquad (7.4)$$

For a completely uncracked column β is equal to 1 and for a completely cracked one equal to 0.

7.2 Calculation according to second order theory

The deflection a_o at the top of the column may be expressed by the equation

$$a_o = \frac{V_o \cdot \ell}{N_o} \cdot \left(\frac{\tan k_2\ell}{k_2\ell} - 1\right) - \frac{M_o}{N_o} + \frac{q \cdot \ell^2}{N_o} \cdot \left(\frac{\tan k_2\ell}{k_2\ell} + \frac{1}{(k_2\ell)^2} - \frac{1}{2}\right) + \\ + \frac{M_r}{N_o} \cdot \left(1 - \left(\frac{k_1\ell}{k_2\ell}\right)^2\right) - \frac{\ell^2 \cdot 1/r_o}{(k_2\ell)^2} - a_1 \qquad (7.5)$$

where

$$a_1 = \frac{1}{\cos k_2\ell} \cdot \frac{k_1\ell}{k_2\ell} \cdot \frac{\sin k_2\ell\beta}{\sin k_1\ell\beta} \cdot \left[\frac{q \cdot \ell^2}{N_o \cdot (k_1\ell)^2} - \frac{M_o}{N_o} - \frac{\ell^2 \cdot 1/r_o}{(k_1\ell)^2} + \right. \\ \left. + \left(\frac{M_r}{N_o} - \frac{q \cdot \ell^2}{N_o \cdot (k_1\ell)^2} + \frac{\ell^2 \cdot 1/r_o}{(k_1\ell)^2}\right) \cdot \left(\cos k_1\ell\beta - \frac{k_1\ell}{k_2\ell} \cdot \frac{\sin k_2\ell\beta}{\tan k_2\ell\beta}\right)\right]$$

and $k_1^2 = N_o/(EI)_o$, $k_2^2 = N_o/(EI)_r$ and the parameters M_r, $1/r_o$, $(EI)_o$ and $(EI)_r$ may be determined according to chapter 5 with consideration of normal force and possible non-uniform shrinkage and creep.

The deflection a_r at the location where the moment is equal to the cracking moment M_r i.e. at the distance $\beta\ell$ from the top may be expressed, in relation to the deflection a_o at the top of the column, by

$$a_o - a_r = \frac{V_o \cdot \ell}{N_o} \cdot \left(\frac{\sin k_2\ell\beta/\cos k_2\ell}{k_2\ell} - \beta\right) - \frac{M_o}{N_o} + \frac{q \cdot \ell^2}{N_o} \cdot \left(\frac{\sin k_2\ell\beta/\cos k_2\ell}{k_2\ell} + \right. \\ \left. + \frac{1}{(k_2\ell)^2} - \frac{\beta^2}{2}\right) + \frac{M_r}{N_o} \cdot \left(1 - \left(\frac{k_1\ell}{k_2\ell}\right)^2\right) - \frac{\ell^2 \cdot 1/r_o}{(k_2\ell)^2} - a_1 \cdot \cos(k_2\ell \cdot (1-\beta)) \qquad (7.6)$$

The distance $\beta\ell$ from the top of the column may be determined from the equation

$$M_r = V_o \cdot \beta\ell + M_o + q \cdot (\beta\ell)^2/2 + N_o \cdot (a_o - a_r) \qquad (7.7)$$

An appropriate calculation procedure is to determine at first β from Eq. 7.7 with $N_o = 0$, and then a_o and $a_o - a_r$ from Eqs 7.5 and 7.6 for this value of β, and after that determine a new value of β from Eq. 7.7 and then repeat the calculation procedure until the deflection is determined with satisfactory accuracy.

If the column is completely uncracked the deflection at the top of the column is equal to

$$a_o = \frac{V_o \cdot \ell}{N_o} \cdot \left(\frac{\tan k_1\ell}{k_1\ell} - 1\right) + \frac{q \cdot \ell^2}{N_o} \cdot \left(\frac{\tan k_1\ell}{k_1\ell} - 1/2\right) +$$

$$+ \left(\frac{M_o}{N_o} - \frac{q \cdot \ell^2}{N_o \cdot (k_1\ell)^2} + \frac{\ell^2 \cdot 1/r_o}{(k_1\ell)^2}\right) \cdot \left(\frac{1}{\cos k_1\ell} - 1\right) \qquad (7.8)$$

and if the column is completely cracked the deflection is equal to

$$a_o = \frac{V_o \cdot \ell}{N_o} \cdot \left(\frac{\tan k_2\ell}{k_2\ell} - 1\right) + \frac{q \cdot \ell^2}{N_o} \cdot \left(\frac{\tan k_2\ell}{k_2\ell} - 1/2\right) +$$

$$+ \left(\frac{M_o}{N_o} - \frac{q \cdot \ell^2}{N_o \cdot (k_2\ell)^2} + \frac{\ell^2 \cdot 1/r_o}{((k_2\ell)^2)}\right) \cdot \left(\frac{1}{\cos k_2\ell} - 1\right) \qquad (7.9)$$

The restraint moment is determined by

$$M_s = V_o \cdot \ell + M_o + q \cdot \ell^2/2 + N_o \cdot a_o \qquad (7.10)$$

7.3 Method for the determination of interaction diagrams for the buckling load

If the cross-section data and the normal force of the column are assumed to be known, the ultimate moment (M_u), the cracking moment (M_r), the rigidities at uncracked and cracked states $(EI)_o$ and $(EI)_r$, and the curvature at zero moment ($1/r_o$) may be calculated as well as $k_1 = \sqrt{N_o/(EI)_o}$ and $k_2 = \sqrt{N_o/(EI)_r}$ with the consideration of possible creep and shrinkage. If the column is completely uncracked, the unknown

magnitude of the force which coacts with the normal force may be calculated by a combination of Eqs 7.8 and 7.10. Otherwise, an iteration procedure must be used which in principle may be performed in the following way.

By a combination of Eqs 7.10 and 7.7 β and the unknown magnitude of the force coacting with the normal force may be expressed as functions of the normal force, the ultimate moment, the cracking moment and the deflections a_o and a_r. If in the first iteration step, the deflections are assumed to be equal to zero, β and the force may be determined. Then a_o and a_r may be calculated with the aid of Eqs 7.5 and 7.6. By using these deflections new values of β and the force may be determined and inserted into Eqs 7.5 and 7.6. This calculation process is repeated until the magnitude of the force is determined with sufficient accuracy. The calculation procedure may then be repeated for a new value of the normal force.

The moment-curvature relations used are established under the assumption of constant moment during the loading time. Since the deflection on account of creep and shrinkage will increase with time there is also an increase of the moment with time. This leads to somewhat larger rigidities than those assumed, a fact which will probably cause a slight underestimation of the buckling load.

8 FRAMES AT SERVICEABILITY LIMIT STATE

A systematized frame calculation model has been established for the calculation of loaded concrete frames subjected to support displacements. The calculation may be performed for short-term load, creep and non-uniform shrinkage and with the consideration of partial cracking. Width, depth, creep and shrinkage may vary between the separate members of the frame and the reinforcement within the members.

The calculation is iterative and is performed according to the deformation method. The frame is divided into joints and members, consisting of beams or columns or parts of these. The system lines of the frame are represented by the centroidal axes of its members. The members are divided into cracked and uncracked sections with the aid of the moment distributions formerly calculated. The flexural rigidities of cracked and uncracked states, the cracking moment and the curvatures at zero moment ($1/r_0$) are determined according to chapter 5 for each section. The flexibility matrix of each member may be established according to the same procedure as the aid formulae of Appendix A4. The deformations of normal force are calculated as if the members are uncracked. The shear deformations are disregarded, but may be included in the analysis without difficulty. The flexibility matrices are inverted to local stiffness matrices. These are transformed to the global coordinate system and collected in the global stiffness matrix. The load vector is set up considering possible load between the joints. The stiffness matrix and the load vector are modified for the boundary conditions. The displacements and rotations of the joints are solved from the system of equations. The section forces are calculated. If the agreement between these section forces and those previously calculated is satisfactory, the calculation is terminated, otherwise it is repeated with the new force distributions of the members as entrance value for a dividing of the members into new cracked and uncracked sections. For more simple frames, where the number of statically indeterminate forces is small, a manual calculation may be performed with an improvised force method where the aid formulae of Appendix A4 in combination with

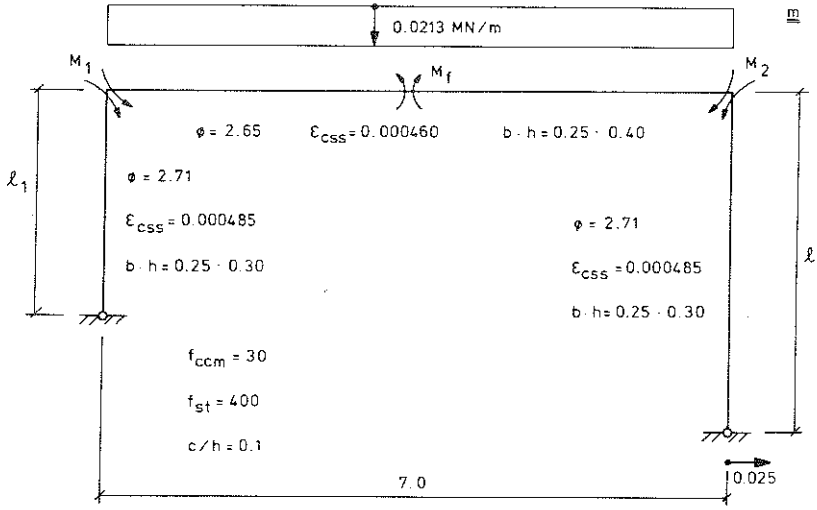

Figure 8.1 Data for the frames, the calculation results of which are accounted for in Table 8.1.

the moment-curvature relations of chapter 5 are used.

A few frames are calculated to illustrate the influence of the effects of imposed deformations as well as the deviations in the moment distributions between the more accurate calculations according to the model described above, where regard is taken to partial cracking, and simplified calculations, where the frames are calculated as uncracked and non-reinforced. In this chapter these methods will be referred to as the accurate one (partial cracking) and the simple one (uncracked) respectively. In the latter method, each frame member is assumed to be uniformly rigid along its length and with the flexural rigidity equal to $E_c \cdot bh^3/12$ at short-term load, and at long-term load the elastic modulus of the concrete is divided by $1+\phi$. Possible curvature at zero moment ($1/r_0$) of normal force and uniform shrinkage are disregarded, but non-uniform shrinkage is considered. Calculation according to this method may be performed with the aid of manuals with frame formulae or in a conventional manner, and the influence of different loading cases and effects of imposed deformation may be superposed.

The shape, serviceability load, support displacement, creep and shrinkage of the first frames are shown in Fig. 8.1. Three frames are symmetric ($\ell_1 = \ell_2$), whereas the fourth frame is unsymmetrical with different lengths of its columns which has the effect that it is subjected to sway. In order to examine how the elastic restraints of the beams influence the effects of imposed deformations and the deviation between the calculation methods described, the length of the columns has been varied for the symmetric frames. The frames are reinforced for the moments calculated according to the simple method for short-term load without support displacement, and are, for this load, cracked in the corners as well as in the spans of the beams. At support displacement this is assumed to take place at the same time as the loading. The influence of other loading histories is dealt with in section 6.1.4. At non-uniform shrinkage this is assumed to take place only in the beams and to be 25 % larger at the upper edge and 25 % smaller at its lower edge than the value stated in the figure with a linear distribution inbetween. The calculation results are accounted for in Table 8.1. For the frames 1, 2 and 3 $M_1 = M_2$, whereas for frame 4 $M_2 = 2M_1$.

Table 8.1 Calculation results for the frames in Fig. 8.1. The corner moments M_1 and their numerical and percentage deviations between the simple and the more accurate calculation method are stated as well as the maximum span moments M_f. If the deviations for M_1, calculated according to the two methods, exceed 15 % of M_1 calculated according to the accurate method for load alone, then the deviations are underlined with one line and with 2 lines if they exceed 30 %.

FRAME NUMBER	1 $\ell_1 = \ell_2 = 1.25$				2 $\ell_1 = \ell_2 = 2.5$				3 $\ell_1 = \ell_2 = 5.0$				4 $\ell_1 = 1.25$ $\ell_2 = 2.5$			
Calculation case	M_1 kNm	M_1 deviation kNm	%	M_f kNm	M_1 kNm	M_1 deviation kNm	%	M_f kNm	M_1 kNm	M_1 deviation kNm	%	M_f kNm	M_1 kNm	M_1 deviation kNm	%	M_f kNm
partial cracking, load	70.8			59.7	59.3			71.2	40.6			89.9	38.1			74.0
uncracked, load	67.4	-3.4	5	63.1	55.5	-3.8	6	75.0	40.8	0.2	0	89.7	36.1	-2.0	5	77.0
partial cracking, load+support movement	33.7			96.8	43.3			87.2	35.1			95.4	21.7			98.2
uncracked, " " "	-16.6	-50.3	149	147.1	20.9	-22.4	52	109.6	28.1	-7.0	20	102.4	6.1	-15.8	73	121.4
partial cracking, " " " -load	-37.1				-16.0				-5.5				-16.4			
uncracked, " " " -load	-84.0	-46.9	126		-34.6	-18.6	116		-12.7	-7.2	131		-30.0	-13.6	83	
partial cracking, load+creep+shrinkage	73.5			57.0	60.2			70.3	39.3			91.2	40.5			70.5
uncracked, " "	64.2	-9.3	13	66.3	54.0	-6.2	10	76.5	40.0	0.7	2	95.5	34.8	-5.7	14	78.9
partial cracking, " " -load	2.7				0.9				-1.3				2.4			
uncracked, " " -load	-3.8	-6.5			-1.5	-2.4			-0.8	0.5			-1.3	-3.7		
partial cracking, load+creep+non-uniform shrinkage	73.9			56.6	60.6			69.9	40.0			95.5	40.9			70.0
uncracked, " "	68.8	-5.1	7	61.7	57.8	-2.8	5	72.7	42.8	2.8	7	87.7	37.3	-3.6	9	75.2
partial cracking, load+creep+shrinkage+movement	53.3			77.2	51.5			79.0	36.1			94.4	31.8			83.3
uncracked, " "	41.2	-12.1	23	89.3	44.5	-7.0	14	86.0	36.6	0.5	1	93.9	26.6	-5.2	16	90.9
partial cracking, " " -(load+creep+shrinkage)	-20.2				-8.7				-3.2				-8.7			
uncracked, " " -(load+creep+shrinkage)	-23.0	-2.8	14		-9.5	-0.8	9		-3.4	-0.2	6		-8.2	0.5	6	

According to the table the moment distribution may be estimated relatively satisfactorily with the simple calculation method at short-term load without support displacement. However, at a reinforcement distribution deviating from the one which belongs to the moment distribution calculated for an uncracked frame the risk increases of a greater deviation between the intended and the real moment distribution. If the frame has such dimensions and such load that cracking takes place either only in the frame corners or only in the span, the deviation may be somewhat larger than the one which appears from these calculations but it will probably not be larger than to make possible a reasonable estimation of the real moment distribution with the simple calculation method. This condition is valid also for the supported cantilever beams and the beams clamped at both ends as described in chapter 6.

Since frames generally have such a design that they are cracked at serviceability limit state and the support displacement generally causes increased cracking and the ratio between the flexural rigidities at uncracked and cracked states for short-term load is large, the difference between the influences of the support displacement according to the different calculation methods will as a rule be large. The frames here accounted for are cracked at serviceability limit state in the frame corners as well as in the spans of the beams, and the table shows that the influence of the support displacement on the moment distribution will be only about one half calculated for a partially cracked frame in comparison with the results from the simple calculation method. Since the influence of the support displacement is largest for frame 1, which is the most rigid one as it has the shortest columns, the total error will be largest for this frame. Consequently, the simple calculation method is not satisfactory for a calculation of the influence of the support displacement at short-term load, if this causes a large moment redistribution when the frame is cracked at serviceability limit state or if the support displacement causes cracking.

The creep has the effect that flexural rigidity decreases. At uncracked state the decrease is larger in percent than at cracked state. This implies that the curve describing the moment-curvature relation becomes

more straigth and that the cracking does not have as large an importance as at short-term load. The influence of the reinforcement on the flexural rigidity is considerably larger at creep than at short-term load, which means that the rigidity of the frame and hence the moment distribution are better adapted to the one for which the frame has been reinforced. These two factors probably have the effect that the agreement between the two calculation methods is better at uniform creep in the structure than at short-term load.

The shrinkage causes a contraction of the beam, a curvature $(1/r_0)$ for non-symmetrically reinforced cross-sections and a reduction of the cracking moment. The two latter factors involve a reduction of flexural rigidity. In the simple calculation method the shortening of the beam causes a decrease of the corner moments in the same way as the support displacement. However, the decrease is considerably smaller on account of the fact that on the one hand the shortening is smaller than the support displacement and on the other hand the creep reduces the rigidity of the frame. The decrease of the corner moments is largest for frame 1 which is the most rigid one. The creep of the columns is larger than the one for the beam which involves that their rigidity decreases more causing in turn a decrease of the corner moments. For frame 2 these reductions will be equal to 1.2 and 0.3 kNm respectively according to the simple method. On calculating with the more accurate method, the shortening of the beam causes a decrease of the corner moments by about as much as according to the simple method. The curvature $1/r_0$ in the span of the beam increases the corner moments, whereas the curvatures $1/r_0$ at the ends of the beam and for the columns decrease them and all this results in a decrease of the corner moments. The reduction of the cracking moment is largest in the span which is simply reinforced, and its influence on the ratio between the flexural rigidities in span and corners together with creep involves an increase of the corner moments. The deviation between the corner moments calculated according to the two methods is larger at creep and shrinkage than at short-term load and exceeds 10 % of the moments at short-term load for three of the four frames. However, the deviation is not larger than that the simple method may be used for an estimation of

the moment distribution for the loaded frames at long-term load.

The corner moments increase at non-uniform shrinkage of the beam and the change of the curvature $1/r_o$ belonging to this. This increase is, however, counteracted by the fact that the cracking moment is comparatively more reduced at the ends of the beam than in its span, causing a decrease in the ratio between the flexural rigidities at support and in span for the beam. The table shows that the influence of the non-uniformity of the shrinkage is very small and that this may be neglected, whereas the simple method heavily overestimates the influence of the non-uniformity of shrinkage.

The influence of the support displacement decreases with time on account of the fact that the rigidity of the frames decreases at increased creep and shrinkage. For the frames shown in the table it decreases to about one half. The difference between the rigidities of the frames calculated with the different methods also decreases considerably. This is due to the fact that the ratio between the flexural rigidities at short-term and long-term load for an uncracked section without considering the reinforcement is $1 + \phi$, whereas the same ratio is smaller if the reinforcement is considered. This compensates the lower flexural rigidity at cracking as well as the increased cracking of shrinkage in the more accurate calculation. A high percentage of reinforcement, large creep, small shrinkage and little cracking may involve that the influence of the support displacement becomes smaller with the simple method than with the more accurate one. This may also be recognized at a study of the rigidity for a calculation of the influence of a support displacement on beams in chapter 6. The factors enumerated are, however, contradictory since a high percentage of reinforcement normally is connected with large cracking and large creep with large shrinkage. The influence of the support displacement on the frames becomes approximately the same for the two calculation methods.

Among the frames calculated, the influence of the effects of imposed deformations and the deviation between the calculation methods will be largest in those cases where the beam is long in relation to the columns. Due to this, comparative calculations have been made for a symmetric two-bay frame the data and load of which are shown in Fig. 8.2, and for which the deviations may be expected to become even

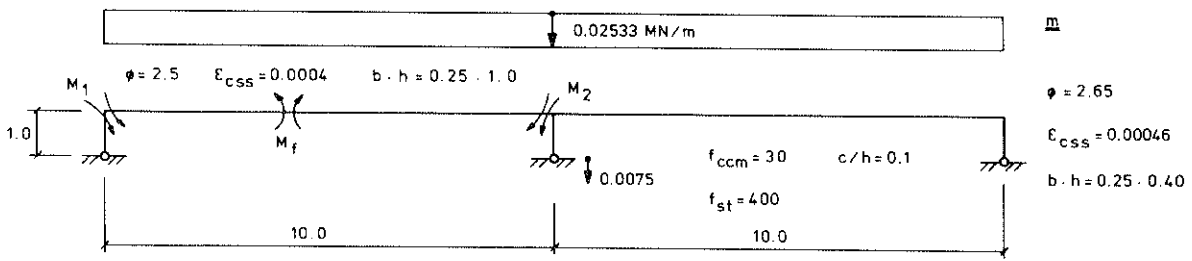

Figure 8.2 Data for the symmetric two-bay frame which is hinged fixed at the ground and the calculation results of which are accounted for in Table 8.2.

larger. The frame is reinforced for the moments calculated according to the simple method at serviceability limit state, and the beams remain uncracked in span at this load. At non-uniform shrinkage this is assumed to take place only in the beams and with the same distribution as for the previous frames. The calculation results are shown in Table 8.2 and about the same conclusions may be drawn from these as from the results from the calculations of the frames above.

In Fig. 8.4 the moment diagrams for a symmetric two-story, two-bay frame according to Fig. 8.3 is accounted for, where one side of the structure is loaded with a uniform lateral horizontal load and the slabs with uniform lateral vertical loads. The walls, with a thickness of 15 cm, are symmetrically reinforced with ρ = 0,004 at each side and the slabs, with a thickness of 10 cm, are reinforced in the top with ρ = 0,007 at the exterior support and with ρ = 0,01 at the interior support. The bottom reinforcement corresponds to ρ = 0,005 in the span and ρ = 0,0025 at the supports. At non-uniform shrinkage this is assumed to take place only in the slabs with the same distribution as for the previous frames. The slabs are uncracked in span at short-term load. The agreement between the two calculation methods is, as is shown in the figure, good except for support displacement at short-term load.

Conclusions

From the calculation results and the discussion concerning these, the following conclusions may be drawn about the reliability of the simple method for the calculation of the influence of effects of imposed deformations on loaded frames.

At short-term load without support displacement the method should give satisfactory results.

At short-term load with support displacement, the method may overestimate the influence of the support displacement by 2 to 3 times if the frame is cracked at serviceability limit state or if the support displacement is of such a magnitude that it causes cracking. If neither the load at serviceability limit state nor the support displacement

Table 8.2 Calculation results for the symmetric two-bay frame in Fig. 8.2. The corner moments M_1 and M_2 and the maximum span moment M_f are accounted for, as well as the numerical and percentage deviation between the more accurate and the simple calculation method. If the deviations between the moments calculated according to the two methods exceed 15 % of the moments, calculated according to the two methods for load alone, then the deviations are underlined with one line and with two lines if they exceed 30 %.

Calculation case	M_1 kNm	M_f kNm	M_2 kNm	deviation M_1 kNm	M_1 %	M_f kNm	M_f %	M_2 kNm	M_2 %
partial cracking, load	62	159	271						
uncracked, load	62	153	284	0		-6	4	13	5
partial cracking, load+support movement	102	205	122						
uncracked, " "	140	191	112	38	37	-14	7	-10	8
partial cracking, " " -load	40	46	-149						
uncracked, " " -load	78	38	-172	38	95	-8	17	-23	15
partial cracking, load+creep+shrinkage	1	178	316						
uncracked, " "	-16	186	323	-17		8	4	7	2
partial cracking, " " -load	-61	19	45						
uncracked, " " -load	-78	33	39	-17	28	14	74	-6	13
partial cracking, load+creep+non-uniform shrinkage	4	174	321						
uncracked, " "	-6	163	369	-10		-11	6	48	15
partial cracking, load+creep+shrinkage+movement	27	179	272						
uncracked, " "	5	191	274	-22	81	12	7	2	1
partial cracking, " " -(load+creep+shrinkage)	26	1	-44						
uncracked, " " -(load+creep+shrinkage)	21	5	-49	-5	19	4		-5	11

causes any cracking, the influence of the support displacement is slightly underestimated.

At long-term load the method should give an acceptable result. The influence of the non-uniformity of shrinkage is neglected.

The moment diagram of the frame for long-term load and support displacement may be estimated with the method with reasonable accuracy. If the influence of the support displacement is great and the creep is small a certain precaution should be taken, and likewise if the frame is uncracked. If the support displacement develops with time at about the same rate as the creep and shrinkage, its influence can be calculated in the same way as for an instantaneous support displacement, but its decrease with time will only be about 2/3 of the decrease for the instantaneous displacement. This is a rather rough approximation. The later the support displacement takes place the smaller the decrease will be.

Consequently the moment distribution in the frames at serviceability limit state may be calculated approximately with a simple calculation method, in which the frames are assumed uncracked and nonreinforced, at short-term load without support displacements and at long-term load with or without support displacements.

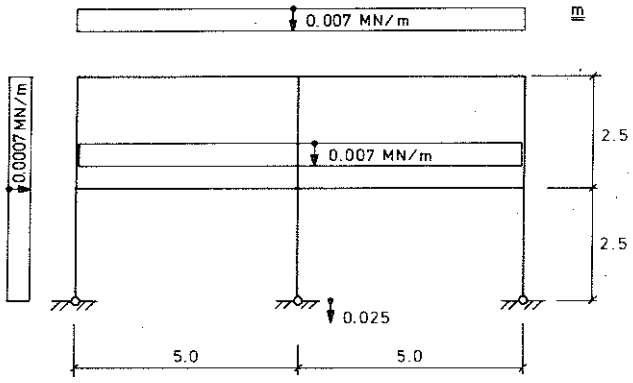

Figure 8.3 Load, design and support displacement for a symmetric two-story two-bay frame the calculation results of which are accounted for in Fig. 8.4. $f_{ccm} = 30$, $f_{st} = 400$, c/h = 0.1. Slabs $\phi = 2.83$, $\varepsilon_{css} = 0.000533$, $b \cdot h = 1.0 \cdot 0.1$. Walls $\phi = 2.67$, $\varepsilon_{css} = 0.000466$, $b \cdot h = 1.0 \cdot 0.15$.

uncracked

load

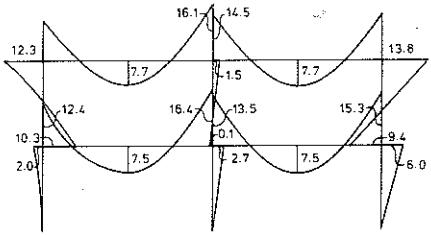

load+support displacement

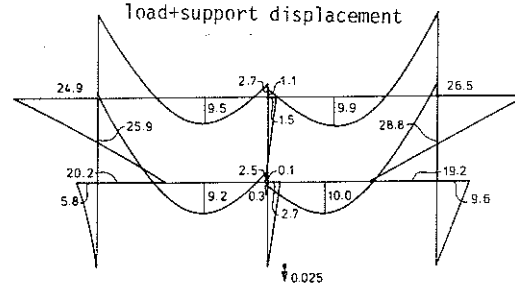

load+creep+shrinkage

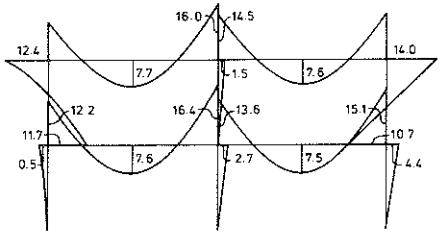

load+creep+shrinkage+support displacement

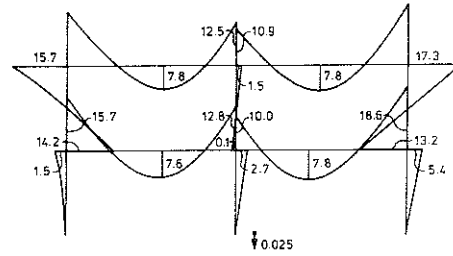

partially cracked

load+support displacement

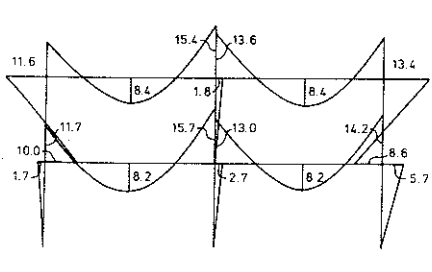

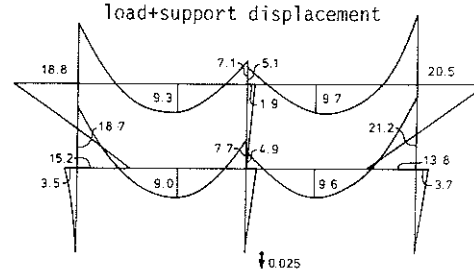

load+creep+shrinkage

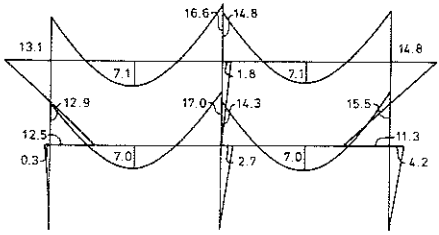

load+creep+shrinkage+support displacement

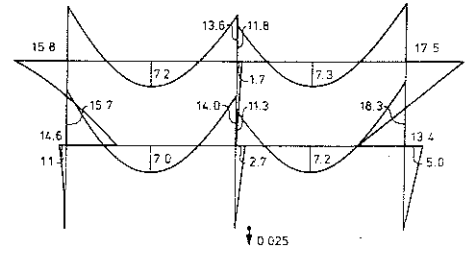

load+creep+shrinkage+non-uniform shrinkage of slabs

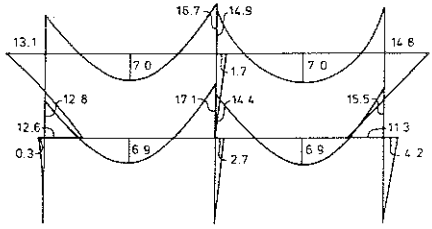

Figure 8.4 Calculation results from the symmetric two-story, two-bay frame in Fig. 8.3. Dimensions kNm and m.

9. ROTATION REQUISITES AT ULTIMATE LIMIT STATE

In the design of concrete structures two states are distinguished, viz. the serviceability limit state and the ultimate limit state. At serviceability limit state deflections and crack widths are controlled with regard to integrity of secondary structures, impenetrability, the risk of corrosion as well as aesthetic demands. The analysis is normally carried out according to the elastic theory.
At ultimate limit state the safety against failure is controlled to be satisfactory. This is performed through stability analysis and a control that the cross-section can carry the section forces. These are generally determined by an analysis according to the plastic theory. Then it must be controlled, for the collapse mechanism assumed, that the rotation requisite at each plastic hinge does not exceed its rotation capacity.

In order to determine the required rotations at the plastic hinges the rotation between the hinges must be calculated. Elastic behaviour is assumed in the regions between the plastic hinges. This implies that the formulae stated in Appendix A4, which are based on the bilinear moment curvature relations stated in chapter 5 considering the cracking, shrinkage and creep of concrete, are appropriate for the determination of the rotations between the plastic hinges. The formulae are established for some common loading cases and will be used in the following. The deformations due to shear forces are not regarded.

Supported cantilever beams and beams clamped at both ends as well as two-hinged portal frames subjected to uniform lateral load and support displacements are studied. Their purpose is, on the one hand, to serve as examples of how to perform the calculations, on the other hand, to examine which parameters govern and how they govern the rotation requisite.

9.1 The rotation requisites for a supported cantilever beam subjected to uniform lateral load and to support displacement.

The beam studied is shown in Fig. 9.1 together with its load, support displacement, moment distribution at ultimate limit state and cracking zones. The figure also shows the division of the load into

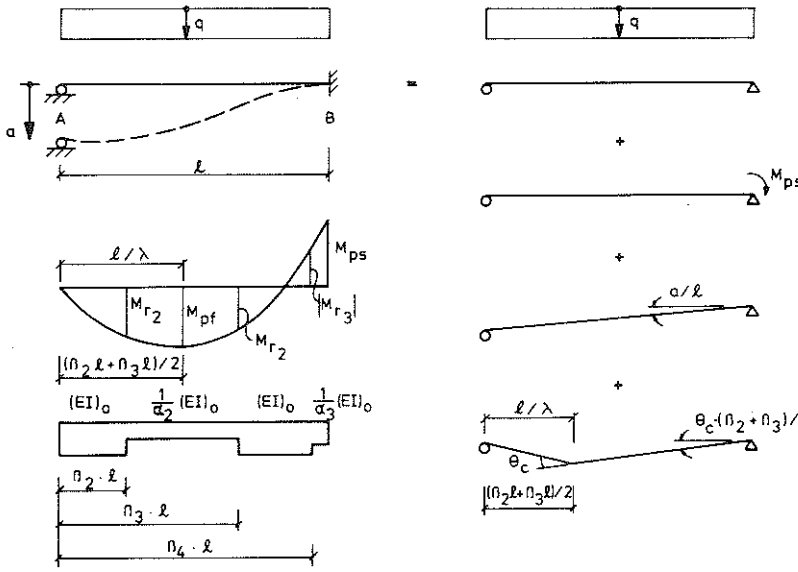

Figure 9.1 Definition of the notations used in the evaluation. Division into subloading cases.

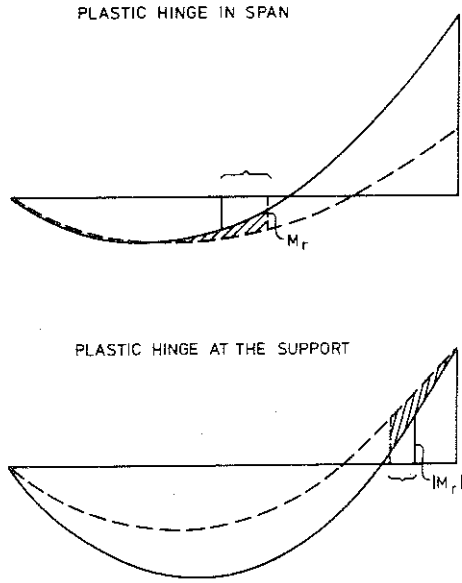

Figure 9.2 Within the areas indicated the flexural rigidity assumed is incorrect since regard is not taken to the loading history. Within certain areas denoted the beam is assumed uncracked despite the fact that in an earlier stage it has been cracked.

appropriate partial loadings. With the aid of these and the aid formulae in Appendix A4 the slope at the support θ_B may be calculated

$$\theta_B = \theta_o + \theta_C \cdot (\beta_2 + \beta_3)/2 + a/\ell \qquad (9.1)$$

where θ_o (due to q and M_{ps}) according to Appendix A4 is equal to

$$\theta_o = \frac{q\cdot\ell^3}{24(EI)_o} \cdot \left[\alpha_3+(\alpha_2-1)\cdot\left[\beta_3^3\cdot(4-3\beta_3)-\beta_2^3\cdot(4-3\beta_2)\right]-(\alpha_3-1)\cdot\beta_4^3\cdot(4-3\beta_4)\right]+$$

$$-\frac{M_{ps}\cdot\ell}{3(EI)_o}\cdot\left[\alpha_3+(\alpha_2-1)\cdot(\beta_3^3-\beta_2^3)-(\alpha_3-1)\cdot\beta_4^3\right]+$$

$$-\frac{\ell}{2(EI)_o}\cdot\left[M_{r2}\cdot(\alpha_2-1)\cdot(\beta_3^2-\beta_2^2)+M_{r3}\cdot(\alpha_3-1)\cdot(1-\beta_4^2)\right]+$$

$$+\frac{\ell}{2}\cdot\left[1/r_{o2}\cdot(\beta_3+\beta_4)^2/4+1/r_{o3}\cdot(1-(\beta_3+\beta_4)^2/4)\right] \qquad (9.2)$$

The other notations are shown in Fig. 9.1 and Appendix A4.

If the plastic hinge is developed first at the support the rotation requisite in the plastic hinge there must be equal to

$$\theta_B = \theta_o + a/\ell \qquad (9.3)$$

in order to attain the plastic moment also in the span.

If a plastic hinge is developed first in span then $\theta_B = 0$ and the rotation requisite will be equal to

$$\theta_C = -2 \cdot (\theta_o + a/\ell)/(\beta_2 + \beta_3) = -\lambda\,(\theta_o + a/\ell) \qquad (9.4)$$

The uniform lateral load q and the parameters β may, with the aid of the equilibrium conditions, be expressed as functions of the plastic and cracking moments

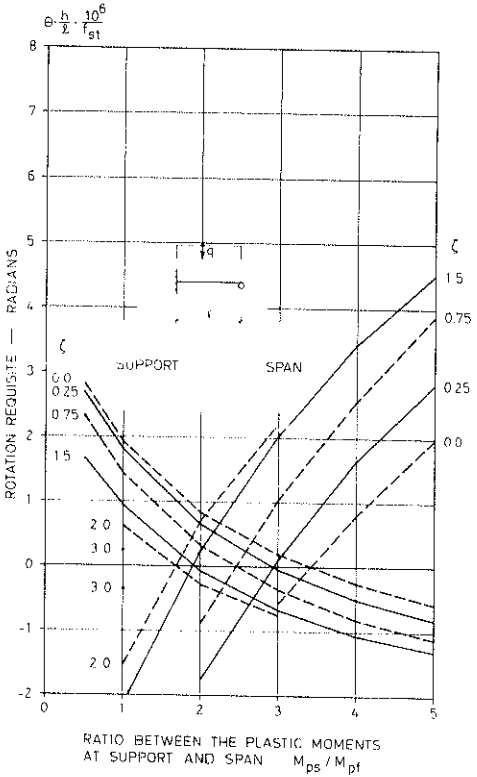

Figure 9.3 The rotation requisite at support and in span for short-term load. The numerals by the curves denote the value of ζ for which they are valid. ζ is determined by Eq. 9.12.

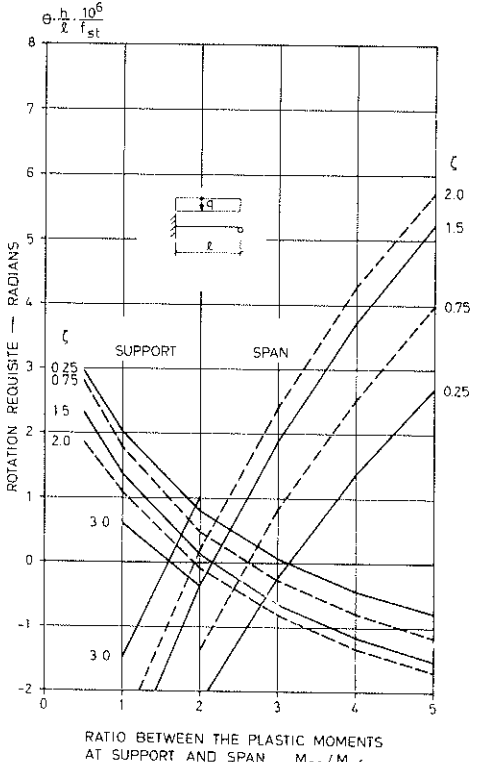

Figure 9.4 The rotation requisite at support and in span for $\phi = 0$ and $\varepsilon_{css} = 0.0004$. The numerals by the curves denote the value of ζ for which they are valid. ζ is determined by Eq. 9.12.

$$q \cdot \ell^2 = 2M_{pf} \cdot \lambda^2 \tag{9.5}$$

$$\lambda^2 = 2 + M_{ps}/M_{pf} + 2\sqrt{1 + M_{ps}/M_{pf}} \tag{9.6}$$

$$\beta_2 = (1 - \sqrt{1 - M_{r2}/M_{pf}})/\lambda \qquad \beta_2 \geq 0 \tag{9.7}$$

$$\beta_3 = (1 + \sqrt{1 - M_{r2}/M_{pf}})/\lambda \qquad \beta_2 \leq \beta_3 \leq 1 \tag{9.8}$$

$$\beta_4 = (1 + \sqrt{1 - M_{r3}/M_{pf}})/\lambda \qquad \beta_3 \leq \beta_4 \leq 1 \tag{9.9}$$

The cracking moments M_r, the curvatures $1/r_o$ and the flexural rigidities $(EI)_o$ and $(EI)_r$ may be calculated according to chapter 5 considering possible nonuniform shrinkage and creep. If these parameters are inserted together with the load and the plastic moments into θ_o the rotation requisites may be expressed as a function multiplied with ℓ/h

$$\theta = \frac{\ell}{h} \cdot f(\rho_f, \rho_f', \rho_s, \rho_s', c/h, 1+\phi, \varepsilon_{css}, \gamma, f_{st}, f_{ccm}, a \cdot h/\ell^2) \tag{9.10}$$

which implies that the rotation requisites increase with the length of the span and decreases with the depth of the beam.

The calculation method used does not take into consideration the loading history, which implies that certain parts of the beam will be considered uncracked although they have already been cracked at a lower load level (Fig. 9.2). This implies that the calculated rotation requisites will be somewhat large. The increase is, however, probably so small that it is insignificant. At shrinkage the influence gets even smaller, since this reduces the cracking moment.

Numerical calculations have been performed to examine how the rotation requisites at support and in span are affected by the cracking and the reinforcement distribution between support and span at both short-term and long-term load. The following calculation assumptions are valid.

The plastic moment is larger than the cracking moment. The plastic moments have been determined by

$$M_p = 0.9 \cdot d \cdot A_s \cdot f_{st} \tag{9.11}$$

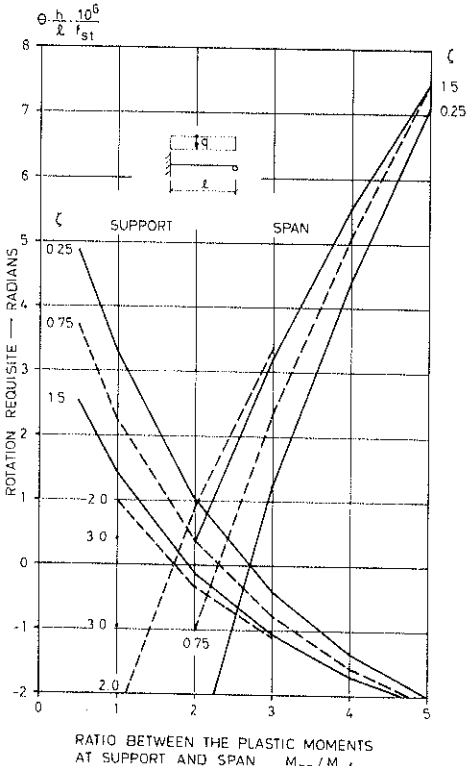

Figure 9.5 The rotation requisite at support and in span for $\phi = 2.5$ and $\varepsilon_{css} = 0$. The numarals by the curves denote the value of ζ for which they are valid. ζ is determined by Eq. 9.12.

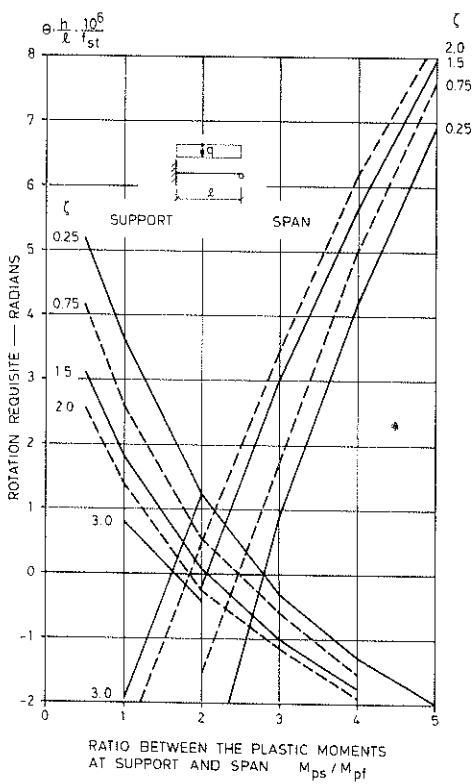

Figure 9.6 The rotation requisite at support and in span for $\phi = 2.5$ and $\varepsilon_{css} = 0.0004$. The numerals by the curves denote the value of ζ for which they are valid. ζ is determined by Eq. 9.12.

Compressive reinforcement does not exist in span and is at support equal to one fourth of the area of the tensile reinforcement in span. No consideration has been given to the cutoff of the reinforcement. The depth and width of the rectangular cross-section are the same for the whole beam. In order to reduce the number of parameters in the presentation of the results, the amount of reinforcement, the strength of concrete and the tensile strength of the reinforcement have been transferred into a parameter ζ which is defined by

$$\zeta = \frac{f_{cbm}}{\rho_{tot} \cdot f_{st}} \tag{9.12}$$

where $\rho_{tot} = \frac{\lambda^2}{4} \cdot \frac{A_{sf}}{b \cdot h}$ (9.13)

with λ^2 according to Eq. (9.6) or $\lambda^2 \approx 4.2 + 1.6 \cdot M_{ps}/M_{pf}$.

The definition of ζ implies that for beams with the same ζ the bearing capacity is not affected by a reinforcement redistribution between support and span. The parameter ζ governs the degree of cracking for the beams and a small value of ζ implies heavy cracking. If the beam is completely cracked ζ is equal to zero.

The result from the calculations is shown in Figs 9.3 - 9.7. The numerals by the curves denote the value of ζ for which they are valid. The maximum deviations of the rotation requisites from the values stated in the figures are about $\pm$ 10 % at short-term load and about $\pm$ 15 % at long-term load, depending on the variation of ρ_{tot}, f_{ccm} ($15 \leq f_{ccm} \leq 60$) and f_{st} ($400 \leq f_{st} \leq 800$). The values stated are the average values when f_{ccm} and f_{st} vary as described.

If the beams are at the same time subjected to both load and a support displacement a, defined according fo Fig. 9.1, the rotation requisites stated in the figures increase with a/ℓ at support and decrease with $\lambda \cdot a/\ell$ in span with λ according to Eq. 9.6 or $\lambda \approx 2.12 + 0.29 \cdot M_{ps}/M_{pf}$.

The figures show that the rotation requisite at support is largest at heavy cracking and when the ratio between the plastic moments at support and in span (M_{ps}/M_{pf}) is small, whereas the opposite is valid for the rotation requisite in span. At a comparison between Figs 9.3 and 9.4 and Figs 9.5 and 9.6, it may be noted that the shrinkage has relatively small influence on the rotation requisite, but increases this

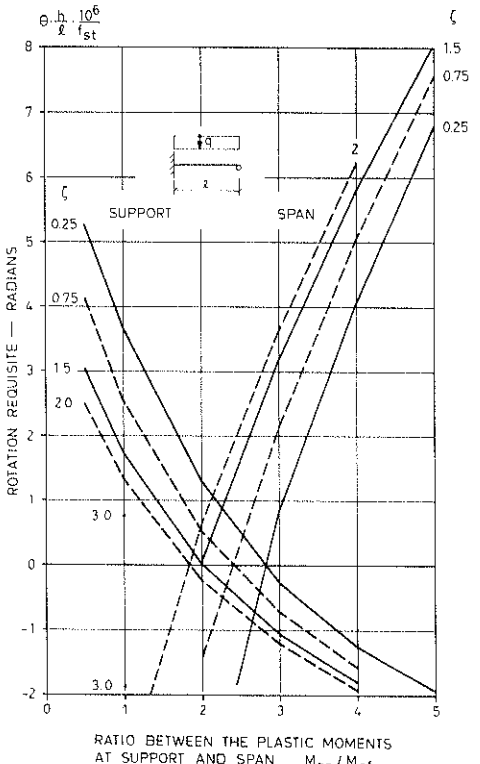

Figure 9.7 The rotation requisite at support and in span for $\phi = 2.5$ and ε_{css} is equal to 0.0003 in the lower edge, 0.0005 in the upper edge and linear in between. The numerals by the curves denote the value of ζ for which they are valid. ζ is determined by Eq. 9.12.

Table 9.1 The slope θ_p according to Eq. 9.29 as a function of $\zeta = \dfrac{f_{cbm} \cdot b \cdot h}{f_{st} \cdot A_s}$ and the normal force N (N positive for tension). The numerals above the values (average values) show the scatter in percent, if this is larger than 10 %, when f_{st} and f_{cbm} vary ($400 \le f_{st} \le 800$, $15 \le f_{ccm} \le 60$). The largest values are obtained for $f_{st} = 400$ and $f_{ccm} = 60$ and the smallest ones for $f_{st} = 800$ and $f_{ccm} = 15$. The slope θ_p is valid when the moment is equal to the plastic moment and c/h = 0.1.

$$\frac{\theta_p \cdot 10^6 \cdot h}{\ell_p \cdot f_{st}}$$

$\frac{N}{b \cdot h}$ \ ζ	4	3	2	1	0.5	0.25
0	±20 0.32	±10 0.78	1.51	2.45	2.94	3.15
-0.5	±25 0.26	±10 0.62	±10 1.32	2.32	2.85	3.12
-1.0	±30 0.23	±25 0.49	±15 1.20	±10 2.21	2.79	3.10
-2.5	±30 0.23	±30 0.35	±40 0.75	±15 1.91	2.62	3.03
-5.0	±30 0.24	±30 0.32	±45 0.56	±40 1.48	±15 2.37	2.86
-10.0	±30 0.25	±35 0.32	±35 0.47	±50 1.08	±25 1.93	±10 2.69

somewhat at support for M_{ps}/M_{pf} = 0.5 - 1 as well as in span for M_{ps}/M_{pf} = 4 - 5. The non-uniformity of shrinkage probably has no effect (Figs 9.6 and 9.7). Figs 9.3 and 9.5 show that creep increases the rotation requisite considerably. According to /76PL/ the rotation capacity also increases considerably under creep.

9.2 The rotation requisites for a beam clamped at both ends subjected to uniform lateral load and to support displacement

Fig 9.8 shows the symmetrically reinforced beam together with its load, support displacement and moments at ultimate limit state. The division into subloading cases is also shown. With the aid of these subloading cases and the aid formulae of Appendix A4, the slopes at the supports and at the centre of the span, after simplifications where regard is taken to the symmetri, may be expressed by

$$\theta_B = \theta_o + \theta_c/2 + a/\ell \tag{9.14}$$

$$\theta_A = \theta_o + \theta_c/2 - a/\ell \tag{9.15}$$

where

$$\theta_o = \frac{q\cdot\ell^3}{24(EI)_o}\cdot\left[\alpha_1-(\alpha_1-1)\cdot(1-2\beta_1)\cdot(1+2\beta_1-2\beta_1^2)+(\alpha_2-1)\cdot(1-2\beta_2)\cdot\right.$$
$$\left.\cdot(1+2\beta_2-2\beta_2^2)\right] - \frac{M_{ps}\cdot\ell}{2(EI)_o}\cdot\left[\alpha_1-(\alpha_1-1)\cdot(1-2\beta_1)+(\alpha_2-1)\cdot(1-2\beta_2)\right] +$$
$$-\frac{\ell}{2(EI)_o}\cdot\left[M_{r1}\cdot(\alpha_1-1)\cdot 2\beta_1+M_{r2}\cdot(\alpha_2-1)\cdot(1-2\beta_2)\right] +$$
$$+\frac{\ell}{2}\cdot\left[1/r_{o1}\cdot(\beta_1+\beta_2)+1/r_{o2}\cdot(1-\beta_1-\beta_2)\right] \tag{9.16}$$

The other notations are shown in Fig 9.8 and Appendix A4.

If the plastic hinge is developed last in the span then $\theta_c = 0$ and the rotation requisites at the supports will be equal to

$$\theta_B = \theta_o + a/\ell \tag{9.17}$$

$$\theta_A = \theta_o - a/\ell \tag{9.18}$$

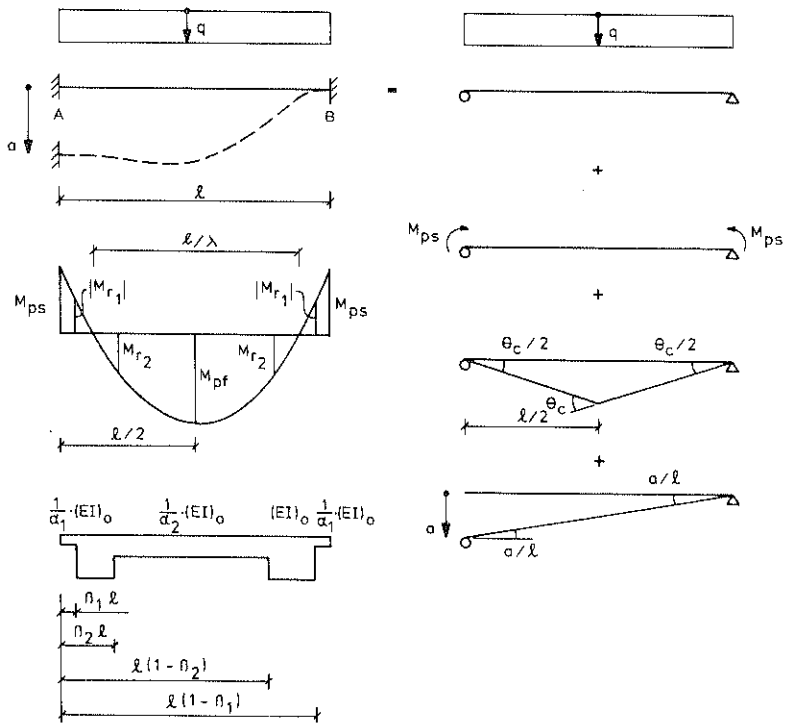

Figure 9.8 Definition of the notations used in the evaluation. Division into subloading cases.

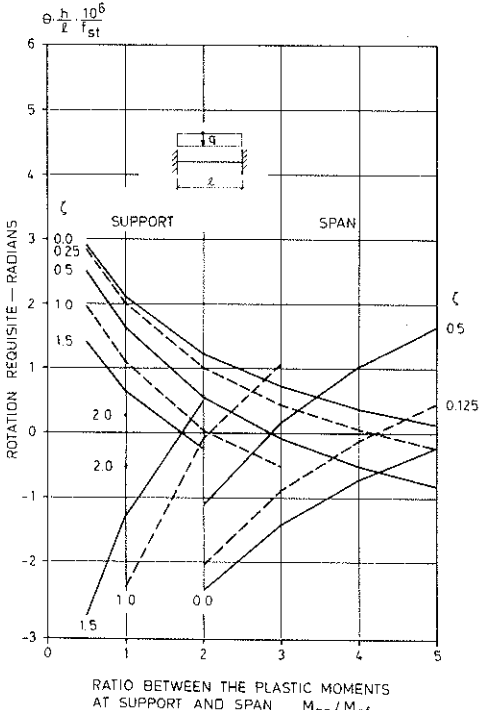

Figure 9.9 The rotation requisite at support and in span for short-term load. The numerals by the curves denote the value of ζ for which they are valid. ζ is determined by Eq. 9.26.

If the plastic hinge is developed last at support A then $\theta_A = 0$ and the rotation requisites in span and at the support B will be equal to

$$\theta_C = -2 \cdot \theta_o + 2 \cdot a/\ell \tag{9.19}$$

$$\theta_B = 2 \cdot a/\ell \tag{9.20}$$

With the aid of equilibrium conditions the uniform lateral load q and the parameters β may be expressed as functions of the plastic and cracking moments

$$q \cdot \ell^2 = 8\, M_{pf} \cdot \lambda^2 \tag{9.21}$$

$$\lambda^2 = 1 + M_{ps}/M_{pf} \tag{9.22}$$

$$\beta_1 = (\lambda - \sqrt{1 - M_{r1}/M_{pf}})/2\lambda \qquad 0 \le \beta_1 \le 1/2 \tag{9.23}$$

$$\beta_2 = (\lambda - \sqrt{1 - M_{r2}/M_{pf}})/2\lambda \qquad \beta_1 \le \beta_2 \le 1/2 \tag{9.24}$$

The cracking moments M_r, the curvatures $1/r_o$ and the flexural rigidities $(EI)_o$ and $(EI)_r$ may be calculated according to chapter 5 considering possible non-uniform shrinkage and creep. If these values together with q, β_1 and β_2 as well as the plastic moments are inserted into θ_o the rotation requisites θ may be expressed by

$$\theta = \frac{\ell}{h} \cdot f(\rho_f, \rho'_f, \rho_s, \rho'_s, c/h, 1+\phi, \varepsilon_{css}, \gamma, f_{st}, f_{ccm}, a \cdot h/\ell^2) \tag{9.25}$$

which implies that the rotation requisites increase with the length of the span and decrease with the depth of the beam.

The calculation is performed for the collapse state and does not consider the effects of those moment redistributions which take place at increasing load after the development of the first plastic hinge. This implies that the calculated rotation requisites become insignificantly larger than the real ones.

The same numerical calculations have been performed for the beams clamped at both ends as for the supported cantilever beam. The same

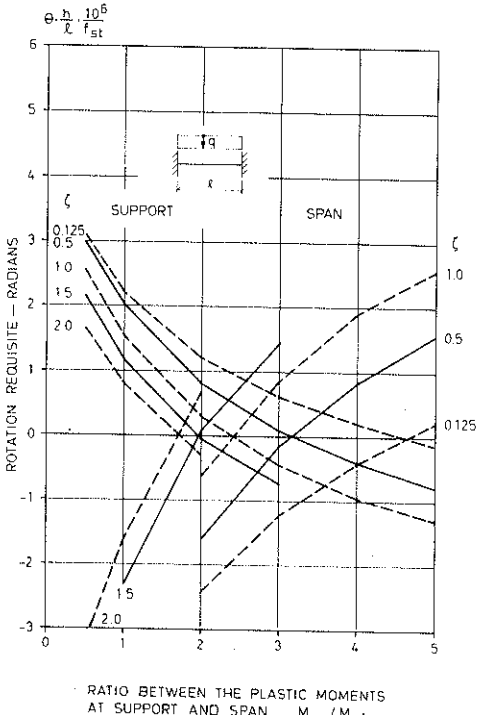

Figure 9.10 The rotation requisite at support and in span for $\phi = 0$ and $\varepsilon_{css} = 0.0004$. The numerals by the curves denote the value of ζ for which they are valid. ζ is determined by Eq. 9.26.

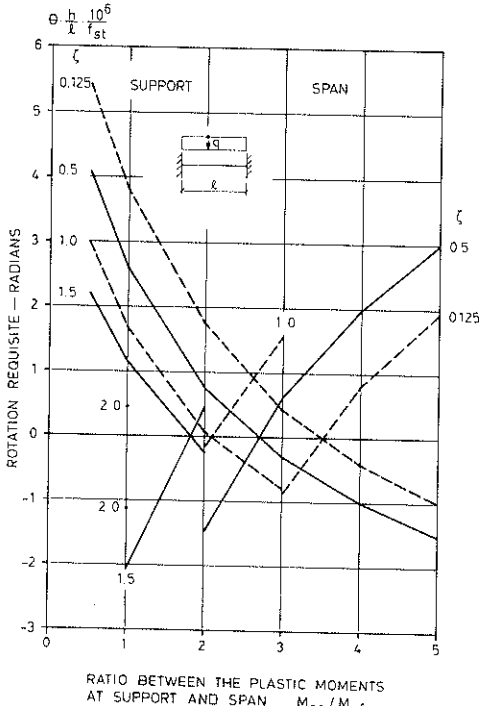

Figure 9.11 The rotation requisite at support and in span for $\phi = 2.5$ and $\varepsilon_{css} = 0$. The numerals by the curves denote the value of ζ for which they are valid. ζ is determined by Eq. 9.26.

calculation assumptions are valid with the exception of ρ_{tot} which is determined according to

$$\rho_{tot} = (A_{sf} + A_{ss})/(b \cdot h) \qquad (9.26)$$

at the determination of ζ according to Eq. 9.12.

The results from the calculations are shown in Figs 9.9 - 9.13 where the numerals by the curves denote the value of ζ for which each curve is valid. The same maximum deviations are valid and the same conclusions may be drawn as for the supported cantilever beams. The rotation requisites at the supports are somewhat larger for the beams clamped at both ends than for the supported cantilever beams, whereas the rotation requisites in span are considerably smaller.

For a support displacement a, according to Fig. 9.8 the rotation requisites are modified as above.

9.3 The rotation requisites for two-hinged frames

The design of frames at ultimate limit state may be performed as follows. The best economy is obtained if the frame is designed such that the whole frame collapses at ultimate load. Therefore a complete collapse mechanism is assumed. The number of plastic hinges will then be one more than the number which is required to render the whole structure statically determinate. Choose the plastic moments so that the equilibrium conditions are fulfilled and determine the moment diagram for the frame for which it is to be reinforced. Determine the rotation requisites. If the rotation requisite is put equal to zero in the plastic hinge developed last, then the rotation requisites may be determined in the remaining plastic hinges. If the rotation requisite somewhere is negative then either the plastic hinge developed last is another one or the wrong direction is assumed for one or some of the plastic moments. If somewhere the rotation requisite exceeds the rotation capacity the frame will collapse before the complete collapse mechanism is attained.

Calculation methods for the determination of the rotation requisites in frames and beams are accounted for in literature in among others /72CEB/.

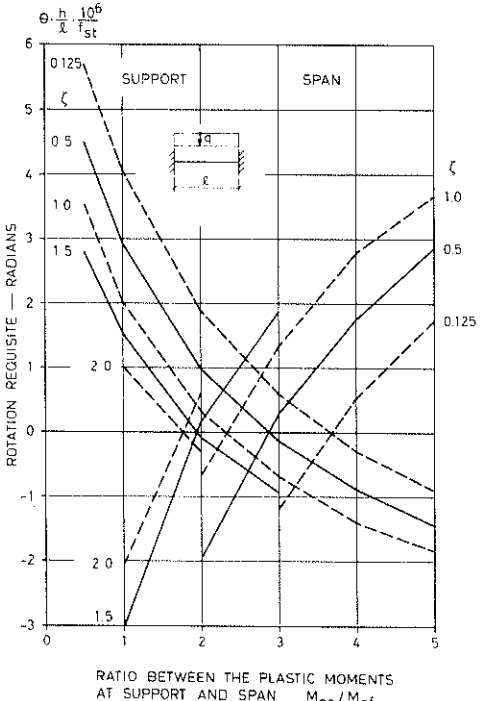

Figure 9.12 The rotation requisite at support and in span for $\phi = 2.5$ and $\varepsilon_{css} = 0.0004$. The numerals by the curves denote the value of ζ for which they are valid. ζ is determined by Eq. 9.26.

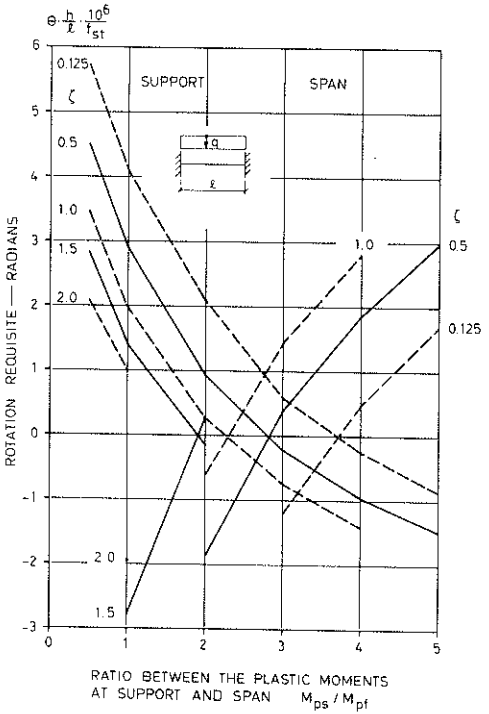

Figure 9.13 The rotation requisite at support and in span for $\phi = 2.5$. ε_{css} is equal to 0.0003 in the lower edge, 0.0005 in the upper edge and linear in between. The numerals by the curves denote the value of ζ for which they are valid. ζ is determined by Eq. 9.26.

Three examples of the calculation of the rotation requisites for loaded two-hinged frames subjected to support displacements will be performed in order to illustrate how the aid formulae of Appendix A4 together with the flexural rigidities and cracking moments calculated according to chapter 5 may be used for the deformation of the rotation requisites.

The first example concerns a frame according to Fig. 9.14, which is symmetric around C. In the figure is also stated an appropriate division into subloading cases. The rotations in the plastic hinges at A and B will be

$$\theta_A = \theta_B = \theta_o + \theta_C/2 - \theta_p - a_x/2\ell_p \tag{9.27}$$

If the plastic hinges are developed last at A and B the rotation requisite in span may be calculated by inserting $\theta_A = \theta_B = 0$.

$$\theta_C = -2\theta_o + a_x/\ell_p + 2\theta_p \tag{9.28}$$

where

$$\theta_p = \frac{M_{ps}\cdot\ell_p}{3(EI)_{op}} \cdot (\alpha_p - (\alpha_p-1)\cdot(1-\beta_p)^3) +$$

$$- \frac{M_{rp}\cdot\ell_p}{2(EI)_{op}} \cdot (\alpha_p-1)\cdot\beta_p\cdot(2-\beta_p) + \frac{1}{r_{op}} \cdot \ell_p/2 \tag{9.29}$$

which may be taken from Tab. 9.1 (page 151) if the moments in the columns are equal to their plastic moments.

The rotation θ_o may be calculated according to Eq. 9.16, or $-2\theta_o$ may be found in Figs 9.9 - 9.13 if the plastic moments of the columns are larger than those of the beam, so that the plastic hinges are developed in the beam. If plastic hinges are developed first at A and B their rotation requisite will be $\theta_A = \theta_B = \theta_o - \theta_p - a_x/2\ell_p$.

The beam may be regarded elastically fixed at the columns. The elastic restraint has the effect that the rotation requisite increases in span.

If the frame is assumed to be a continuous beam simply supported at A and B also, then the rotation requisite decreases at the supports A and B with θ_p and increases in span with $2\theta_p$ compared to the rotation requisite for a beam clamped at A and B.

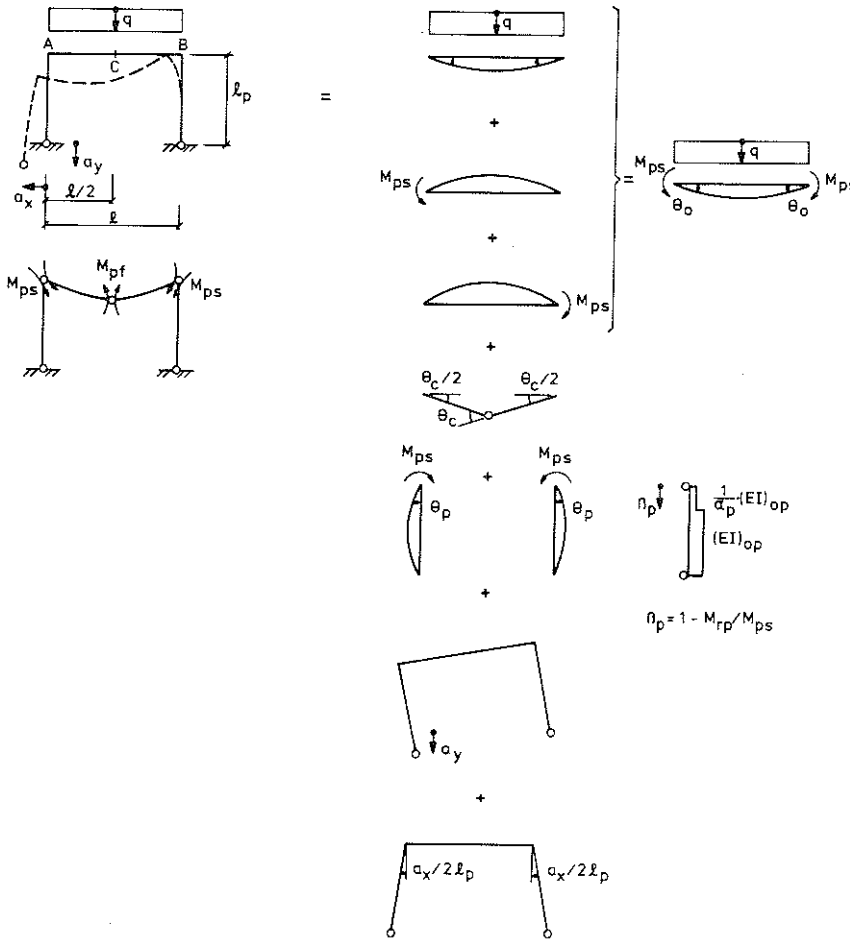

Figure 9.14 Loading, support displacements, collapse mechanism, notations and the division into subloading cases for the determination of the rotation requisites.

In the second example one of the columns is loaded with a uniform lateral load according to Fig. 9.15 and the frame is assumed to be reinforced so that plastic hinges at ultimate limit state are developed at A and B. With the aid of the subloading cases in the figure, the rotations at the plastic hinges may be determined as

$$\theta_A = -\theta_{Ap}^{M_{pA}} - \theta_{Ap}^{q} + a/\ell_p + a_x/2\ell_p - \theta_{Ab}^{M_{pA}} + \theta_{Ab}^{M_{pB}} \tag{9.30}$$

$$\theta_B = -\theta_{Bp}^{M_{pB}} + a/\ell_p - a_x/2\ell_p + \theta_{Bb}^{M_{pA}} - \theta_{Bb}^{M_{pB}} \tag{9.31}$$

If the plastic hinge is developed in B, the rotation requisite in B may be determined by inserting $\theta_A = 0$ and eliminating $a/\ell p$.

$$\theta_B = \theta_o \tag{9.32}$$

where

$$\theta_o = -\theta_{Bp}^{M_{pB}} + \theta_{Ap}^{M_{pA}} + \theta_{Ap}^{q} - a_x/\ell_p + \theta_{Bb}^{M_{pA}} + \theta_{Ab}^{M_{pA}} + -\theta_{Bb}^{M_{pB}} - \theta_{Ab}^{M_{pB}} \tag{9.33}$$

If θ_o becomes negative, the assumption that the plastic hinge is developed first at B is incorrect. Instead it is developed at A and its rotation requisite will be

$$\theta_A = -\theta_o \tag{9.34}$$

In the third example the plastic moments are of the same magnitude in the whole frame and a collapse mechanism according to Fig. 9.19 is obtained. With the notations of the figure, the rotations at A and B will be

$$\theta_A = \theta_{Ap}^{M_A} - \theta_{Ap}^{q} - \theta_C \cdot \ell_{pl}/\ell_p + a/\ell_p + a_x/2\ell_p - \theta_{Ab}^{M_A} + \theta_{Ab}^{M_p} \tag{9.35}$$

$$\theta_B = -\theta_{Bp}^{M_{pB}} + a/\ell_p - a_x/2\ell_p + \theta_{Bb}^{M_A} - \theta_{Bb}^{M_p} \tag{9.36}$$

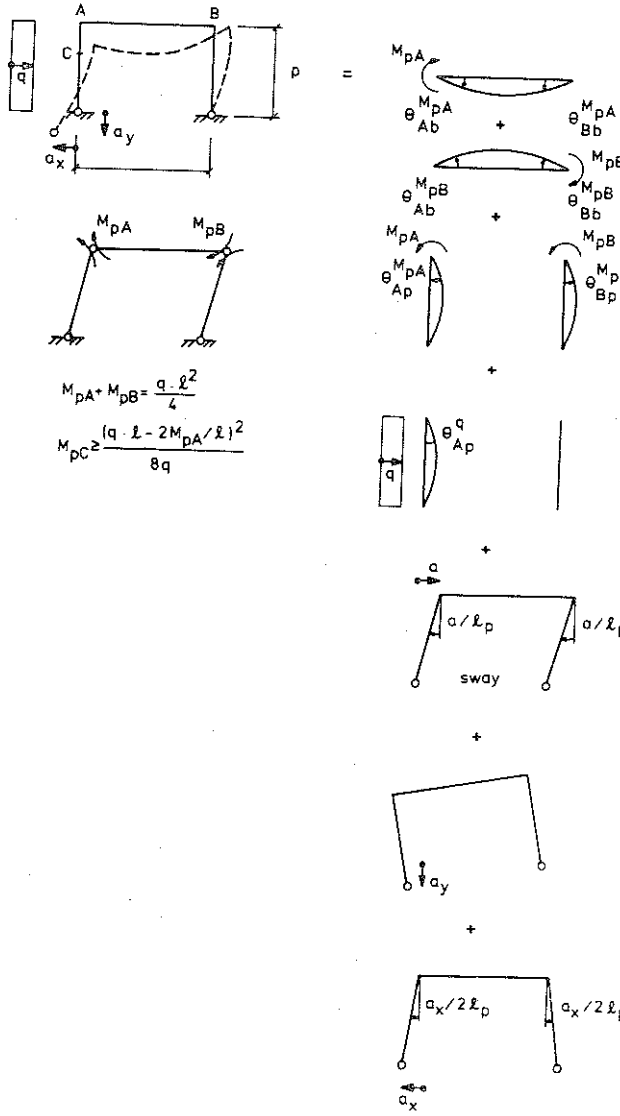

Figure 9.15 Loading, support displacements, collapse mechanism, notations and the division into subloading cases for the determination of the rotation requisites.

If the plastic hinge is developed first at B, the rotation requisite may be determined by inserting $\theta_A = \theta_C = 0$ and eliminating a/ℓ_p.

$$\theta_B = \theta_o \tag{9.37}$$

where

$$\theta_o = -\theta_{Bp}^{M_{pB}} + \theta_{Ap}^{M_A} + \theta_{Ap}^{q} - a_x/\ell_p + \theta_{Bb}^{M_A} + \theta_{Bb}^{M_A} - \theta_{Bb}^{M_p} - \theta_{Ab}^{M_p} \tag{9.38}$$

If the plastic hinge is developed first at C, then θ_o will be negative and the rotation requisite in C may be calculated by inserting $\theta_A = \theta_B = 0$ and eliminating a/ℓ_p.

$$\theta_C = -\frac{\ell_p}{\ell_{pl}} \cdot \theta_o \tag{9.39}$$

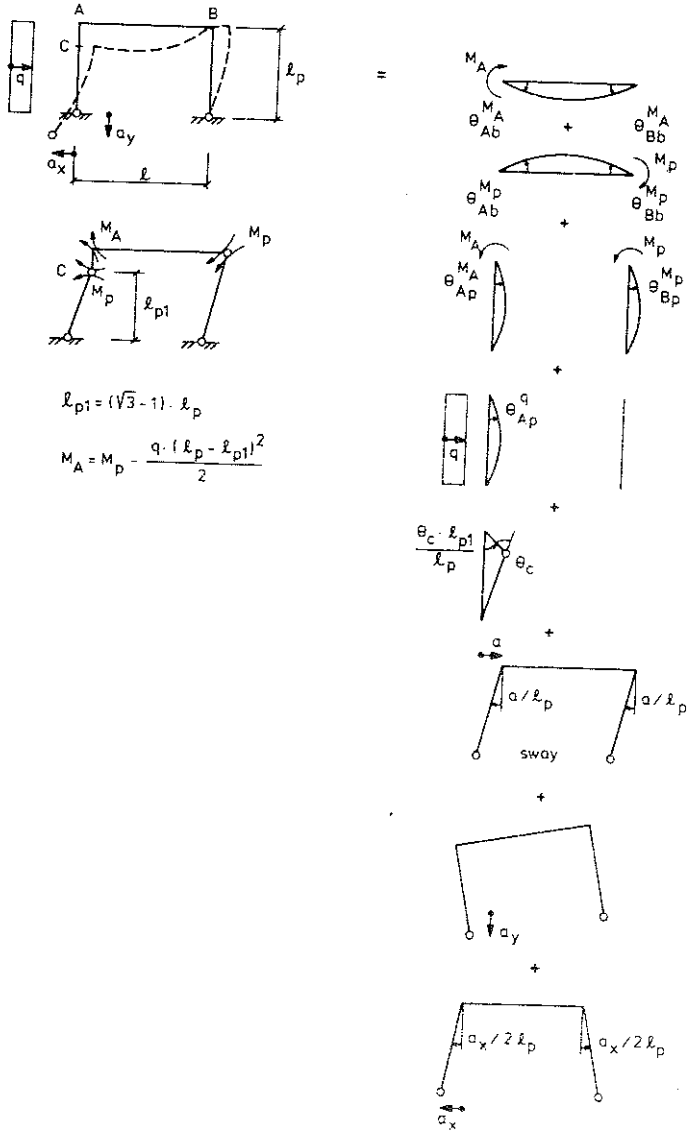

Figure 9.16 Loading, support displacements, collapse mechanism, notations and the division into subloading cases for the determination of the rotation requisites.

10 CONCLUSIONS

A refined calculation model can be established, which carefully describes the behaviour of concrete, considering among other things the stress-strain relation for concrete in tension, the basic creep when the stresses change signs, the drying process and the drying creep.

For structures, however, it has been shown that simplified models based on the creep coefficient (including the drying creep) and the final shrinkage can be used with satisfactory accuracy in spite of the cracking and the large stress variations, which take place in structures during a drying process.

The deformation caused by normal force can be calculated by superposing the influences of the stress-related deformation, the creep (including drying creep) and the shrinkage.

A simple bilinear moment-curvature relation for bending can be established considering cracking, creep (including drying creep), non-uniform shrinkage and normal force and where the parameters, curvature at zero moment, cracking moment and the flexural rigidities at uncracked and cracked state, can be described by a combination of formulae and diagrams.

By using this relation the influence of the imposed deformations may be determined and for beams moment distribution, deflection and influence of support displacement may be accounted for by diagrams, tables and calculation methods. For supported cantilever beams and beams clamped at both ends subjected to uniform lateral load at serviceability limit state the following may be mentioned.

A redistribution of the reinforcement between support and span has little influence on the deflection as long as the redistribution does not change the carrying capacity of the beams and the influence of the shear deformations is small. At creep and shrinkage the ratio between the deflections at long-term and short-term load is largest for an initial uncracked or slightly cracked beam.

For a beam clamped at both ends and reinforced for the moments calculated for a beam with the same flexural rigidity along its length, the support moments calculated in this way decrease at short-term load with maximally about 10 percent if only cracking takes place at the support and increase maximally about 7 percent at heavy cracking. At long-term load the support moments increase because of creep by 0 - 8 percent in comparison with those at short-term load. If shrinkage takes place at the same time as creep the support moments decrease at small cracking by maximally about 6 percent and increase at heavy cracking by maximally about 8 percent. The corresponding moment changes at the clamped end for supported cantilever beams will be a few percent larger than the values mentioned above.

The rigidity of the beam to be used for a calculation of the support moment change for a support displacement at short-term load is only about 40 to 50 percent of the flexural rigidity for an uncracked segment. Heavier cracking and larger displacement decrease the rigidity. If loading and support displacement take place at the same time the rigidity for the calculation of the support moment change at creep and shrinkage is only about 15 to 20 percent of the flexural rigidity for an uncracked segment which is not exposed to creep and shrinkage. The differences will be larger if the shear deformations are of importance. As long as both loading and support displacement take place in a short period the influence of the sequence is small at short-term and negligible at long-term load. If the support displacement develops with time at about the same rate as the creep and shrinkage, its influence can be calculated in the same way as for an instantaneous support displacement, but its decrease with time will only be about 2/3 of the decrease for the instantaneous displacement. This is a rather rough approximation. The later the support displacement takes place the smaller the decrease will be.

Calculation models according to the second order theory can be established for columns for the determination of the deflection and moments by using the bilinear moment-curvature relations mentioned.

These models can also be used in the determination of inter-action diagrams. In the models regard may be taken to cracking, creep, non-uniform shrinkage and different areas of the tensile and compressive reinforcement.

The moment distribution in frames at serviceability limit state may be calculated approximately with a simple calculation method, in which the frames are assumed uncracked and nonreinforced, at short-term load without support displacements and at long-term load with and without support displacements, if the frames are reinforced according to the moment distribution at short-term load calculated by this method. Thus the influence of an instantaneous support displacement at short-term load should not be calculated with this simple method. The influence of the nonuniformity of shrinkage should be neglected, since the simple method very strongly overestimates its influence.

For beams the rotation requisites at ultimate limit state increase at increased ratio between span and depth, and an elastic restraint increases the rotation requisite in span and decreases it at support. Heavier cracking increases the rotation requisite at support and decreases it in span. Creep increases the rotation requisites considerably both at support and in span. Uniform and nonuniform shrinkage increase the rotation requisites insignificantly.

11 PRACTICAL APPLICATIONS

In this section an enumeration of the formulae and figures which are applicable for the problem in question will be done.

1 Deformation due to concentrical normal force under creep and shrinkage

Unreinforced cross-section: Eq. 5.1, Figs 5.2 - 5.5
Symmetrically reinforced cross-section: Eq. 5.2, Figs 5.2 - 5.5

2 Moment-curvature relations due to bending

The simplified moment-curvature relations are defined by the parameters in the following figure.

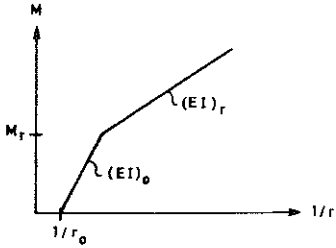

2.1 Short-term load

$1/r_o = 0$
$(EI)_o$: Eq. 5.3 Fig. 5.8
M_r : Eq. 5.5 Fig. 5.9
$(EI)_r$: Eq. 5.4

2.2 Long-term load, basic creep

$1/r_o = 0$
$(EI)_o$: Eq. 5.6 Fig. 5.8
M_r : Eq. 5.5 Fig. 5.9 (ϕ=0)
$(EI)_r$: Eqs 5.7 Fig. 5.16

2.3 Long-term load, creep and shrinkage

$1/r_o$: Eq. 5.8 Fig. 5.20

$(EI)_0$	: Eq. 5.9	Fig. 5.8
M_r	: Eqs 5.11 and 5.12	Figs 5.9 and 5.21
$(EI)_r$	: Eq. 5.7	Fig. 5.16

2.4 Long-term load, creep, shrinkage and normal force

$1/r_0$	: Eq. 5.13	Figs 5.20 and 5.22
$(EI)_0$	: Eq. 5.9	Fig. 5.8
M_r	: Eqs 5.16 and 5.12	Figs 5.9, 5.21 and 5.23
$(EI)_r$	: Eqs 5.15 and 5.7	Fig. 5.16 and Table 5.1

3 Beams at serviceability limit state

3.1 Moment distribution

3.1.1 Supported cantilever beams and beams clamped at both ends subjected to uniform lateral load.

Short-term load: Figs 6.1, 6.2.
Long-term load, basic creep: Figs 6.1, 6.2 and page 104.
Long-term load, creep and shrinkage: Figs 6.1, 6.2 and page 108.

3.1.2 Supported cantilever beams and beams fixed at both ends subjected to uniform lateral load and support displacement.

The influence of the support displacement: Tables 6.1 and 6.2.

3.1.3 Nonloaded supported cantilever beams and beams clamped at both ends subjected to support displacements.

Eq. 6.7.

3.1.4 Moment distribution for beams with other loadings and end conditions.

Use the calculation method and the aid formulae in Appendix A4.

3.2 Deflection (only bending deformations are regarded)

3.2.1 Simply supported beams, supported cantilever beams and beams clamped at both ends subjected to uniform lateral load.

Short-term load: Figs 6.4, 6.5 and 6.6.
Long-term load, basic creep: Figs 6.7, 6.8 and 6.9.
Long-term load, basic creep and shrinkage: Figs 6.10, 6.11 and 6.12.

3.2.2 Other types of beams, loadings and end conditions.

The moment distribution may be determined according to Appendix A4 and the simplified moment-curvature relations stated may be used in the integration processes in order to determine the deflection.

4 Columns

4.1 Moment distribution and deflection for a laterally loaded column fixed at the one end and free at the other one or hinged at both ends

Calculation according to first order theory: Formulae in section 7.1.
Calculation accoridng to second order theory: Formulae in section 7.2.

4.2 Moment distribution and deflection for columns with other loadings or end conditions

Calculation according to first order theory: Use the aid formulae and calculation method described in Appendix A4.

4.3 Method for the determination of inter-action diagrams for the buckling load for the columns described above (4.1)

Use the calculation method described in section 7.3 and the formulae which are mentioned.

5 Frames at serviceability limit state

The moment distribution in frames at serviceability limit state may be calculated approximately with a simple calculation method, in

which the frames are assumed uncracked and nonreinforced, at short-term load without support displacements and at long-term load with and without support displacements, if the frames are reinforced according to the moment distribution at short-term load calculated by this method. The influence of the nonuniformity of shrinkage should be neglected, since the simple method very strongly overestimates its influence. At short-term load with support displacements the method described in Appendix A4 can be used. This method may also be used if a more accurate moment distribution is desired for the other loading cases or if the reinforcement distribution diverges from the moment distribution calculated by the simple method described.

6 Rotation requisites at ultimate limit state

Supported cantilever beams subjected to uniform lateral load and support displacement: Eqs 9.3 and 9.4 and Figs 9.1 and 9.3 - 9.7.

Beams clamped at both ends subjected to uniform lateral load and support displacement: Eqs 9.17 - 9.20 and Figs 9.8 - 9.13.

Beams elastically clamped at both ends subjected to uniform lateral load and support displacement: page 158, Figs 9.8 - 9.13 and Eq. 9.29 or Table 9.1.

Two-hinged portal frames: Calculation descriptions in section 9.3 with references to the rotation requisites for beams.

REFERENCES

/58GR/ GRANHOLM, H, 1958, Sprickbildning i armerad betong. Division of Building Technology, Chalmers University of Technology, Gothenburg, Sweden.

/58RO/ ROSS, A.D, 1958, Creep of Concrete under Variable Stress. ACI Journal, Proc. 54, 1958 pp. 739-757.

/59HE/ L'HERMITE, R, 1959, What do we know about plastic deformation and creep of concrete? RILEM Bulletin No. 1, March 1959.

/59PE/ de la PEÑA, C, 1959, Shrinkage and creep of specimens of thin section. RILEM Bulletin No. 3, juillet 1959.

/59RU/ RÜSCH, H, 1959, Physikalische Fragen der Betonprüfung. Zement-Kalk-Gips, V. 12, No. 1, 1959.

/63HSU/ HSU, T.T.C et al., 1963, Microcracking of Plain Concrete and the Shape of the Stress-Strain Curve. ACI Journal, Proc. 60, 1963, pp. 209-224.

/64SAE/ SAENZ, L.P, 1964, Discussion of "Equation for Stress-Strain Curve of Concrete" by Desayi, P, Krishnan, S. ACI Journal, Proc. 61, 1964, pp. 1229-1235.

/65EN/ ENGLAND, G.L, ILLSTON, J.M, 1965, Methods of computing stress in concrete from a history of measured strain. Civil Engineering and Public Works Review 60, Parts 1, 2 and 3, April, May June 1965, pp. 513-517, 692-694, 846-847.

/65HE/ L'HERMITE, R, et al., 1965, Nouveaux résultats de recherches sur la déformation et la rupture du béton. Annales I.T.B.T.P mars-avril 1965, pp. 323-354.

/65ST/ STURMAN, G.M, et al., 1965, Effects of Flexural Strain Gradients on Microcracking and Stress-Strain Behaviour of Concrete. ACI Journal, Proc. 62, 1965, pp. 805-822.

/66DI/ DILGER, W, 1966, Veränderlichkeit der Briege - und Schubsteitigkeit der... . Deutscher Ausschuss für Stahlbeton, Heft 179, 1966.

/66HA/ HANSEN, T.C, MATTOCK, A.H, 1966, Influence of Size and Shape of Member on the Shrinkage and Creep of Concrete. ACI Journal, Proc. 63, 1966, pp. 267-290.

/66HAN/ HANSEN, T.C, ERIKSSON, L, 1966, Temperature Change Effect on Behavior of Cement Paste, Mortar and Concrete Under Load. ACI Journal, Proc. 63, 1966 pp. 489-504.

/66HU/ HUGES, B.P, CHAPMAN, G.P,1966, The complete stress-strain curve for concrete in direct tension. RILEM, Bulletin No. 30, March 1966, pp. 95-97.

/66HUG/ HUGES, B.P, CHAPMAN, G.P, 1966, The deformation of concrete and microconcrete in compression and tension with particular reference to aggregate size. Magazine of Concrete Research, Vol. 18, No. 54, March 1966, pp. 19-24.

/66RU/ RUETZ, W, 1966, Das Kriechen des Zementsteins im Beton und seine Beeinflussung durch gleichzeitiges Schwinden. Deutscher Ausschuss für Stahlbeton, Heft 183, 1966.

/66WE/ WELCH, G.B, 1966, Tensile strains in unreinforced concrete beams. Magazine of Concrete Research, Vol. 18, No. 54, March 1966,pp. 9-18

/67MA/ MAYER, H, 1967, Die Berechnung der Durchbiegung von Stahlbetonbauteilen. Deutscher Ausschuss für Stahlbeton, Heft 194, 1967.

/68EV/ EVANS, R.H, MARATHE, M.S, 1968,Microcracking and Stress-Strain Curves for Concrete in Tension. Matériaux et Constructions, No. 1, January-February, 1968, pp. 61-64.

/68HE/ L'HERMITE, R, MAMILLAN, M, 1968, Further results of shrinkage and creep tests. International Conference on the Structure of Concrete, London 1965, Cement,Concrete association. London 1968. pp. 423-433.

/68HU/ HUGES, B.P, ASH, J.E, 1968, Short-term loading and deformation of concrete in uniaxial tension on pure torsion. Magazine of Concrete Research, Vol. 20, No. 64, September 1968, pp. 145-154.

/68IL/ ILLSTON, J.M, 1968, Components of Creep in Mature Concrete. ACI Journal, Proc. 65, 1968, pp. 219-227.

/68MA/ MAMILLAN, M, 1968, Influnence de la dimension et de la forme sur le retrait des pièces de bêton. Annales I.T.B.T.P., No. 249, Septembre, 1968, pp. 1319-1324.

/69BA/ BAZANT, Z.P, 1969, Thermodynamic Theory of Deformation of Concrete with Explanation of Drying Creep. ACI, SP-27, 1969. In this paper is given a short description of Bazants philosophy. It is further described in
BAZANT, Z.P, 1974, Thermoviscoelasticity of Aging Concrete. Journal of the Engineering Mechanics Division, ASCE, Vol. 100, No. EM3, Proc. Paper 10621, June, 1974, pp. 575-597.

/69BE/ BERGSTRÖM, S.G, NIELSEN, A, 1969, Beräkning av krypning hos betong. Byggmästaren, No 6,1969, pp. 16-20.

/69HE/ HEILMANN, H.G et al., 1969, Festigkeit und Verformung von Beton unter Zugspannungen. Deutscher Ausschuss für Stahlbeton, Heft 203, 1969.

/69KO/ KOMLOS, K, 1969, Factors Affecting the Stress-Strain Relation of Concrete in Uniaxial Tension. ACI Journal, Proc. 66, 1969, pp. 111-114.

/69MA/ MAMILLAN, M, 1969, Influence de la dimension des éprouvettes sur le retrait. Annales I.T.B.T.P, No. 258, Juin, 1969, pp. 905-909.

/69MO/ MONNIER, Th, 1969, The behaviour of continuous beams in reinforced concrete. Institute TNO for building materials and building structures, IBBC, Delft, The Netherlands, Report No BI-69-70, 1969.

/69MON/ MONNIER, Th, 1969, The moment-curvature relation of reinforced concrete. Institute TNO for building materials and building structures, IBBC, Delft, The Netherlands, Report No BI-69-72, 1969.

/69SA/ SARGIN, M, HANDA, V.K, 1969, A General Formulation for the Stress-Strain Properties of Concrete. Solid Mechanics Division, University of Waterloo, Report No. 3, May, 1969.

/70ACI/ ACI Building Code (ACI 318 - 71).

/70BE/ BERGSTRÖM, S.G et al., 1970, Kompendium Byggnadsmateriallära AK. Division of Building Technology, the Lund Institute of Technology, Lund, Sweden.

/70CEB/ COMITÉ EUROPEÉN DU BÉTON: International recommendations for the design and construction of concrete structures. Principles and recommendations. June, 1970.

/70IM/ IMBERT, I.D.C, 1970, The Effect of Holes on Tensile Deformations in Plain Concrete. Highway Research Record, No. 324, 1970, pp. 54-65.

/70JO/ JOHNSTON, C.D, 1970, Strength and deformation of concrete in uniaxial tension and compression. Magazine of concrete Research, Vol. 22, No. 70, March 1970, pp. 5-16.

/70KA/ KARSAN, I.D, JARSA, J.O, 1970, Behaviour of Concrete under Varying Strain Gradients.Journal of the Structural Division, Proc. of the American Soc. of Civ. Eng., August, 1970, pp. 1675-1695.

/70KO/ KOMLOS, K, 1970, Comments on the long-term tensile strength of plain concrete. Magazine of Concrete Research, Vol. 22, No. 73, December 1970, pp. 232-238.

/70NE/ NEVILLE, A.M, 1970, Creep of Concrete: Plain, Reinforced and Prestressed. (North-Holland Publishing Company), Amsterdam, 1970.

/70PO/ POPOVICS, S, 1970, A Review of Stress-Strain Relationship for Concrete. ACI Journal, Proc. 67, 1970, pp. 243-248.

/70SW/ SWAMY, N, 1970, The Inelastic Deformation of Concrete. Highway Research Record, No. 324, 1970, pp. 90-99.

/71AB/ ABELES, P.W, HU, C.H, 1971, Flexural Microcracking in Unreinforced Concrete Beams.ACI Journal, Proc. 68, 1971, pp. 779-787.

/71CE/ CEDERWALL, K, 1971, Time-dependent behaviour of reinforced concrete structures. National Swedish Building Research, D3:1971.

/71KE/ KEE, C.F, 1971, Relation Between Strength and Maturity of Concrete. ACI Journal, Proc. 68, 1971, pp. 196-203.

/71NE/ NEVILLE, A.M, 1971, Hardened Concrete: Physical and Mechanical Aspects. ACI Monograph, No. 6, 1971.

/72BA/ BAZANT, Z.P, NAJJAR, L.J, 1972, Nonlinear water diffusion in nonsaturated concrete. Matériaux et constructions, Vol. 5, No. 25, 1972, pp. 3-20.

/72CEB/ BAKER, A.L.L, 1972, Calcul des structures hyperstatiques par la méthod simplifiée bi-linearie de la charge ultime. C.E.B. Annexes aux recommendations internationales pour le calcul et L'execution des ouvrages en beton, Supplément extraordinaire au N^{O} 8 - AOUT 1972 - Roma,Tome 3, Structures hyperstatiques, Document Annexe 6. pp. 218-312.

/72KE/ KESLER, C.E, 1972, Control of Shrinkage, Creep and Temperature Volume Changes Through Variations of Material Properties. ASCE-IABSE, International Conference Preprints Reports, Vol. III-25, 1972, pp. 17-27.

/72LIU/ LIU, T.C.Y et al., 1972, Stress-Strain Response and Fracture of Concrete in Uniaxial and Biaxial Compression. ACI Journal, Proc. 69, 1972, pp. 291-295.

/73CEB/ COMITÉ EUROPÉEN DU BÉTON: Bulletin d'information No. 94, Aout, 1973.

/73SA/ SANDBERG, P.I, 1973, Moisture balance in building elements exposed to natural climate conditions. Division of Building Technology,the Lund Inst. of Tech., Lund, Sweden, Report 43, 1973.

/74HI/ HILLERBORG, A, 1974, Kompendium Byggnadsmateriallära FK I. Division of Building Technology, the Lund Inst. of Tech., Lund, Sweden.

/74KU/ KULICKI, J.M, KOSTEN, C.N, 1974, Inelastic Response of Prestressed Concrete Beams. Fritz Eng. Laboratory, Lehigh University, Bethlehem, Pennsylvania, USA.

/74TH/ THELANDERSSON, S, 1974, Mechanical Behaviour of Concrete under Torsional Loading at Transient, Hightemperature Conditions.Division of Structural Mechanics and Concrete Construction, Lund Inst. of Tech., Lund, Sweden, Bulletin 46, 1974.

/75MA/ MADU, R.M, 1975, Characterization of the stress-stain curves for reinforced concrete under uniaxial tension. Magazine of Concrete Research, Vol. 27, No. 93, December 1975, pp. 210-218.

/76NI/ NILSSON, L.O, 1976, Still unpublished report, Division of Building Technology, the Lund Inst. of Tech., Lund, Sweden.

/76PE/ PETERSON, P-E, MODÉER, M, 1976, Model based on Fracture Mechanics for the Calculation of Crack Propagation in Concrete. Division of Building Technology, the Lund Inst. of Tech., Lund, Sweden, Report 70, 1976.

/76PL/ PLEM, E, 1976, Still unpublished report, Division of Structural Mechanics and Concrete Construction, Lund Inst. of Tech., Lund, Sweden.

A1. Determination of the average stress of concrete in a concentrically reinforced prismatic bar in tension, as a function of the strain of the prism according to the theory of constant slip modulus /58GR/.

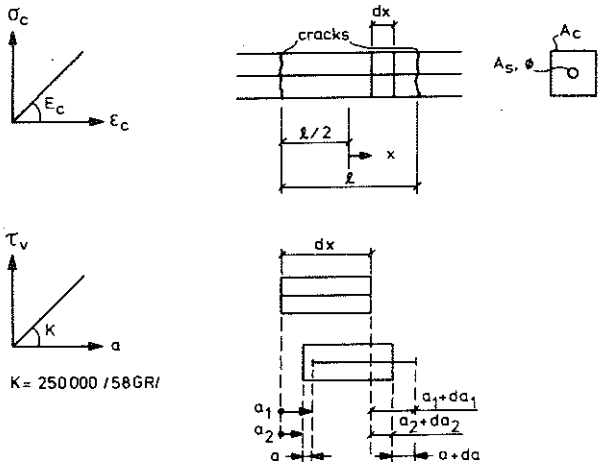

Figure A1.1 Notations used at the derivation of the equations.

With notations according to Fig. A1.1 the following equations may be derived. A linear relation is assumed between the shear stress τ_v and the slip a between concrete and reinforcement (constant slip modulus).

$$\tau_v = K \cdot a = K \cdot (a_1 - a_2) \qquad (A1.1)$$

The derivation of this gives

$$\frac{d\tau_v}{dx} = K \cdot \left(\frac{da_1}{dx} - \frac{da_2}{dx}\right) = K \cdot (\varepsilon_s - \varepsilon_c) = K \cdot \left(\frac{\sigma_s}{E_s} - \frac{\sigma_c}{E_c}\right) \qquad (A1.2)$$

The force in the crack is equal to the force of the prism

$$\sigma_s^o \cdot A_s = \sigma_s \cdot A_s + \sigma_c \cdot A_c \qquad (A1.3)$$

where σ_s^o is the stress of the reinforcement in the crack.

If σ_s from Eq. A1.3 is inserted in Eq. A.1.3 we get

$$\frac{d\tau_v}{dx} = \frac{K}{E_s} \cdot (\sigma_s^o - \sigma_c \cdot (\alpha + 1/\rho)) \qquad (A1.4)$$

where $\alpha = E_s/E_c$ and $\rho = A_s/A_c$.

The force increment in the concrete is equal to the force transferred from the bond surface of the reinforcement

$$\frac{d\sigma_c}{dx} = - \tau_y \cdot \frac{\pi \cdot \phi}{A_c} = - \frac{4\rho}{\phi} \cdot \tau_y \qquad (A1.5)$$

where ϕ is the diameter of the reinforcement bar.

If this equation is derivated and $\frac{d\tau_v}{dx}$ from Eq. A1.4 is inserted we get

$$\frac{d^2\sigma_c}{dx^2} = - \frac{4\rho \cdot K}{\phi \cdot E_s} \cdot (\sigma_s^o - \sigma_c \cdot (\alpha + 1/\rho)) \qquad (A1.6)$$

which can be transformed into

$$\frac{d^2\sigma_c}{dx^2} - \kappa^2 \cdot \sigma_c = - \frac{\kappa^2 \cdot \rho \cdot \sigma_c^o}{1 + \alpha \cdot \rho} \qquad (A1.7)$$

where

$$\kappa^2 = \frac{4K}{\phi \cdot E_s} \cdot (1 + \alpha \cdot \rho)$$

The solution of the equation is

$$\sigma_c = k_1 \cdot \sinh(\kappa \cdot x) + k_2 \cdot \cosh(\kappa \cdot x) + \frac{\sigma_s^o \cdot \rho}{1 + \alpha \cdot \rho} \qquad (A1.8)$$

where the constants k_1 and k_2 may be determined by considering the boundary conditions.

For $x = 0$ $\quad \frac{d\sigma_c}{dx} = 0$ which gives $k_1 = 0$

For $x = \ell/2$ $\quad \sigma = 0$ which gives $k_2 = \frac{- \sigma_s^o \cdot \rho}{(1 + \alpha \cdot \rho) \cdot \cosh(\kappa \cdot \ell/2)}$

By inserting the constants into Eq. A1.8 the stress of concrete may be expressed

$$\sigma_c = \frac{\sigma_s^o \cdot \rho}{1 + \alpha \cdot \rho} \cdot \left(1 - \frac{\cosh(\kappa \cdot x)}{\cosh(\kappa \cdot \ell/2)}\right) \qquad (A1.9)$$

This equation combined with Eq. A1.3 gives an expression for the reinforcement stress

$$\sigma_s = \frac{\sigma_s^0}{1 + \alpha\cdot\rho} \cdot \left(\frac{\cosh\ (\kappa\cdot x)}{\cosh\ (\kappa\cdot \ell/2)} + \alpha\cdot\rho\right) \qquad (A1.10)$$

For x = 0 the stress of concrete has its maximum value

$$\sigma_c^{max} = \frac{\sigma_s^0 \cdot \rho}{1 + \alpha\cdot\rho}\cdot\left(1 - \frac{1}{\cosh\ (\kappa\cdot\ell/2)}\right) \qquad (A1.11)$$

By an integration of Eq. A1.9 and A1.10 from x = 0 to $\ell/2$ the average values of the stresses may be determined.

$$\sigma_{cta} = \frac{2}{\ell} \cdot \int_0^{\ell/2} \sigma_c \cdot dx = \frac{\sigma_s^0 \cdot \rho}{1 + \alpha\cdot\rho}\cdot\left(1 - \frac{\text{tgh}\ (\kappa\cdot\ell/2)}{\kappa\cdot\ell/2}\right) \qquad (A1.12)$$

$$\sigma_{sa} = \frac{2}{\ell} \cdot \int_0^{\ell/2} \sigma_s \cdot dx = \frac{\sigma_s^0}{1 + \alpha\cdot\rho} \cdot \left(\alpha\cdot\rho + \frac{\text{tgh}\ (\kappa\cdot\ell/2)}{\kappa\cdot\ell/2}\right) \qquad (A1.13)$$

The strain of the prism is equal to the average strain of the reinforcement

$$\varepsilon_{sa} = \frac{\sigma_{sa}}{E_s} = \frac{\sigma_s^0}{E_s \cdot (1 + \alpha\cdot\rho)} \cdot \left(\alpha\cdot\rho + \frac{\text{tgh}\ (\kappa\cdot\ell/2)}{\kappa\cdot\ell/2}\right) \qquad (A1.14)$$

Assuming that the maximum concrete stress in Eq. A1.11 is equal to the tensile strength of concrete, the cracking distance may be calculated as a function of σ_s^0.

$$\ell = \frac{2}{\kappa} \cdot \text{arccosh}\ \left(\frac{\sigma_s^0 \cdot \rho}{\sigma_s^0 \cdot \rho - f_{ctm} \cdot (1 + \alpha\cdot\rho)}\right) \qquad (A1.15)$$

If the reinforcement stress in the crack is put equal to the yield stress of reinforcement the maximum shortest cracking distance ℓ_{max} may be calculated with the aid of Eq. A1.15. Since the cracking distances, at increasing load are halved successively, the shortest cracking distance of the prism will vary between ℓ_{max} and $\ell_{max}/2$ depending on the cracking distances which will occur at the first cracks.

The calculations forming the basis for Figs. 3.5 and 3.6 have been performed in the following way. At first ℓ_{max} has been determined

with Eq. A1.15. The values of ℓ and σ_s^o have then been inserted into Eqs A1.12 and A1.14. After that ℓ has been doubled successively and new values of σ_{ca} and ε_{sa} have been determined. The corresponding calculations have also been performed for $\ell = 3/4 \cdot \ell_{max}$. Since the figures are valid for a constant strain rate the average stresses have been calculated also shortly after the occurrence of a new cracking.

A2.1 Basic creep at varying stresses for strain hardening concrete

Notations:

ε_{cci} basic creep after time step i
σ_i stress during time step i
Δt_i time step i, days

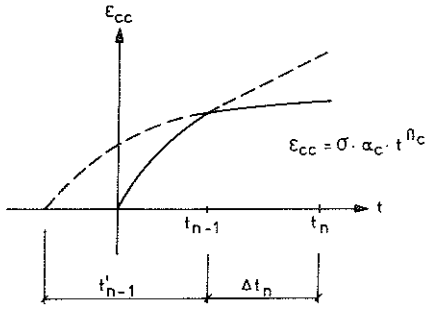

Figure A2.1 Principle for the calculation of basic creep at t_n when the creep is known at the beginning of the time step

The creep after time step n may according to Fig. A2.1 be calculated with

$$\varepsilon_{ccn} = \sigma_n \cdot \alpha_c \cdot (t'_{n-1} + \Delta t_n)^{\beta_c} \qquad (A2.1)$$

where

$$(t'_{n-1})^{\beta_c} = \frac{\varepsilon_{ccn-1}}{\sigma_n \cdot \alpha_c} \qquad (A2.2)$$

By inserting t'_{n-1} into Eq. A2.1 we get

$$\varepsilon_{ccn} = \sigma_n \cdot \alpha_c \cdot \left(\left(\frac{\varepsilon_{ccn-1}}{\sigma_n \cdot \alpha_c}\right)^{1/\beta_c} + \Delta t_n\right)^{\beta_c} \qquad (A2.3)$$

which can be transformed into

$$\varepsilon_{ccn}^{1/\beta_c} = \varepsilon_{ccn-1}^{1/\beta_c} + (\sigma_n \cdot \alpha_c)^{1/\beta_c} \cdot \Delta t_n \qquad (A2.4)$$

In the same way as ε_{ccn} is expressed with the aid of ε_{ccn-1} we may express ε_{ccn-1} with the aid of ε_{ccn-2}

$$\varepsilon_{ccn-1}^{1/\beta_c} = \varepsilon_{ccn-2}^{1/\beta_c} + (\sigma_{n-1} \cdot \alpha_c)^{1/\beta_c} \cdot \Delta t_{n-1} \qquad (A2.5)$$

By expressing creep successively with the aid of previous creep and then summaring up the contributions we get

$$\varepsilon_{ccn}^{1/\beta_c} = \varepsilon_{cc1}^{1/\beta_c} + \alpha_c^{1/\beta_c} \cdot \sum_{i=2}^{n} (\sigma_i^{1/\beta_c} \cdot \Delta t_i) \qquad (A2.6)$$

or if stress may be expressed as a function of time

$$\varepsilon_{cct}^{1/\beta_c} = \varepsilon_{cco}^{1/\beta_c} + \alpha_c^{1/\beta_c} \cdot \int_0^t \sigma(t)^{1/\beta_c} \cdot dt \qquad (A2.7)$$

If no creep has occured at time 0 ($\varepsilon_{cco} = 0$) the basic creep at time t may be calculated with

$$\varepsilon_{cc}(t) = \alpha_c \cdot \left(\int_0^t \sigma(t)^{1/\beta_c} \cdot dt\right)^{\beta_c} \qquad (A2.8)$$

A2.2 Relaxation at basic creep

At relaxation the deformation at time t days may be expressed in two ways

$$\sigma/E_c + \varepsilon_{cc}(t) = \Delta \qquad (A2.9)$$

where Δ is equal to the original deformation at t = 0 which at linear relation between stress and strain is equal to

$$\Delta = \sigma_0/E_c \qquad (A2.10)$$

where σ_0 is the stress at the beginning of the relaxation.

By combining Eqs A2.9 and A2.10 and inserting $\varepsilon_{cc}(t)$ according to Eq. A2.8 we get

$$\sigma_0 - \sigma = E_c \cdot \alpha_c \cdot \left(\int_0^t \sigma^{1/\beta_c} \cdot dt\right)^{\beta_c} \qquad (A2.11)$$

which can be transformed into

$$\left(\frac{\sigma_o - \sigma}{E_c \cdot \alpha_c}\right)^{1/\beta_c} = \int_0^t \sigma^{1/\beta_c} \cdot dt \qquad (A2.12)$$

The derivation of this gives

$$\frac{1}{\beta_c} \cdot \left(\frac{\sigma_o - \sigma}{E_c \cdot \alpha_c}\right)^{1/\beta_c - 1} \cdot \frac{-1}{E_c \cdot \alpha_c} \cdot \frac{d\sigma}{dt} = \sigma^{1/\beta_c} \qquad (A2.13)$$

If $1/\beta_c$ is replaced by

$$d = 1/\beta_c \qquad (A2.14)$$

Eq. A2.13 may be transformed into

$$\left(\frac{\sigma_o - \sigma}{\sigma}\right)^{d-1} \cdot d\sigma = -\frac{(E_c \cdot \alpha_c)^d}{d} \cdot dt \qquad (A2.15)$$

Performing the following substitution

$$\left[\sigma_o/\sigma = x \qquad dx = \frac{-\sigma_o}{\sigma^2} \cdot d\sigma\right] \qquad (A2.16)$$

and inserting into Eq. A2.15 we get

$$x^{d-1} \cdot \frac{(1 - 1/x)^{d-1}}{\sigma} \cdot \frac{-\sigma^2}{\sigma_o} \cdot dx = -\frac{(E_c \cdot \alpha_c)^d}{d} \cdot dt \qquad (A2.17)$$

which may be transformed into

$$x^{d-2} \cdot (1 - 1/x)^{d-1} \cdot dx = \frac{(E_c \cdot \alpha_c)^d}{d} \cdot dt \qquad (A2.18)$$

Through a series expansion we get

$$(1 - 1/x)^{d-1} \approx 1 - \frac{(d-1)}{x} + \frac{(d-1)\cdot(d-2)}{1 \cdot 2 \cdot x^2} - \frac{(d-1)\cdot(d-2)\cdot(d-3)}{1 \cdot 2 \cdot 3 \cdot x^3} + \ldots. \qquad (A2.19)$$

If Eq. A2.18 is integrated we get

$$\int_1^x x^{d-2} \cdot (1 - 1/x)^{d-1} \cdot dx = \frac{(E_c \cdot \alpha_c)^d}{d} \int_0^t dt \qquad (A2.20)$$

and if the integration is performed with the aid of Eq. A2.19 the following equation is obtained

$$\frac{x^{d-1}-1}{d-1} - \frac{(d-1)\cdot(x^{d-2}-1)}{d-2} + \frac{(d-1)\cdot(d-2)\cdot(x^{d-3}-1)}{2(d-3)} +$$

$$- \frac{(d-1)\cdot(d-2)\cdot(d-3)\cdot(x^{d-4}-1)}{6(d-4)} + \frac{(d-1)\cdot(d-2)\cdot(d-3)\cdot(d-4)\cdot(x^{d-5}-1)}{24(d-5)} +$$

$$- \frac{(d-1)\cdot(d-2)\cdot(d-3)\cdot(d-4)\cdot(d-5)\cdot(x^{d-6}-1)}{120(d-6)} \approx \frac{(E_c \cdot \alpha_c)^d}{d} \cdot t \qquad \text{(A2.21)}$$

By using Eq. A2.21, the time t necessary for a decrease of stress to a certain value of the original one, as well as the amount of the original stress left at a certain time, may be calculated. The number of terms which must be included in the series expansion depends on $x = \sigma_0/\sigma$ and the desired accuracy.

A3. Evaluation of moment-curvature relations for reinforced concrete

Assumptions:
- plane cross-sections remain plane
- linear relation between stress and strain
- creep is governed by the stress prevailing when the moment-curvature relation is determined
- shrinkage is fully developed
- normal force N is positive at tension and is acting at the centroid of the concrete cross-section
- the cross-sections are rectangular

A3.1 Flexural rigidity at uncracked state (EI_o) and curvature when the moment is zero ($1/r_o$).

The stresses may be expressed as a function of the strains according to Fig. A3.1.

$$\sigma_u = E_c \cdot \left[1/r \cdot x + \varepsilon_{\sigma=0} - \gamma \cdot \varepsilon_{css} - \sigma_u \cdot \varepsilon'_{cc}\right] \qquad (A3.1)$$

$$\sigma_\ell = E_c \cdot \left[1/r \cdot (h-x) - \varepsilon_{\sigma=0} + \varepsilon_{css} - \sigma_\ell \cdot \varepsilon'_{cc}\right] \qquad (A3.2)$$

$$\sigma'_s = E_s \cdot \left[1/r \cdot (x-c) + \varepsilon_{\sigma=0}\right] \qquad (A3.3)$$

$$\sigma_s = E_s \cdot \left[1/r \cdot (h-x-c) - \varepsilon_{\sigma=0}\right] \qquad (A3.4)$$

The strain at the neutral axis is equal to

$$\varepsilon_{\sigma=0} = \varepsilon_{css} + (\gamma-1) \cdot \varepsilon_{css} \cdot (h-x)/h \qquad (A3.5)$$

If the strain at the neutral axis together with the creep coefficient $\phi = E_c \cdot \varepsilon'_{cc}$ and $\alpha = E_s/E_c$ are inserted into the stress equations we get

$$\sigma_u = \frac{E_s}{(1+\phi)\cdot\alpha} \cdot \left[1/r - \varepsilon_{css} \cdot (\gamma-1)/h \cdot x\right] \qquad (A3.6)$$

$$\sigma_\ell = \frac{E_s}{(1+\phi)\cdot\alpha} \cdot \left[1/r - \varepsilon_{css} \cdot (\gamma-1)/h \cdot (h-x)\right] \qquad (A3.7)$$

$$\sigma'_s = E_s \cdot \left[1/r \cdot (x-c) + \varepsilon_{css} \cdot ((\gamma-1)\cdot(h-x) + h)/h\right] \qquad (A3.8)$$

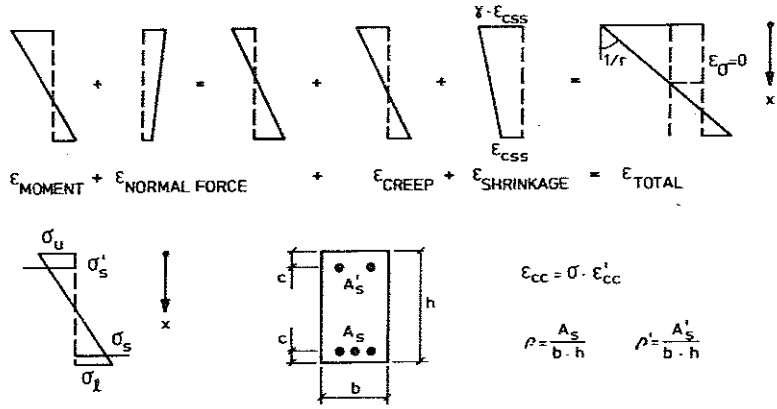

Figure A3.1 Notations and definitions of strain components used for the derivation of the moment-curvature relations for reinforced concrete

$$\sigma_s = E_s \cdot \left[1/r \cdot (h-x-c) - \varepsilon_{css} \cdot ((\gamma-1)\cdot(h-x) + h)/h\right] \qquad (A3.9)$$

Horizontal equilibrium requires that

$$N = \sigma_\ell \cdot b \cdot (h-x)/2 + \sigma_s \cdot b \cdot h \cdot \quad - \sigma_u \cdot b \cdot x/2 +$$

$$- \sigma_s' \cdot b \cdot h \cdot \rho' \qquad (A3.10)$$

By using

$$\psi = (1 + \phi) \cdot \alpha \cdot \rho \qquad \psi' = (1 + \phi) \cdot \alpha \cdot \rho' \qquad (A3.11)$$

and inserting the stresses according to Eqs A3.6 - A3.9 into Eq. A3.10 the position of the neutral axis may be determined

$$\frac{x}{h} = \frac{\alpha_1}{\alpha_2} \qquad (A3.12)$$

where

$$\alpha_1 = 1 + 2\psi \cdot (1 - c/h) + 2\psi' \cdot c/h - \varepsilon_{css} \cdot r \cdot \left[(\gamma - 1)\cdot(1 + 2\psi +\right.$$

$$\left. + 2\psi') + 2(\psi + \psi')\right] /h - 2N \cdot (1 + \phi) \cdot \alpha \cdot r/(b \cdot h^2 \cdot E_s)$$

and

$$\alpha_2 = 2(1 + \psi + \psi') \cdot (1 - (\gamma - 1) \cdot \varepsilon_{css} \cdot r/h)$$

Moment equilibrium requires that

$$M = \sigma_u \cdot b \cdot x/2 \cdot (h/2 - x/3) + \sigma_s' \cdot b \cdot h \cdot \rho' \cdot (h/2 - c) +$$

$$+ \sigma_s \cdot b \cdot h \cdot \rho \cdot (h/2 - c) + \sigma_\ell \cdot b \cdot (h - x)/2 \cdot (h/2 - (h - x)/3) \qquad (A3.13)$$

By inserting the stresses of Eqs A3.6 - A3.9 and Eq. A3.11 into Eq. A3.13 we get

$$\frac{12\ M \cdot (1 + \phi) \cdot \alpha}{b \cdot E_s} = h^3 \cdot (1/r - \varepsilon_{css}\cdot(\gamma - 1)/h + 6h \cdot (h - 2c) \cdot$$

$$\left[x \cdot (1 - \varepsilon_{css} \cdot r \cdot (\gamma - 1)/h) \cdot 1/r \cdot(\psi' - \psi) +\right.$$

$$+ \varepsilon_{css} \cdot \gamma \cdot (\psi' - \psi) + 1/r \cdot (\psi \cdot (h - c) - \psi' \cdot c) \Big] \qquad \text{(A3.14)}$$

If x from Eq. A3.12 is inserted into this equation the following relation is obtained

$$M = (EI_o) \cdot (1/r - 1/r_o) \qquad \text{(A3.15)}$$

where

$$(EI_o) = \frac{b \cdot h^3 \cdot E_s}{12\,(1+\phi) \cdot \alpha} \cdot \frac{1 + \psi + \psi' + 3\,(1 - 2\,c/h)^2 \cdot (\psi + \psi' + 4\psi \cdot \psi')}{1 + \psi + \psi'} \qquad \text{(A3.16)}$$

and

$$1/r_o = \frac{\varepsilon_{css} \cdot (\gamma-1)(1+\psi+\psi')/h + 3(1-2c/h) \cdot (\psi-\psi') \cdot (\varepsilon_{css} \cdot (1+\gamma)/h - 2N \cdot (1+\phi) \cdot \alpha / b \cdot h^2 \cdot E_s)}{1+\psi+\psi' + 3(1-2c/h)^2 \cdot (\psi+\psi'+4\psi \cdot \psi')} \qquad \text{(A3.17)}$$

A3.2 The cracking moment (M_r)

The cracking moment is attained when σ_ℓ (Eq. A3.7) is equal to the tensile strength σ_r.

$$\sigma_\ell = \frac{E_s}{(1+\phi) \cdot \alpha} \cdot \Big[1/r - \varepsilon_{css} \cdot (\gamma-1)/h\Big] \cdot (h-x) = \sigma_r \qquad \text{(A3.18)}$$

If x from Eq. A3.12 is inserted into this equation the curvature corresponding to the cracking moment may be determined.

$$\frac{1}{r} = \frac{2\sigma_r \cdot (1+\phi) \cdot \alpha \cdot (1+\psi+\psi')/(E_s \cdot h) + \varepsilon_{ccs} \cdot ((\gamma-1) - 2(\psi+\psi'))/h - 2N \cdot (1+\phi) \cdot \alpha / (b \cdot h^2 \cdot E_s)}{1 + 2\psi \cdot c/h + 2\psi' \cdot (1-c/h)} \qquad \text{(A3.19)}$$

If this curvature is inserted into Eq. A3.15 together with (EI_o) and $1/r_o$ from Eqs A3.16 and A3.17 respectively, the cracking moment may be determined.

$$M_r = \sigma_r \cdot \frac{b \cdot h^2}{6} \cdot \frac{1 + \psi + \psi' + 3\,(1 - 2c/h)^2 \cdot (\psi + \psi' + 4\psi \cdot \psi')}{\alpha_3} +$$

$$- \frac{b \cdot h^2 \cdot E_s}{3(1+\phi) \cdot \alpha} \cdot \varepsilon_{css} \cdot (\gamma - 1) \cdot \frac{\psi \cdot (2-3c/h) \cdot c/h - \psi' \cdot (1-c/h) \cdot (1-3c/h)}{\alpha_3} +$$

$$- \frac{b \cdot h^2 \cdot E_s \cdot \varepsilon_{css}}{3\,(1+\phi)\cdot\alpha} \cdot \frac{\psi\cdot(2-3c/h)-\psi'(1-3c/h)+6\psi\cdot\psi'\cdot(1-2c/h)^2}{\alpha_3} +$$

$$- \frac{N \cdot h}{6} \cdot \frac{1-6(1-2c/h)\cdot(\psi\cdot c/h-\psi'\cdot(1-c/h))}{\alpha_3} \qquad (A3.20)$$

where

$$\alpha_3 = 1 + 2\psi \cdot c/h + 2\psi' \cdot (1 - c/h)$$

A3.3 Flexural rigidity at cracked state $(EI)_r$

Assumptions: The concrete does not carry any tensile stresses

Horizontal equilibrium requires that

$$N = \sigma_s \cdot b \cdot h \cdot \rho - \sigma_u \cdot b \cdot x/2 - \sigma_s' \cdot b \cdot h \cdot \rho' \qquad (A3.21)$$

If the stresses according to Eqs A3.6, A3.8, A3.9 and A3.11 are inserted into this equation the curvature may be determined as a function of, among other things, x

$$\frac{1}{r} = \frac{\varepsilon_{css}\cdot\left[(\gamma-1)\cdot(x^2-2h\cdot(h-x)\cdot(\psi+\psi'))-2h^2\cdot(\psi+\psi')\right] - 2N\cdot(1+\phi)\cdot\alpha\cdot h/(b\cdot E_s)}{h(x^2-2\psi\cdot h\cdot(h-x-c)+2\psi'\cdot h(x-c))} \qquad (A3.22)$$

Moment equilibrium requires that

$$M = \sigma_u\cdot b\cdot x/2\cdot(h/2-x/3)+\sigma_s'\cdot b\cdot h\cdot\rho'\cdot(h/2-c)+\sigma_s\cdot b\cdot h\cdot\rho\cdot(h/2-c) \qquad (A3.23)$$

If the stresses according to Eqs A3.6, A3.8, A3.9 and A3.11 are inserted into this equation the moment may be determined as a function of, among other things, 1/r and x.

$$\frac{12M\cdot(1+\phi)\cdot\alpha}{b\cdot E_s} = 1/r\cdot\left[x^2\cdot(3h-2x)+6h\cdot(h-2c)\cdot(\psi\cdot(h-x-c)+\psi'\cdot(x-c))\right] +$$

$$+ \varepsilon_{css}\cdot 6h\cdot(h-2c)\cdot(\psi'-\psi) + \varepsilon_{css}\cdot(\gamma-1)\cdot\left[6h\cdot(h-2c)\cdot(h-x)\cdot(\psi'-\psi) +\right.$$

$$\left. - x^2\cdot(3h-2x)\right]/h \qquad (A3.24)$$

In order to determine the flexural rigidity the following procedure has been chosen

$$(EI)_r = dM/d(1/r) \tag{A3.25}$$

According to Eq. A3.22 the curvature may be written

$$1/r = f(x)/g(x) \tag{A3.26}$$

Derivation with respect to x gives

$$d(1/r)/dx = (g(x) \cdot f'(x) - f(x) \cdot g'(x))/g(x)^2 \tag{A3.27}$$

According to Eq. A3.24 the moment may be expressed

$$M = 1/r \cdot h(x) + k(x) \tag{A3.28}$$

If this is derivated with respect to x we get

$$dM/dx = d(1/r)/dx \cdot h(x) + 1/r \cdot h'(x) + k'(x) \tag{A3.29}$$

which may be transformed into

$$\frac{dM/dx}{d(1/r)/dx} = h(x) + \frac{1/r \cdot h'(x)}{d(1/r)/dx} + \frac{k'(x)}{d(1/r)/dx} \tag{A3.30}$$

If Eqs A3.26 and A3.27 are inserted into A3.30 we get

$$\frac{dM}{d(1/r)} = \frac{h(x)\cdot g(x)\cdot f'(x)-h(x)\cdot f(x)\cdot g'(x)+f(x)\cdot g(x)\cdot h'(x)+g(x)^2\cdot k'(x)}{g(x)\cdot f'(x)-f(x)\cdot g'(x)} \tag{A3.31}$$

If the functions according to Eqs A3.22 and A3.24 are inserted into Eq. A3.31 and if $y = x/h$ the flexural rigidity at cracked state will be equal to

$$(EI)_r = \frac{b \cdot h^3 \cdot E_s}{3\,(1+\phi)\cdot\alpha} \cdot \frac{\alpha_4}{y + \psi + \psi'} \tag{A3.32}$$

where

$$\alpha_4 = y^4/4+y\cdot(y^2-3y\cdot(1-c/h)+3(1-c/h)^2)\cdot\psi+y\ (y^2-3y\cdot c/h+3(c/h)^2)\cdot\psi' +$$

$$+ 3(1-2c/h)^2\cdot\psi\cdot\psi'$$

By eliminating 1/r from Eq. A3.24 with the aid of Eq. A3.22 an equation of the third degree in y is obtained from which y may be determined.

$$\alpha_{10} + \alpha_{11}\cdot y + \alpha_{12}\cdot y^2 + \alpha_{13}\cdot y^3 = 0 \qquad \text{(A3.33)}$$

where

$$M_1 = M\cdot(1+\phi)\cdot\alpha/(b\cdot h^2\cdot E_s\cdot\varepsilon_{css})$$

and

$$N_1 = N\cdot(1+\phi)\cdot\alpha/(b\cdot h\cdot E_s\cdot\varepsilon_{css})$$

$$\alpha_{10} = 6\left[N_1\cdot(1-2c/h)\cdot(\psi\cdot(1-c/h)-\psi'\cdot c/h)-2M_1\cdot(\psi\cdot(1-c/h)+\psi'\cdot c/h)+2(1-2c/h)^2\cdot\gamma\cdot\psi\cdot\psi'\right]$$

$$\alpha_{11} = 6\left[-N_1\cdot(1-2c/h)\cdot(\psi-\psi')+2M_1\cdot(\psi+\psi')-2(1-2c/h)^2\cdot(\gamma-1)\cdot\psi\cdot\psi'\right]$$

$$\alpha_{12} = 6\left[N_1/2+M_1+\psi\cdot(1-c/h)+\psi'\cdot c/h+(\gamma-1)\cdot c/h\cdot(1-c/h)\cdot(\psi+\psi')\right]$$

$$\alpha_{13} = -2\left[N_1+\psi+\psi'+(\gamma-1)\cdot(\psi\cdot c/h+\psi'\cdot(1-c/h))\right]$$

The flexural rigidity may be determined by solving x from Eq. A3.33 and inserting it into Eq. A3.32.

A3.4 The flexural rigidity at cracked state when there is neither shrinkage nor normal force.

In this case the position of the neutral axis may easily be determined from Eq. A3.22

$$x^2 - 2\psi\cdot h\cdot(h-x-c) + 2\psi'\cdot h\cdot(x-c) = 0 \qquad \text{(A3.34)}$$

If x is replaced by $z\cdot h$ the following relations is valid

$$z^2 - 2\psi\cdot(1-z-c/h) + 2\psi\cdot(z-c/h) = 0 \qquad \text{(A3.35)}$$

which has the solution

$$z = -(\psi + \psi')(\pm)\sqrt{(\psi + \psi')^2 + 2\psi \cdot (1 - c/h) + 2\psi' \cdot c/h} \qquad (A3.36)$$

According to Eq. A3.24 the following is valid

$$\frac{M}{1/r} = \frac{b \cdot h^3 \cdot E_s}{12(1+\phi)\cdot\alpha} \cdot \left[z^2 \cdot (3-2z) + 6(1-2c/h)\cdot(\psi\cdot(1-z-c/h)+\psi'\cdot(z-c/h))\right] \qquad (A3.37)$$

By inserting z^2 according to Eq. A3.35 it may be transformed into

$$\frac{M}{1/r} = \frac{dM}{d(1/r)} = (EI)_r = \frac{b \cdot h^3 \cdot E_s}{12(1+\phi)\cdot\alpha} \cdot \left[\psi\cdot(1-c/h-z)\cdot(3-3c/h-z) + \right.$$

$$\left. + \psi'\cdot(z-c/h)\cdot(z-3c/h)\right] \qquad (A3.38)$$

By calculating z from Eq. A3.36 and inserting it into Eq. A3.28 the flexural rigidity may be calculated.

A4. Calculation method for the determination of the moment distribution in a partially cracked statically indeterminate beam with a bilinear moment-curvature relation and aid formulae

In the manual calculation the force method is used. The structure is made statically determinate by insertion of unknown forces. The deformations of the unknown forces and the load are determined and inserted into the compatibility equations.

The following procedure is the most appropriate for the calculation. The moment distribution of the beam is estimated by assuming that the flexural rigidity is constant along the length. Then the beam is divided into cracked and uncracked sections respectively according to the assumed moment distribution and a new moment distribution is calculated. After this the beam is again divided into cracked and uncracked sections according to the new moment distribution and another moment distribution is calculated. This procedure is repeated until an acceptable accuracy between the moment distribution assumed and the one calculated is obtained. Generally one or two iterations are sufficient.

For a bilinear moment-curvature relation according to Fig. A.4-1 the curvature may be expressed as a function of the moment as

$$\frac{1}{r} = \frac{1}{r_0} + \frac{M}{(EI)_0} \qquad 0 < M \leq M_r$$

$$\frac{1}{r} = \frac{1}{r_0} - \frac{M_r}{(EI)_0} \cdot \left(\frac{(EI)_r}{(EI)_0} - 1\right) + \frac{M}{(EI)_r} \qquad M_r < M < M_y$$

The terms $1/r_0$, $(EI)_0$, $(EI)_r$ and M_r may be determined according to chapter 5 and if creep and shrinkage exist, this is considered. The calculation is best performed by taking into account the effects of the factors M/EI, $\frac{M_r}{(EI)_0} \cdot \left(\frac{(EI)_0}{(EI)_r} - 1\right)$ och $1/r_0$ separately. This may be performed with the aid of the moment area method and below aid formulae for the most common loading cases are stated. In order to simplify the formulae, the rigidity $(EI)_0$ is assumed to be the same for the whole beam, which is a reasonable approximation. The ratio used in the formulae between the rigidities and the lengths of the uncracked and cracked sections respectively are shown in Fig. A.4-2.

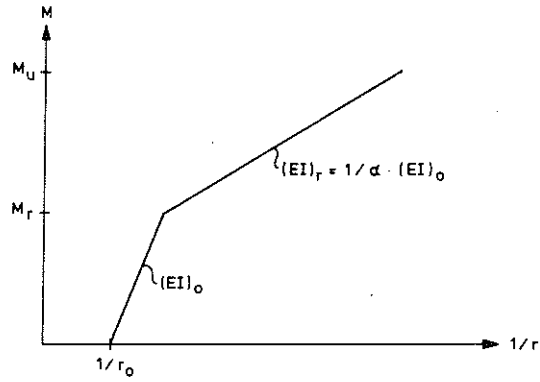

Figure A4.1 The parameters of the bilinear moment-curvature relation used.

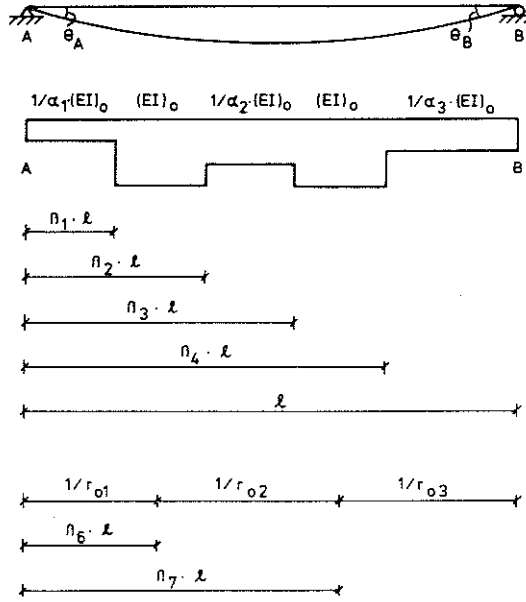

Figure A4.2 Definition of the notations used in the aid formulae

1. The slopes at the supports for a uniform lateral load q.

$$\theta_A + \theta_B = \frac{q \cdot \ell^3}{12(EI)_o} \cdot \left[\alpha_3 + (\alpha_1 - 1) \cdot \beta_1^2 \cdot (3 - 2\beta_1) + (\alpha_2 - 1) \cdot \right.$$

$$\left. \cdot \left[\beta_3^2 \cdot (3 - 2\beta_3) - \beta_2^2 \cdot (3 - 2\beta_2)\right] - (\alpha_3 - 1) \cdot \beta_4^2 \cdot (3 - 2\beta_4)\right]$$

$$\theta_B = \frac{q \cdot \ell^3}{24(EI)_o} \cdot \left[\alpha_3 + (\alpha_1 - 1) \cdot \beta_1^3 \cdot (4 - 3\beta_1) + (\alpha_2 - 1) \cdot \right.$$

$$\left. \cdot \left[\beta_3^3 \cdot (4 - 3\beta_3) - \beta_2^3 \cdot (4 - 3\beta_2)\right] - (\alpha_3 - 1) \cdot \beta_4^3 \cdot (4 - 3\beta_4)\right]$$

2. The slopes at the supports for a concentrated lateral load F applied at the centre of the beam.

$$\theta_A + \theta_B = \frac{F \cdot \ell^2}{4(EI)_o} \cdot \left[\alpha_3 - \alpha_2/2 + (\alpha_1 - 1) \cdot \beta_1^2 + (\alpha_2 - 1) \cdot \right.$$

$$\left. \cdot \left[\beta_3 \cdot (2 - \beta_3) - \beta_2^2\right] - (\alpha_3 - 1) \cdot \beta_4 \cdot (2 - \beta_4)\right]$$

$$\theta_B = \frac{F \cdot \ell^2}{12(EI)_o} \cdot \left[\alpha_3 - \alpha_2/4 + (\alpha_1 - 1) \cdot 2\beta_1^3 + (\alpha_2 - 1) \cdot \right.$$

$$\left. \cdot \left[\beta_3^2 \cdot (3 - 2\beta_3) - 2\beta_2^3\right] - (\alpha_3 - 1) \cdot \beta_4^2 \cdot (3 - 2\beta_4)\right]$$

The equations are valid only when $\beta_2 \leq 1/2$ and $\beta_3 \geq 1/2$.

3. The slope at the supports for a concentrated lateral load F at the distance $\beta_5 \cdot \ell$ from the support A.

$$\theta_A + \theta_B = \frac{F \cdot \ell^2}{2(EI)_o} \cdot \left[(1 - \beta_5) \cdot \left[(\alpha_1 - 1) \cdot \beta_1^2 - (\alpha_2 - 1) \cdot \beta_2^2\right] + \right.$$

$$\left. - \beta_5^2 \cdot \alpha_2 + \beta_5 \cdot \left[\alpha_3 + (\alpha_2 - 1) \cdot \beta_5 \cdot (2 - \beta_3) - (\alpha_3 - 1) \cdot \beta_4 \cdot (2 - \beta_4)\right]\right]$$

$$\theta_B = \frac{F \cdot \ell^2}{6(EI)_o} \cdot \left[(1 - \beta_5) \cdot \left[(\alpha_1 - 1) \cdot 2\beta_1^3 - (\alpha_2 - 1) \cdot 2\beta_2^3 - \beta_5^3 \cdot \alpha_2 + \right.\right.$$

$$\left.\left. + \beta_5 \cdot \left[\alpha_3 + (\alpha_2 - 1) \cdot \beta_3^2 \cdot (3 - 2\beta_3) - (\alpha_3 - 1) \cdot \beta_4^2 \cdot (3 - 2\beta_4)\right]\right]\right]$$

The equations are valid only when $\beta_2 \leq \beta_5$ and $\beta_3 \geq \beta_5$.

4. The slopes at the supports for a couple M applied at the end A.

$$\theta_A + \theta_B = \frac{M \cdot \ell}{2(EI)_o} \cdot \left[\alpha_1 - (\alpha_1 - 1) \cdot (1 - \beta_1)^2 + (\alpha_2 - 1) \cdot \right.$$

$$\left. \cdot \left[(1 - \beta_2)^2 - (1 - \beta_3)^2\right] + (\alpha_3 - 1) \cdot (1 - \beta_4)^2\right]$$

$$\theta_A = \frac{M \cdot \ell}{3(EI)_o} \cdot \left[\alpha_1 - (\alpha_1 - 1) \cdot (1 - \beta_1)^3 + (\alpha_2 - 1) \cdot \right.$$

$$\left. \cdot \left[(1 - \beta_2)^3 - (1 - \beta_3)^3\right] + (\alpha_3 - 1) \cdot (1 - \beta_4)^3\right]$$

5. The slopes of the supports for a couple M applied at the end B.

$$\theta_A + \theta_B = \frac{M \cdot \ell}{2(EI)_o} \cdot \left[\alpha_3 + (\alpha_1 - 1) \cdot \beta_1^2 + (\alpha_2 - 1) \cdot (\beta_3^2 - \beta_2^2) + \right.$$

$$\left. - (\alpha_3 - 1) \cdot \beta_4^2\right]$$

$$\theta_B = \frac{M \cdot \ell}{3(EI)_o} \cdot \left[\alpha_3 + (\alpha_1 - 1) \cdot \beta_1^3 + (\alpha_2 - 1) \cdot (\beta_3^3 - \beta_2^3) + \right.$$

$$\left. - (\alpha_3 - 1) \cdot \beta_4^3\right]$$

6. The slope at the supports for the terms $\frac{M_r}{(EI)_o} \cdot (\frac{(EI)_r}{(EI)_o} - 1)$

$$\theta_A + \theta_B = \frac{-\ell}{(EI)_o} \cdot \left[M_{r1} \cdot (\alpha_1 - 1) \cdot \beta_1 + M_{r2} \cdot (\alpha_2 - 1) \cdot (\beta_3 - \beta_2) + \right.$$

$$\left. + M_{r3} \cdot (\alpha_3 - 1) \cdot (1 - \beta_4)\right]$$

$$\theta_B = \frac{-\ell}{2(EI)_o} \cdot \left[M_{r1} \cdot (\alpha_1 - 1) \cdot \beta_1^2 + M_{r2} \cdot (\alpha_2 - 1) \cdot (\beta_3^2 - \beta_2^2) + \right.$$

$$\left. + M_{r3} \cdot (\alpha_3 - 1) \cdot (1 - \beta_4^2)\right]$$

The cracking moments M_r are assumed positive at cracking in the lower edge of the beam.

7. The slope at the supports for the terms $1/r_o$.

$$\theta_A + \theta_B = \ell \cdot \left[1/r_{o1} \cdot \beta_6 + 1/r_{o2} \cdot (\beta_7 - \beta_6) + 1/r_{o3} \cdot (1 - \beta_7)\right]$$

$$\theta_B = \frac{\ell}{2} \cdot \left[1/r_{o1} \cdot \beta_6^2 + 1/r_{o2} \cdot (\beta_7^2 - \beta_6^2) + 1/r_{o3} \cdot (1 - \beta_7^2)\right]$$

The curvatures $1/r_o$ are assumed positive if they cause tensile strains in the lower edge of the beam.

A5. Reinforcement stress in a crack for segment in pure bending

Under the assumptions that plane cross-sections remain plane, that the tensile zone of concrete is neglected, that the creep is governed by the final stress, and that at shrinkage the final stage is studied, it is possible, with the aid of two equilibrium equations and compatibility equations, to derive the tensile stress of the reinforcement to

$$\sigma_s = \frac{M}{A_s \cdot h} \cdot \xi \qquad (A5.1)$$

where, if no shrinkage takes place

$$1/\xi = 1 - c/h - (x/h)/3 + \psi'/\psi \cdot ((x/h)/3-c/h) \cdot (x/h-c/h)/(1 - c/h - x/h)$$

and where

$$x/h = \sqrt{(\psi + \psi')^2 + 2\psi \cdot (1 - c/h) + 2\psi' \cdot c/h} - (\psi + \psi'),$$

$$\psi = (1 + \phi) \cdot \alpha \cdot \frac{A_s}{b \cdot h}, \quad \psi' = (1 + \phi) \cdot \alpha \cdot \frac{A_s'}{b \cdot h}, \quad \alpha = E_s/E_c \text{ and}$$

c is the distance from the centroid of the tensile and compressive reinforcements respectively to the edges in tension and compression. The parameter ξ is shown in Fig. A5.1 for c/h = 0.1. At short-term load $\phi = 0$.

If shrinkage takes place then

$$1/\xi = 1-c/h-(x/h)/3-\psi'/\psi\cdot((x/h)/3-c/h)\cdot\left(1-\frac{\psi + \psi'}{\psi'+(x/h)^2/(2(1-2c/h))}\right)$$

with x/h according to Eq. A3.33.

Fig. A5.2 shows the parameter ξ for c/h = 0.1 and the parameter

$\eta = \frac{(1 + \phi) \cdot M}{b \cdot h^2 \cdot E_c \cdot \varepsilon_{css}}$ equal to 1. The peaks of the vertical lines are valid for $\eta = 4$. When $\eta \to \infty$ ξ at shrinkage gets the same value as when skrinkage does not exist. (Fig. A5.1).

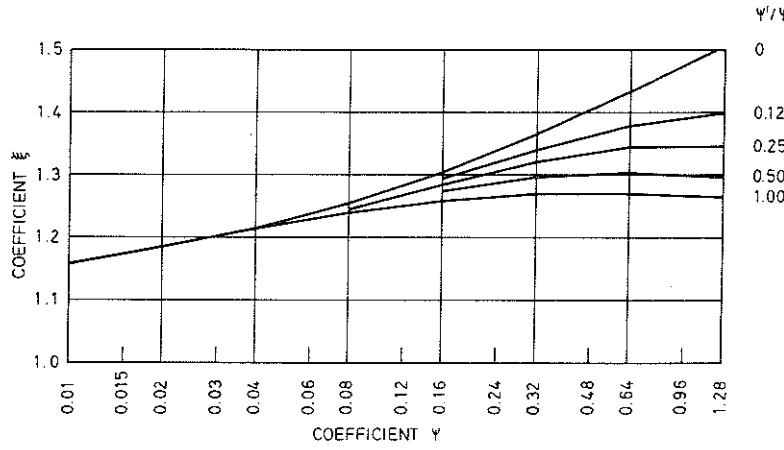

Figure A5.1 The coefficient ξ for the determination of the reinforcement stress in a crack at short-term load and creep according to Eq. A5.1. c/h = 0.1

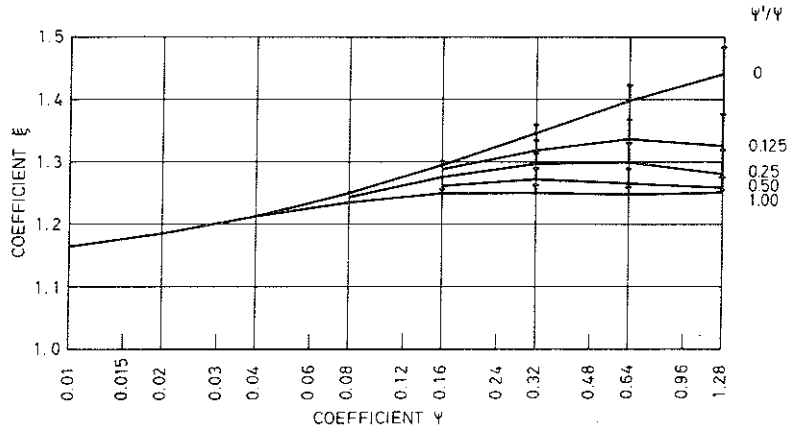

Figure A5.2 The coefficient ξ for the determination of the reinforcement stress in a crack at creep and shrinkage according to Eq. A5.1. c/h = 0.1